Developing a hybrid agent-based mathematical model to study bladder infections

Anas Lasri Doukkali

A thesis submitted for the degree of PhD
at the
University of St Andrews

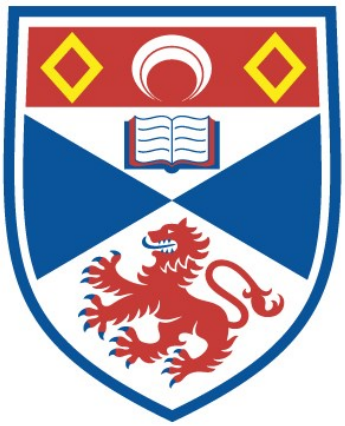

2024

Full metadata for this item is available in
St Andrews Research Repository
at:
https://research-repository.st-andrews.ac.uk/

Identifier to use to cite or link to this thesis:
DOI: https://doi.org/10.17630/sta/890

This item is protected by original copyright

Candidate's declaration

I, Anas Lasri Doukkali, do hereby certify that this thesis, submitted for the degree of PhD, which is approximately 60,000 words in length, has been written by me, and that it is the record of work carried out by me, or principally by myself in collaboration with others as acknowledged, and that it has not been submitted in any previous application for any degree. I confirm that any appendices included in my thesis contain only material permitted by the 'Assessment of Postgraduate Research Students' policy.

I was admitted as a research student at the University of St Andrews in September 2019.

I received funding from an organisation or institution and have acknowledged the funder(s) in the full text of my thesis.

Date 03/05/2024 Signature of candidate

Supervisor's declaration

I hereby certify that the candidate has fulfilled the conditions of the Resolution and Regulations appropriate for the degree of PhD in the University of St Andrews and that the candidate is qualified to submit this thesis in application for that degree. I confirm that any appendices included in the thesis contain only material permitted by the 'Assessment of Postgraduate Research Students' policy.

Date 03/05/2024 Signature of supervisor

Permission for publication

In submitting this thesis to the University of St Andrews we understand that we are giving permission for it to be made available for use in accordance with the regulations of the University Library for the time being in force, subject to any copyright vested in the work not being affected thereby. We also understand, unless exempt by an award of an embargo as requested below, that the title and the abstract will be published, and that a copy of the work may be made and supplied to any bona fide library or research worker, that this thesis will be electronically accessible for personal or research use and that the library has the right to migrate this thesis into new electronic forms as required to ensure continued access to the thesis.

I, Anas Lasri Doukkali, confirm that my thesis does not contain any third-party material that requires copyright clearance.

The following is an agreed request by candidate and supervisor regarding the publication of this thesis:

Printed copy

No embargo on print copy.

Electronic copy

No embargo on electronic copy.

Date 03/05/2024 Signature of candidate

Date 03/05/2024 Signature of supervisor

Underpinning Research Data or Digital Outputs

Candidate's declaration

I, Anas Lasri Doukkali, understand that by declaring that I have original research data or digital outputs, I should make every effort in meeting the University's and research funders' requirements on the deposit and sharing of research data or research digital outputs.

Date 03/05/2024 Signature of candidate

Permission for publication of underpinning research data or digital outputs

We understand that for any original research data or digital outputs which are deposited, we are giving permission for them to be made available for use in accordance with the requirements of the University and research funders, for the time being in force.

We also understand that the title and the description will be published, and that the underpinning research data or digital outputs will be electronically accessible for use in accordance with the license specified at the point of deposit, unless exempt by award of an embargo as requested below.

The following is an agreed request by candidate and supervisor regarding the publication of underpinning research data or digital outputs:

No embargo on underpinning research data or digital outputs.

Date 03/05/2024 Signature of candidate

Date 03/05/2024 Signature of supervisor

ACKNOWLEDGEMENTS

I am deeply grateful to my supervisor Dr. Ruth Bowness for her invaluable advice, continuous support and insightful comments at every stage of my research journey. I would also like to thank my family, friends and colleagues.

This work was supported funding from the Academy of Medical Sciences (London), the Wellcome Trust (London), the UK Government Department of Business, Energy and Industrial Strategy (London), the British Heart Foundation (London), and the Global Challenges Research Fund (Swindon, UK; grant number SBF003052).

ABSTRACT

Urinary Tract Infections (UTIs) are amongst the most common infections worldwide, affecting well over 150 million people each year. UTIs now account for 40% of all hospital-acquired infections and they are becoming harder to treat, with an estimated 1 in 3 being resistant to the most commonly used antibiotics. UTIs are also notorious for recurring. Using agent-based modelling techniques we have developed a model that describes the infection process in bladder infections. Gaining a better understanding of the pathophysiology can prove key to the development of new treatment strategies with greater success and less resistance rates. Data arising from animal and cell culture models are incredibly valuable but can be limited by ethical considerations and time constraints. Simulations from in silico models can be analysed and their results can complement clinical findings, adding to the understanding of how the infection behaves and how we might improve treatment. We simulate discrete agents in the system: *E. Coli* bacteria and the immune cell types reported to have critical roles in lower UTIs (LY6C macrophages, neutrophils and mast cells). The capacity of the bacteria to penetrate the bladder epithelial barrier and seek refuge in the bladder epithelial cells is a critical initiating step of infection and this process is simulated in our model. We also integrated in our model a treatment framework which we have used to investigate the effects of Trimethoprim, the most commonly used antibiotic for bladder infections, on the infection outcome.

TABLE OF CONTENTS

LIST OF ILLUSTRATIONS

LIST OF TABLES

Chapter 1

INTRODUCTION

1.1 Urinary tract infections

Urinary tract infections (UTIs) are infections affecting the urethra, bladder and kidneys. Lower UTIs affect the bladder and urethra, and upper UTIs affect the kidneys. Simple or uncomplicated[1] UTIs are caused by a number of pathogens in people with a normal urinary tract and kidney function, and no predisposing co-morbidities. They can often be asymptomatic, self-limiting or readily cleared with a short course of antibiotics. One in four uncomplicated UTIs patients, however, experience persistent or recurrent infection and/or treatment failure. Conversely, complicated[2] UTIs pose a greater risk of such outcomes due to associated comorbidities or structural abnormalities within the urinary tract. Discriminating between uncomplicated and complicated UTIs is pivotal for tailoring appropriate management strategies and mitigating potential complications [33].

UTIs are some of the most common bacterial infections, with an infection toll of 150 million people each year worldwide [105]. UTIs are a significant cause of morbidity, particularly affecting females, older men and infant boys [33]. These infections can lead to several complications such as pyelonephritis (infection of the kidneys), potentially with sepsis, renal damage in young children, pre-term labour in pregnant women and problems that arise from frequent antimicrobial use (for example, antibiotic resistance). Patients who suffer from symptomatic UTI are normally treated with the use of antibiotics. Currently, the antibiotics most commonly used include Nitrofurantoin, Trimethoprim, Cotrimoxazole (a combination of Trimethoprim and

[1] infection limited to the lower urinary tract (bladder and urethra) in individuals with normal urinary tract and kidney function, and without underlying health conditions or predisposing factors

[2] infection affecting the urinary tract, often involving the upper urinary tract (kidneys) or occurring in individuals with underlying health conditions, structural abnormalities, or other predisposing factors.

Sulfamethoxazole), Fosfomycin or Nitrofurantoin. However, the rise we have seen in antibiotic resistance in addition to the highly recurrent profile of UTIs means health-care professionals may have to use alternative lines of treatment, which have greater risk of complications, such as of infection with *Clostridioides difficile*. Extended-spectrum beta-lactamase (ESBL)-producing Enterobacteriaceae are increasing and these bacteria are often multi-drug resistant. With limited treatment options and a lack of new antibiotics being developed, it is essential to focus on prevention of UTIs and gain more understanding of the cellular and molecular dynamics of how uropathogens adhere, colonise and adapt to the nutritionally lacking environment of the bladder; elude the immune system; persevere and spread through the urinary tract [50, 65, 106].

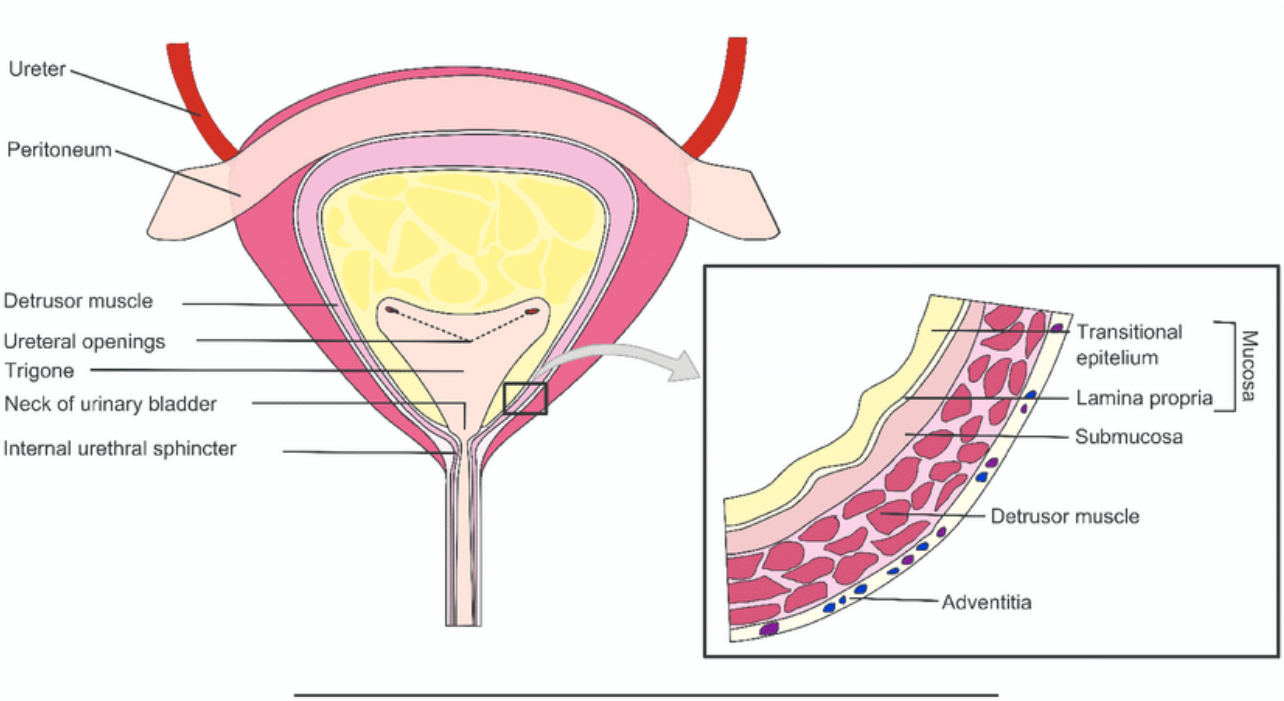

Figure 1.1: Schematic of the anatomical regions of the human urinary bladder (UB). [89]

UTIs are highly recurrent and may persist through different rounds of treatments. This recurrence is due to either relapse (symptomatic recurrent UTIs with the same organism following adequate therapy) or re-infection (recurrent UTIs with

previously isolated bacteria after treatment and with a negative intervening urine culture, or a recurrent UTI caused by a second bacterial isolate). In the majority of cases however, recurrent UTIs are thought to represent reinfection with the same organism. UTIs are caused by both Gram-negative[3] and Gram-positive[4] bacteria, and in some cases by specific fungi, but the majority are caused by the bacterial species Uropathogenic *Escherichia coli* (UPEC) [33]. Although the causes of recurrence are multifactorial - with at least a dozen mechanisms, some acting in tandem - one key factor could be the ability of UPEC to establish quiescent intracellular reservoirs (QIRs) which is a phenomenon exhibited by bacteria during urinary tract infections (UTIs) in the bladder. It involves the ability of certain bacteria to establish reservoirs within the cells lining the bladder epithelium. These reservoirs provide a protected environment where bacteria can evade the host immune response and antibiotic treatment. Thus, the establishment of these bacterial communities at deeper levels of the urothelium may allow them to evade immune cell interaction and other mechanisms, such as bacterial shedding—where bacteria are expelled from the bladder lining into the urinary tract. This shedding can play a dual role, serving as a host defense mechanism to eliminate bacterial invaders, but also potentially contributing to the spread and persistence of urinary tract infections by facilitating bacterial dissemination within the urinary tract or expulsion into the urine, leading to recurrent infections or systemic dissemination. Hence, The focus on intracellular bacteria, particularly those forming quiescent intracellular reservoirs (QIRs), is justified due to their unique ability to evade traditional immune responses and antibiotic treatments.

The bladder has a number of strategies to protect itself against microbial invaders. First and foremost, the urinary tract has anatomical barriers, alongside the flushing

[3]Bacteria with a thick peptidoglycan layer in their cell wall that retains the crystal violet dye in the Gram staining process, appearing purple or blue under the microscope.

[4]Bacteria with a thinner peptidoglycan layer in their cell wall that does not retain the crystal violet dye, appearing red or pink when counterstained with safranin in the Gram staining process.

action of urination, which usually suffice to prevent pathogenic elements from entering the tract and establishing a persistent infection. The presence of virulence factors in some bacteria, however, can help them to bypass these barriers and successfully establish infection. Virulence factors are any set of characteristics that will help bacteria in eluding the primary line of defence, and hence increase the risk of successful infection [33]. A crucial step during the infection process of a number of species of UTI pathogens, including the most common uropathogen, *Escherichia coli* (responsible for approximately 80% of UTIs), is the ability to permeate and invade the bladder epithelial barrier and seek refuge within the bladder epithelial cells (BECs). This is normally done by hijacking the capacity of the epithelial cells to regulate bladder volume [2]. Another important thing to note is, due to the presence of toxic compounds in urine, the bladder must maintain a tight epithelial barrier. Thus any immune reaction has to carefully balance the response to microbial challenge with the need to maintain the structural integrity of the epithelial barrier [52]. This will sometimes lead to premature termination of the anti-inflammatory response, resulting in chronic or recurrent infections due to residual bacteria. The innate immune response refers to the non-specific defence mechanisms that are deployed by the immune system usually hours after a pathogen is established. This is particularly important in bladder infections, as the role of the adaptive immune system in UTIs is less straightforward, and is still being studied [69]. The innate immune system is composed of various recruited and resident cells that express a wide range of pattern recognition receptors (PRRs). These receptors allow for early recognition of the pathogen which will be translated to induce a quick and robust pro-inflammatory response [101]. As noted earlier, although these immune responses are important, they have to be controlled to avoid any substantial damage to the epithelial barrier. As a last line of defence, the bladder sheds cells from its internal walls to reduce bacterial load. These host shedding mechanisms are modulated, however, to avoid adverse effects that can result if these processes occur

too frequently [108, 64].

Patients who suffer from symptomatic UTIs are normally treated with the use of antibiotics; this can, in some cases, cause the alteration of the micro-biota of the vagina and gastro-intestinal tract and also play a key role in the development of multi-drug resistant organisms [65]. Hence, while the 'Golden Era' of antibiotics is abaning, the need for carefully designed and individualised treatment increases with it. In addition to the rise in antibiotic resistance, there are other considerations such as patient allergies, drug interactions, and the presence of underlying health conditions that can impact the effectiveness of treatment. As a result, healthcare professionals must take a holistic approach to UTI management, considering factors such as patient history, symptoms, and laboratory results when making treatment decisions [106].

During this thesis we will focus on bladder infections, with potential future work looking at when these infections progress to the rest of the urinary tract.

1.2 Host-Pathogen Interactions

1.2.1 Introduction

As a primary line of protection against microbial infection and colonization of the urinary tract, the immune system presents various soluble compounds that are secreted into urine, and anatomical barriers [2] which in the majority of cases suffice to prevent pathogenic elements entering the tract and establishing a persistent infection. Examples of the physical and chemical barriers include but are not limited to:

- Layer of hydrated mucus.
- Glycoprotein plaque urooplakins (cell membrane proteins that form urothelial plaques on the surface of each urothelial cell).
- Epithelial cell lining.
- Resident immune cells.

Nevertheless, one may wonder, how do infections withstand and bypass these barriers in order to establish infections and eventually colonize growing parts of the urinary tract? This can be explained by the presence of virulence factors that pathogens can possess.

1.2.2 Virulence Factors

Virulence factors are any set of characteristics that will help a certain bacterium in eluding the primary line of defense, and hence increase the risk of successful infection. In the case of urinary tract infections, these virulence factors may present in a variety of ways, as outlined in [59]. These include:

- The presence of fimbriae[5] which assists in the adherence of the bacteria to specific receptors on the urothelium.
- Possessing a flagella[6] will help the pathogen swim along the urinary tract, even in the instances where it needs to swim upwards.
- In some cases, pathogens will secrete toxins that will compromise the structural integrity of the epithelial barrier allowing for iron chelation, which is an important step for uropathogenic growth.
- The expression of cell surface capsules which will protect the uropathogen against bactericidal actions of complement and phagocitic cells which are specialized immune cells capable of engulfing and digesting foreign particles, such as bacteria, viruses, and cellular debris.

A crucial step during the infection process is the ability of the pathogen to permeate and invade the bladder epithelial barrier and seek refuge in the BECs. This is normally done by hijacking the capacity of the cells to regulate bladder volume [101]. Under normal physiological conditions, BECs meticulously regulate bladder volume through intricate signaling pathways, orchestrating coordinated responses to accommodate urine storage and facilitate voiding. These cellular processes involve the dynamic modulation of ion channels, transporters, and receptors, finely tuned to balance bladder distension and contraction. However, uropathogenic bacteria have evolved mechanisms to subvert these cellular dynamics, exploiting vulnerabilities within the host's regulatory machinery to facilitate their survival and proliferation. For instance, certain bacterial species possess virulence factors that disrupt key signaling pathways involved in bladder volume regulation. By perturbing the delicate

[5] short, hair-like appendages found on the surface of bacteria. They play a crucial role in bacterial adhesion to surfaces, including host cells and environmental substrates.

[6] whip-like appendages protruding from the surface of certain bacteria. They function primarily in bacterial motility, allowing bacteria to move towards favorable environments or away from harmful ones.

balance of ion fluxes and cellular signaling cascades, pathogens can induce aberrant bladder contractions or impair relaxation mechanisms, leading to urinary retention and stasis. Incorporating these cellular responses into computational models enables us to simulate the complex interplay between bacterial virulence factors and host immune defenses, shedding light on the mechanisms driving UTI progression and guiding the development of targeted therapeutic interventions. Hence, within our model, we intricately incorporate these interactions by simulating bladder dynamics. This involves capturing the shedding of bladder epithelial cells (BECs) induced by bacterial invasion, which disrupts the integrity of the bladder epithelial barrier. Additionally, we integrate the dynamics of chemokines, key signaling molecules involved in immune responses, to model the host's inflammatory reaction to bacterial intrusion. Another important thing to note is, due to the function of the urinary tract of urine storage, and due to the presence of toxic and noxious compounds in urine, this has to be contained within a tight epithelial barrier. Thus any immune reaction has to carefully balance between the response to microbial challenge with the need to maintain the structural integrity of the epithelial barrier [52]. This will sometimes lead to premature termination of the anti-inflammatory response resulting in chronic or recurrent infections due to residual bacteria.

1.2.3 Innate Immune Response

The innate immune system refers to the non-specific defense mechanisms that will be deployed by the immune system usually hours after a pathogen is established. The reason we focus on this type of defense is because the adaptive immune system will mostly be inactive while the infection is concentrated in the bladder. In cases where the infection spreads to the kidneys, the immune system is known to produce antigen specific antibodies [86]. The innate immune system is composed of various recruited and resident cells that express a wide range of pattern recognition receptors (PRRs). These receptors allow for early recognition of the pathogen which will be translated to mount a quick and robust pro-inflammatory response [101]. As noted earlier, although these immune responses are important, they have to be controlled to avoid any substantial damage to the epithelial barrier. We now briefly review the main innate immune cells that operate in the urinary tract and focus on their unique antimicrobial activities.

1.2.3.1 Epithelial Cells

These cells, lining the interior of the urinary tract, will form the first line of defense against the infection. As such, an excessive amount of chemical compounds will be released, with the inclusion of pro-inflammatory cytokines and antibacterial agents. The first cytokines that will be detected after infection will be IL-1, IL-6 and IL8. This group of cytokines will be important for the recruitment of phagocytes into the infected bladder [23]. Although our initial model will focus on the bladder, it is important to mention a chemical compound called Uromodulin. This compound, produced by the epithelial cells lining the ascending limb of Henle's loop in kidney nephrons is known to protect the epithelial cells from infection by preventing interactions between them and pathogens, while at the same time, inducing pathogens to aggregate for an easier elimination through urine [2]. While many other immune-modulatory functions of Uromodulin are still being studied, it has been shown in

various experiments that a higher concentration than average of Uromodulin in urine is correlated with a lower risk of UTIs [38]. Additional chemicals secreted by epithelial cells will hinder bacterial growth by eliminating growth factors present in urine. Following bacterial infection of BECs, the pathogens are then encapsulated in RAB27b+ fusiform vesicles with exocytic properties, meaning, BECs will hence be able to expel intracellular bacteria back into the extracellular medium [28]. If any bacteria avoids expulsion, by escaping the RAB27b+ vacuoles, it is then met with a second wave of elimination in which such pathogens are recognised and captured by autophagy. After this second elimination attempt, autophagy will lead to degradation of the bacteria, making sure this will be eliminated through urine. Some studies have shown that in rare cases this degradation produced on the second wave can be mediated by block acidification [2]. If BECs become heavily infected, a preventive measure will be the shedding of the superficial epithelial cell layer through urine [32, 62]. This, however, will leave the underlying tissue exposed to urine toxins, potentially followed by severe consequences. As a prevention of these harmful effects, the shedding of BECs is immediately followed by a shift of the urothelium to a highly active and proliferative phase to restore the previous loss [76].

1.2.3.2 Neutrophils

Neutrophils are the first type of immune cells to be recruited to the bladder. Initially, they answer to CXC-chemokine ligand 1 (CXCL1) and other chemo-attractants produced by superficial epithelial cells, macrophages and mast cells [42].

In mouse experiments, neutrophils are detected in urine as early as 2 hours post-infection although their peak is approximately at 6 hours post-infection [97]. The number of neutrophils is proportional to that of the bacteria in the urinary tract. Neutrophils control the infection via numerous mechanisms. However, activated neutrophils are also responsible for substantial toxicity to the surrounding bladder

tissue [51].

1.2.3.3 Macrophages

A substantial population of macrophages reside in the submucosa of the urinary tract, and more cells are added to these sites following the infection. Once activated, macrophages produce important chemokines and cytokines that regulate the activity of these and other immune cells in the vicinity, hence, influencing the timing and the intensity of inflammatory responses during UTIs [2]. Communication between bladder macrophages leads to mobilisation of neutrophils into the epithelium and their subsequent activation alongside neighbouring immune cells. These responses ensure efficient bacterial clearance while minimising unnecessary and damaging inflammation.

1.2.3.4 Mast Cells

Mast cells are also resident immune cells located underneath the uroepithelium next to blood vessels and lymphatic vessels that traverse the mucosal region while also being found in high numbers in the detrusor muscle region. These type of cells have a pivotal sentinel and key immunomodulatory role during UTIs, which is partly due to their ability to release many pre-stored inflammatory mediators upon activation. These chemicals are kept within cytoplasmic granules and gradually release the chemical mediators after being released extracellularly [102, 107, 58]. Although it is currently unknown what causes the activation of bladder mast cells when the epithelium is still intact, it is believed that chemicals released from stressed epithelial cells such as ATP, LL-37 and IL-33 could contribute to this process. The number of mast cells in the bladder increases during bladder infections, which points to an important dynamic role for these cells in the fight against the infection. Although mast cells are considered pro-inflammatory immune cells, experiments in mice show that once the infection progresses, such cells adopt anti-inflammatory responses (by

releasing cytokines, IL-10) [17]. This switch in function seems to happen in parallel with the breaking down of the epithelial barrier and could facilitate the regeneration of the epithelium.

Due to the high recurrence rates associated with UTIs, a better understanding of the interactions between the immune cells responsible for clearing the infection is needed. This allows for clinicians to make better informed and more individualised decisions when considering therapy options.

1.3 Review of Antibiotic Protocols

The standard treatment for bladder infections caused by bacteria is a course of antibiotics. The choice of antibiotic depends on the type of bacteria causing the infection, the severity of the infection, and the patient's medical history. For most infections, antibiotics are prescribed for a period of three to seven days, although the duration of treatment may vary depending on the specific antibiotic and the severity of the infection.

Trimethoprim is the most commonly prescribed antibiotic for the treatment of bladder infections. Trimethoprim kills bacteria by stopping them from producing a substance called folic acid, which many species of bacteria, such as *E. Coli* need to survive, hence why this antibiotic is effective against many of the bacteria that cause bladder infection.

The prescription protocols for treatment of bladder infections with the use of Trimethoprim vary largely depending on the severity of infection, patients' medical history and the motive for use. Trimethoprim can be used to treat and to prevent bladder infections and UTIs. It is often prescribed as a prevention tool for bladder infections in patients who present a past profile showing recurrence or other factors making them more susceptible to infection. The current treatment protocols for the use of Trimethoprim, as stated by the NHS (National UK Health Service) can be summarised as follows:

- When taking Trimethoprim to treat an established infection the prescribed dose is 200 mg twice a day. This dose can later be adjusted by the physician to better suit the patients needs. The duration of this course of treatment is usually $3 - 7$ days depending on the severity of the infection and patient profile.
- When taking Trimethoprim to prevent infections, the prescribed dose is 100 mg once a day. This course of treatment is often reserved for patients with

increased risk of infection, hence, the duration of treatment is usually extended and undefined, depending on the progression of the infection.

The exact length of time for the treatment depends on how severe the infection is, the age, gender and underlying health problems that the patients may have. Usually, women with uncomplicated UTIs take a 3 day course of treatment, while men and pregnant women take a longer course of treatment of 7 days. Patients presenting with complicated and severe profiles, or a catheter, will usually follow a 2 week treatment course. When Trimethoprim is taken to prevent bladder infections the length of treatment is extended, with the patient following a treatment protocol of up to 6 months.

Although patients who take Trimethoprim are unlikely to get side effects, some report a mild itching or skin rash which is usually resolves after discontinuing the treatment. A more complete list of the known side effects that take place in more than 1 in 100 people is as follows:

- Itching or mild rash
- Feeling or being sick (nausea or vomiting)
- Diarrhoea
- Headaches

Other serious side effects that happen in less than 1 in 1000 people may include long lasting, severe stomach cramps and bruising or bleeding with an unidentified source or generally any issues indicating problems with the patients blood circulation.

1.4 Mathematical models

1.4.1 Introduction

The main goal of my research is to develop a mathematical model to study bladder infections. Specifically, an Agent Based Model (ABM), otherwise known as, an individual-based model. The core idea behind ABMs, is that many, if not all, of the worlds phenomena can be successfully modelled with the use of 'agents' and an 'environment', along with a description of agent-agent and agent-environment interactions [113]. According to Wilensky et al., an agent is an 'autonomous individual or object with particular properties, actions, and possibly goals'. The environment on the other hand, is the landscape on which said agents interact. These interactions between agents and between some agents and their environment can be quite complex, not only can these interactions change with time but so can the strategies used to decide what action will be employed at any particular time. These actions are generally constituted by the exchange of information which as a result, agents can either update their internal state or take other actions [113]. One might question why this approach to modelling is chosen over other approaches and techniques and what makes agent based modelling different to other approaches. Agent based modelling as opposed to the vast majority of other modelling techniques allows for heterogeneity in population and environment, while other models, such as continuous approaches typically, do not [114, 109].

Another difference is the nature of the model results, often the interaction results in the real world are discrete and not continuous, making discrete models perhaps a better fit. This can be seen by considering the population dynamics and modelling issues that would arise from using equation based modelling (EBMs). Evidently, the population variable is a discrete one, however, when using EBMs we consider it to be continuous and this mismatch between the continuous nature of EBMs and the discrete nature of real population causes what is known as the nano-wolf problem [100]. The nano-wolf problem arises from the mismatch between the discrete nature

of real-world phenomena and the continuous framework of equation-based models (EBMs), particularly in modeling population dynamics. This discrepancy can lead to errors in analysis, especially when considering very small numbers of cells, such as in limiting conditions. Therefore, careful consideration of modeling approaches is essential to ensure accurate insights into population dynamics.

Another advantage of ABMs worth noting is that no knowledge of the aggregate phenomena is required. While modelling with EBMs you certainly need a good understanding of the aggregate behaviour and then test your hypothesis against the aggregate result of the model [113]. Finally, the results generated by ABMs are always more detailed than those generated by EBMs [113]. This is the case because in ABMs you can analyze the life trajectory of a single agent along with the aggregate behaviour of the system as well, as opposed to EBMs, where only the aggregate results are achieved.

It is however necessary to also look at the challenges associated with ABMs such as difficulty of analysis and use due to the lack of mathematical tools that are normally available. Much of the recent progress in the life sciences field, especially in biology and the health-care sectors, is in great part due to the technological advances in hardware and software which has freed studies from the technical constraints placed on mathematical models and their analysis. However, even with the recent developments in computational power many of the mathematical models based on simulations, such as ABMs, still reach their computational limits quickly [3]. Hence, instead of disregarding such type of models, we should divert our focus to the use of mathematical tools such as optimal control and optimization in parallel with ABMs. The goal would be to develop mathematical approximations of ABMs, in particular for optimization and control purposes, to overcome the computational limitations placed on such models. This is achieved by following the outlined steps [4]:

- Firstly, ABMs should be considered as "Middle-ware"[7] investigatory objects: The complexity, behind biological systems especially, is currently out of reach for traditional formal mathematical analysis. This complexity mainly arises from the multi-scale nature of interactions, particularly at the cellular level, which are less easily captured in a continuum model. Agent-based models (ABMs) provide a suitable approach to address this multi-scale complexity, allowing for the simulation of spatial heterogeneity and intricate agent-agent interactions that are characteristic of real-world systems. As such, ABMs serve as sufficiently complex proxies for real-world systems, enabling researchers to explore emergent behaviors and phenomena that may not be readily captured by traditional analytical methods.

- Secondly, the nature of ABMs as simulation models, increases the range of experimental conditions that we are able to apply versus real world physical proxy models.

- Due to the computational power limitations placed on brute-force simulations, we need to consider identifying methodological bridges between ABMs and formally tractable SLMs (System Level Models)[8].

- This new hybrid model will hence be a sufficiently complex proxy system, and hence, all information and knowledge obtained by examination of such model may provide insight into how to effectively control the real-word system.

[7] In a conceptual sense, "middle-ware" refers to a layer of software or technology that acts as an intermediary or bridge between different components or systems. In the context of agent-based models (ABMs) as "Middle-ware" investigatory objects, it signifies that ABMs serve as an intermediate tool that facilitates investigation and analysis of complex phenomena, particularly within biological systems.

[8] SLMs are simplified representations of complex systems that capture overall system behavior and interactions without focusing on individual-level details.

1.5 Agent-based models in Computational Biology

In biology, ABMs are used to study a wide range of phenomena, from the behavior of individual cells and organisms to the dynamics of populations and ecosystems. ABMs offer a powerful tool for exploring the emergent properties of biological systems, such as evolution, self-organisation and adaptation[12, 13].

One of the key advantages of ABMs is their ability to capture the heterogeneity and complexity of biological systems, as we will see in Chapter 2. Agents in ABMs can be programmed to have a variety of attributes and behaviors, allowing for a more realistic representation of biological systems than traditional modelling approaches that rely on simplified assumptions. Additionally, ABMs can incorporate stochasticity and multi-scale ability, which are often important factors in biological systems, especially when dealing with bacterial infections.

ABMs have been applied to a variety of biological questions, such as understanding the dynamics of infectious diseases, exploring the emergence of patterns in biological systems. For example, ABMs have been used to simulate the within-host spread of diseases, such as TB to study relapse, COVID-19, and to explore the effectiveness of different intervention strategies [14, 91, 68, 6].

Despite the many advantages of ABMs, they also present several challenges. Developing an ABM requires significant computational resources and programming skills, as well as careful validation and testing to ensure that the model is a faithful representation of the biological system being studied. Additionally, ABMs are often highly specific to the system being studied, which can limit their generalizability and make it difficult to compare results across different studies.

As mentioned in the previous section, ABMs have been used to study the properties of many biological systems. In this section, we will look at some of the most relevant studies and available models.

In our work we adapt an established hybrid ABM to focus on bladder infections. This

established model [14] uses a hybrid agent-based approach to study the effects of bacterial cell state and spatial location on tuberculosis (TB) treatment. Tuberculosis (TB) is an infectious disease caused by the bacterium *Mycobacterium tuberculosis*. It primarily affects the lungs but can also affect other parts of the body. As well as modelling discrete bacterial and immune agents, this model incorporates important attributes of the progression of TB such as oxygen dynamics, caseation and antibiotic treatments. Through this model, it is shown that the spatial location of the bacteria with regards to the source of the drugs alters the outcome of simulations and how the bacterial state affects the infection outcome. All of this is done through analysing multiple simulations of the ABM model which represent different varying initial parameters of the infection. This allows for a deeper insight into the infection development and gives the researcher the opportunity to analyse a greater range of data about the infection progression and its attributes.

ABMs have also been recently used to study the SARS-CoV-2 virus. Due to the complexity of the SARS-CoV-2 progression profiles, traditional mathematical models may not fully capture the various factors that influence the progression and establishment of the virus. Hence, agent-based models such as [91, 40] can aid us in better understanding the within host spread of the disease. In contrast to the traditional mode of experimental study of host-pathogen dynamics which usually involves numerous stages of data collection and processing, these types of mathematical and computational models are able to complement the available data and provide a different perspective.

In addition to the highlighted models, many more have been used in the medical field to study the within-host progression of diseases. ABM models have been used to simulate the progression of viral diseases within the human body such as HIV[9] and influenza [81, 6]. These models take into account factors such as the dynamics of the immune system, the replication of the virus, and the effects of antiretroviral

[9] human immunodeficiency virus

therapy to predict the course of the infection and the response to treatment.

Away from the field of infections disease research, other diseases such as cancer have been extensively modelled using agent-based techniques [83, 68]. These models take into account factors such as the growth and spread of cancer cells, the interactions between cancer cells and the immune system, and the effects of treatment to predict the course of the disease and the response to therapy.

1.5.1 Existing models investigating bladder infections and UTIs

1.5.1.1 *In vitro* experiments

Many *in vitro*, animal and mathematical models have been used to investigate UTIs and bladder infections. *in-vitro* models can provide valuable information about the mechanisms of bacterial infection and the effectiveness of treatment. A common *in-vitro* model for studying bladder infections is to use cultured bladder cells by exposing them to bacterial pathogens that cause UTIs such as *E. Coli*. Researchers then investigate how the bacteria interacts with the bladder cells, including how they adhere to the bladder cells and invade them causing damage. This type of experiment is also used to test the effectiveness of different antibiotics or other treatments for bladder infections. These studies have shown that uropathogenic bacteria, such as *E. Coli*, can attach to bladder cells and invade them. This process is facilitated by bacterial adhesins that interact with specific receptors on the surface of bladder cells. [88, 29]

in vitro models are also used to study the host immune response to bladder infections [31, 5]. Researchers use immune cells isolated from the bladder like macrophages and neutrophils, and study how such cells respond to bacterial infection. This can help researchers understand how the immune system recognises and responds to UTIs, which can inform the development of new treatments. These studies have shown that bladder cells and immune cells, such as macrophages and neutrophils, can recognise and respond to uropathogenic bacteria. The immune response involves the activation of various signaling pathways and the release of cytokines and chemokines.

Overall *in vitro* models and experiments provide valuable insights into the mechanisms of bladder infections and help researchers identify new targets for treatment. However, it is important to note that *in vitro* models have limitations and may not fully capture the complexity of bacterial infections in living organisms. Thus, it is essential to also conduct experiments using other types of models and clinical studies

to confirm the findings obtained from *in vitro* models. Computational models can also be used to complement biological and clinical studies. They provide a way of testing multiple scenarios quickly, and with minimal cost and ethical implications. As seen in Chapter 4, we also use *in vitro* experiments in order to complement and better parameterise our model. The experiments carried out will allow us to better estimate the replication speed of *E. Coli* and the effects of treatment, more specifically Trimethoprim.

1.5.1.2 Animal models

Animal models have been widely used in research to study bladder infections. In these models, animals are infected with bacteria, and the response of the bladder to infection is observed. This approach allows researchers to better understand the mechanisms behind bladder infections and to test new treatments. Mice are commonly used as an animal model for studying bladder infections. The murine bladder shares many similarities with the human bladder, making it a useful model for studying host-pathogen interactions during infection. Murine models have revealed important insights into the host immune response to bladder infections. For example, such models have shown that the immune response involves the recruitment of neutrophils and macrophages to the bladder, the activation of inflammatory pathways, and the production of cytokines and chemokines [48, 92]. In addition to this, murine models have been used to test the efficacy of antibiotics for treating bladder infections and have shown that the choice of antibiotic, dose, and duration of treatment is key to the outcome of the infection.

Animal models can provide important insights into the pathogenesis of bladder infections and can help guide the development of new therapies and prevention strategies. However, it is important to note that animal models have limitations and may not always accurately reflect the complexity of human disease.

1.5.1.3 Mathematical and Computational models

Although mathematical and computational models have long been used to study biological systems and diseases such as cancer, TB and HIV [81, 14], we are not able to find any models within the literature describing the full urinary tract during an infection process. The complexity of the system, the organs and tissues it spans, may be a reason for this.

At present, there is a lack of mathematically predictive models that can accurately describe the behavior of the lower urinary tract. Consequently, the only viable approach to enhance our understanding of the lower urinary tract behavior and develop new treatments is through time-consuming *in vivo* experiments. Given that a staggering 60% of adults experience at least one lower urinary tract by the age of 40 [33], a mathematical model of the lower urinary tract would greatly enhance our capacity to investigate and devise effective treatments for this significant and growing public health concern.

The currently available models describe compartments of the urinary tract focusing on specific processes related to urinary tract infections [19, 24, 39]. These models can usually be divided into ODE models that describe the time rate of change in certain physiological values, and spatio-temporal models which do take into account spatial variation at the cost of computational complexity.

- The bladder: The modeling of the bladder encompasses two interrelated themes: the dynamics of fluid flow in and out of the bladder, and the biomechanical behavior of the bladder walls during the filling and emptying processes. The most common method for fluid dynamic modelling is through ODEs describing the bladder volume changes over time. On the other hand, The study of the visco-elastic properties of the bladder walls falls under the category of bladder biomechanics. As the bladder expands during the filling process, it creates tension in its walls. The conventional approach to model

this phenomenon is by using the linear solid model (SLS), which utilizes a combination of springs and dashpots. Various SLS models have been developed, and some include an active element that mimics detrusor contraction, to better capture the bladder's behavior. The bladder is usually simplified in such models as a spherical shell of a specified thickness, radius and volume. This assumption is further examined through spatio-temporal models using nano-spherical geometries to describe the bladder and assesing the correction of such simplifaction in regards to the low-state volumes not considered by the spherical geometry assumption. Some models, also avoid the geomterical simplification of the bladder by incorporating voiding based on the Navier-Stokes equation. Such models are able to detect areas of the bladder of slow flow, making these areas a cause of concern during the process of urine evacuation [19, 39].

- The urethra: models of the urethra typically look at the fluid flow through a rigid tube. The urethra also possesses a varied shape and structure along its length, which implies that incorporating position information via a spatio-temporal models could yield a more comprehensive examination of fluid flow. In reality the urethra has a complex geometry and interacts differently with both the internal and external urethral sphincters in three dimensions (3-D) along its length. To explore more complex urethral flow regimes, researchers have developed 2-D and 3-D models, which provide analytical and numerical results [24].

Hence, through developing an agent-based model of a section of the bladder we will be able to investigate bladder infections through a unique new lens, looking at cellular level interactions, spatio-temporal effects of the environment, and how cellular level interactions develop leading to either the establishment or clearance of infection. With the continuous validation of our work against the available data

we are able to produce a novel approach to investigating bladder infections.

1.6 Summary

As we've seen thus far, UTIs are proving to be a growing concern in the medical community, both for the high recurrence rates and the rising antimicrobial resistance. 30% of women who have had a UTI will experience a recurrence within six months. Furthermore, about 80% of women who have had at least one UTI will have a recurrence at some point in their lives. Recurrence rates tend to be higher in women who have a history of recurrent UTIs, those who have certain anatomical abnormalities, and those who have underlying medical conditions that impair immune function or urinary tract function. We have reviewed the available literature on *E. Coli*, which is the causing agent in 80% of UTIs, the virulence factors that help bacteria establish infection and the innate immune response to such an infection. A response in which the role of cells like Neutrophils, Macrophages and Mast cells is essential to early bacterial detection and clearance. We also investigated the use of agent-based modelling, and how these computational techniques can be useful in modelling infections and other diseases, allowing researchers and clinicians to gain a better insight. However, UTIs and bladder infections are investigated through other models also. Murine models have been extensively used due to the similarities in the bladder structure. Lastly, *in vitro* experiments are also of great importance to the advancements made in the understanding of UTIs over recent years.

However, the issue of recurrence in UTIs persists.

1.7 Goal of this thesis

We aim to utilise the introduced techniques of agent-based modelling to investigate bladder infections, in doing so, adding a new perspective in tackling this type of infection that allows for individualised treatment based on the patient profile. First however, our model must be correctly parameterised and must also be validated by the current vast sea of literature on bladder infections. The next chapter will outline the design and implementation of the ABM, which we name *UTImodel*, including the model assumptions, input parameters, and simulation algorithms. We will also present the results of the model validation and sensitivity analysis, which will demonstrate the model's ability to reproduce key features of UTI pathogenesis and generate insights into the underlying mechanisms of infection.

In Chapter 3 we will investigate the effects of initial bacterial load, I_B on the progression and outcome of the infection. In doing so, we are able to investigate also the individual arising profiles along with the aggregate infection outcome. We also use our model to simulate an immuno-compromised environment. In Chapter 4 we conduct laboratory experiments that will allow us to validate the replication profile of *E. Coli* in addition to conducting experiments to determine the antibiotic susceptibility profile of *E. Coli* under the effects of Trimethoprim. This allows us to parameterise our treatment model which is later introduced in Chapter 5. Through the analysis of this incorporated treatment model we simulate a full treatment course for uncomplicated bladder infections and we verify the results from our experiments in Chapter 4. Having done so, we will have a model capable of simulating bladder infections with an incorporated treatment framework that will allow us to investigate optimal treatment strategies and even tailoring the treatment to the patient.

Chapter 2

AN AGENT-BASED MODEL TO DESCRIBE BLADDER INFECTIONS

2.1 Introduction

We have developed a simple agent-based mathematical model, *UTImodel* [67], to simulate an infection in a section of the bladder. agent-based models simulate individual elements or 'agents' on a computational grid. The grid describes the environment, here the bladder, and the model includes rules to describe agent-agent and agent-environment interactions. These interactions between agents and between some agents and their environment can be quite complex; not only can these interactions change with time but so can the strategies used to decide what action will be employed at any particular time. These actions are generally constituted by the exchange of information which as a result, agents can either update their internal state or take other actions [113]. Agent-based modeling (ABM) distinguishes itself from conventional modeling approaches by its unique multi-scale ability, allowing for the representation of diverse characteristics across populations and environments [109, 114]. Unlike traditional modeling techniques that often rely on aggregated representations or uniform assumptions, ABM embraces the intricacies of individual agents and their surrounding context at multiple scales. This flexibility enables the simulation of complex systems where agents exhibit varied attributes, behaviors, and interactions, reflecting the richness and heterogeneity of real-world dynamics. Also, interaction results in the real world are discrete and not continuous, making discrete models arguably a better fit. Our model is a hybrid model; as well as discrete agents (bacteria and immune cells), it also contains a generic chemokine molecule that acts as a chemoattractant, directing the immune cells to the site of infection. This generic chemokine is modelled via a Partial Differential Equation (PDE).

2.2 Model Overview

For our model [67], we define five types of agents: bacteria, resident macrophages ($LY6C^-$), helper macrophages ($LY6C^+$), neutrophils and mast cells. We have chosen not to include BECs as agents within this version of the model, in order for computational simplicity. The interaction between such agents will be set by specific rules defined within our model. Functions for all these interactions are stored in separate classes in the code created for each specific agent.

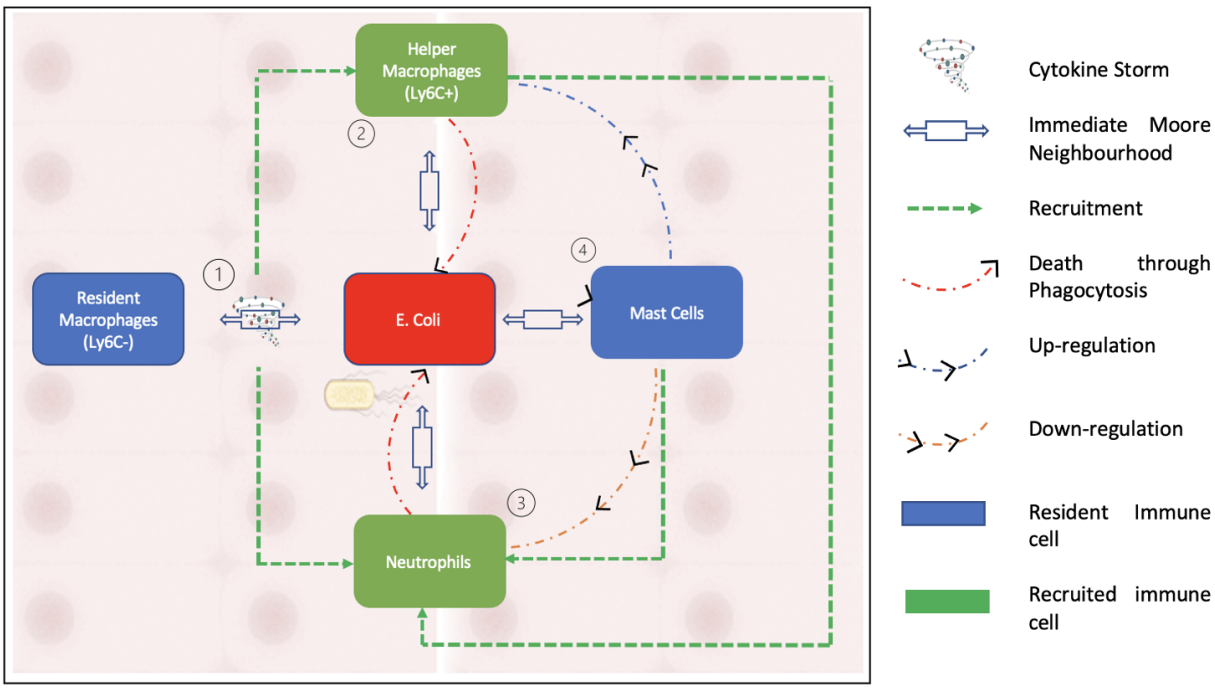

Figure 2.1: This figure illustrates the interactions between the agents that form our model. As can be seen in the schematic, neutrophils are recruited by resident macrophages and helper macrophages while being down regulated by mast cells. Bacterial clearance is possible through helper macrophages or neutrophils.

2.2.1 Model Environment

The spatial domain is formed by the innermost bladder layer, the urothelium, where the two-dimensional model domain is of size $L_g \times L_g$, where $L_g = 200$ for the simulations presented in this thesis. The size of each grid cell within our environment is constructed in order to contain the largest agent within the biological system to be

described, the macrophage. The diameter of a human macrophage is approximately 20 μm, hence each grid cell will be equivalent to a 400 μm^2 section of the bladder. We therefore model over a 16 mm^2 section of the superficial urothelium. Each grid cell will represent a location instance within our model, which can adopt the following states: empty, occupied by immune cell, bacteria or blood vessel. Although blood vessels do not appear on the urothelium in reality, we assume that these are the spatial locations of the blood vessels at deeper levels. Future iterations of the model will study a three-dimensional space where we can simulate the representation of the vasculature more realistically. On our 2-D spatial domain, we fix grid cells to be locations to represent cross-sections of 4 blood vessels, with locations [(175, 25), (25, 175), (175, 175), (25, 25)]. We place bacteria in the centre of the domain. See Figure 2.2 to see the spatial domain and initial cell distributions for our simulations.

2.2.2 Bacteria

In our model, we simulate Uropathogenic *E. Coli* (UPEC) bacteria. Initially, I_B bacteria are seeded at the centre of the grid. We place bacteria in the centre of the domain as our computational environment represents a section of a initially healthy bladder, which is then seeded with bacteria, in order to investigate bacterial growth without the infection approaching the computational boundary. This set-up is also optimal for using experimental results to verify model output, work shown in Chapter 4. Initial bacterial placement can easily be changed to either random allocation or to be located at the boundaries, which is intended to be studied in future work. The bacteria are able to replicate according to a growth rate of B_{sp}. See Table 2.1 for model parameter values, with corresponding references to the experimental data these are based on. Bacteria can be found in either a replicating or "resting" state, where bacteria are deemed to be resting when there is no space on the computational grid for them to replicate into. At each time point, the neighborhoods are checked

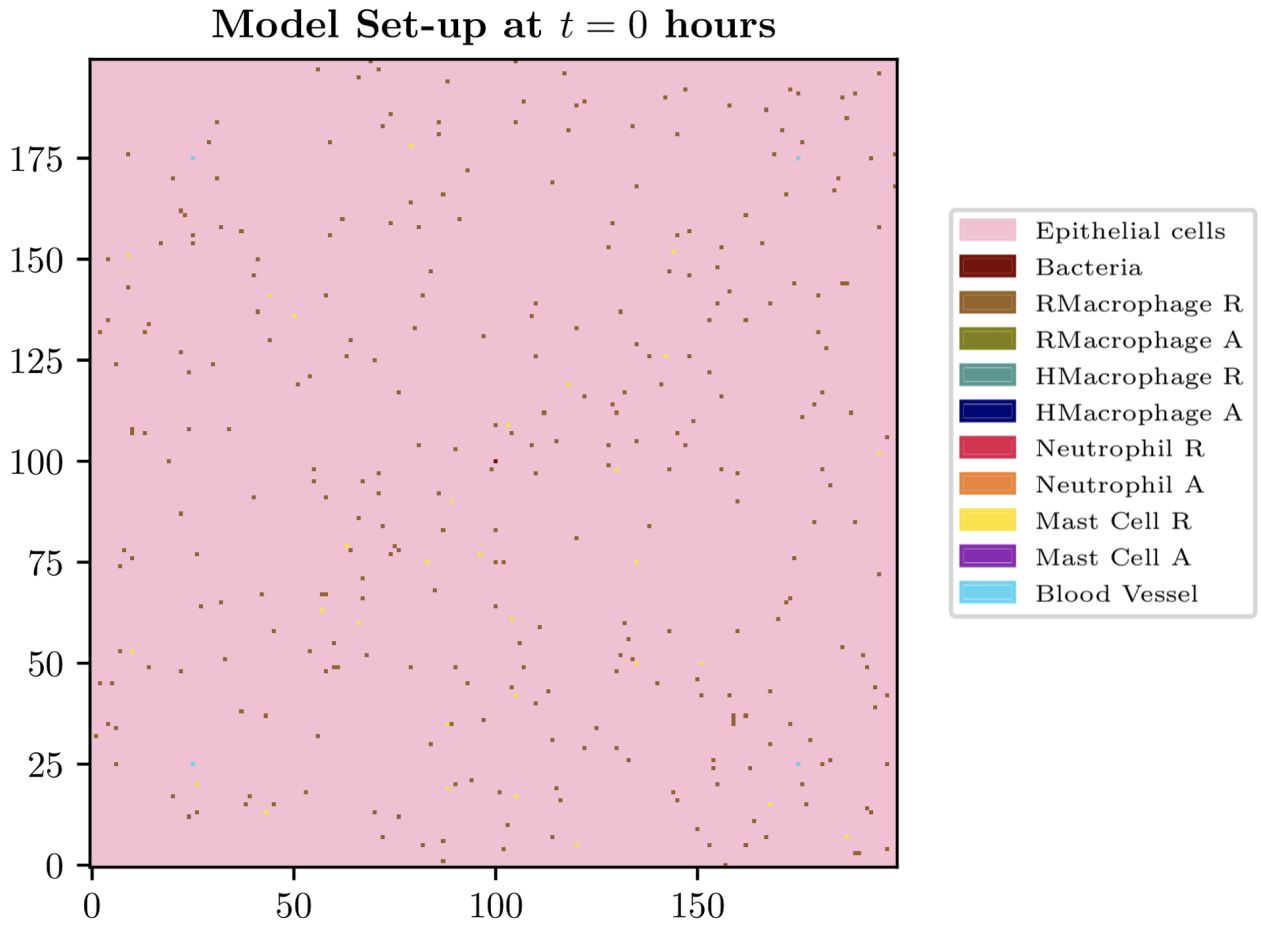

Figure 2.2: Spatial domain and example of initial cell distribution.

and when empty spaces in the proximity of the bacteria are available, the bacteria are able to switch back to a replicating state and spread across the domain. Bacterial replication within our model is assumed to have a neighborhood depth of $N_{db} = 2$. Hence, if bacteria are able to replicate, an empty location within the specified depth is chosen and populated with a new bacterium. If all locations are occupied, the replication state is switched temporarily to resting.

The neighborhood type alternates between Moore and von Neumann at each time step to accurately model bacterial cluster shapes. A Moore neighborhood includes the eight cells surrounding the cell of interest, resulting in square shapes, while a von Neumann neighborhood comprises the four adjacent grid cells (above, below, right,

and left), leading to diamond shapes. This alternating approach ensures a more precise representation of bacterial clusters, with Moore neighborhoods producing square shapes and von Neumann neighborhoods yielding diamond shapes. In future model developments, a 3-D version of this domain will be explored to simulate the environment more realistically, allowing for less restricted bacterial growth.

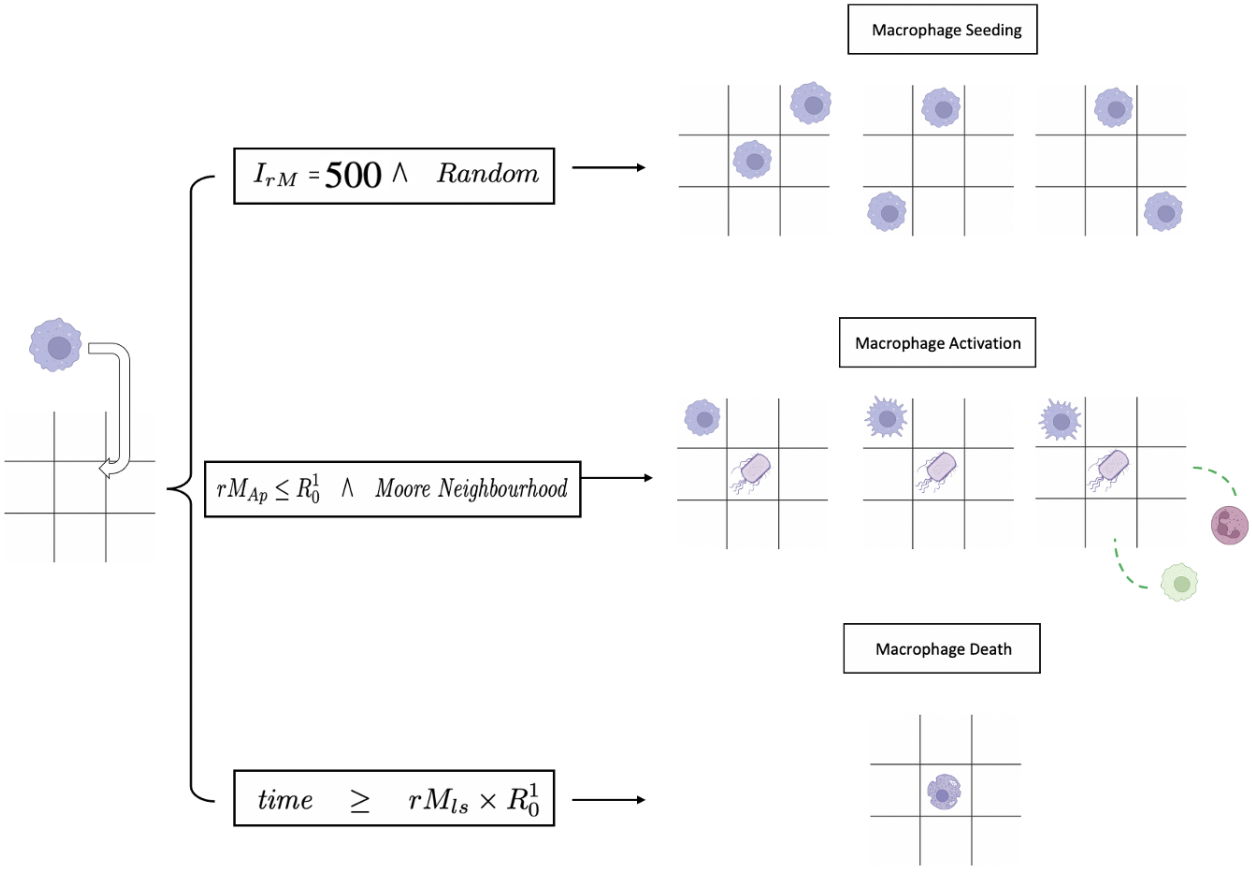

Figure 2.3: Schematic describing resident macrophage seeding, activation and death. R_0^1 is a randomly generated number using the uniform distribution on the interval $(0, 1]$.

2.2.3 Macrophages

Macrophages are represented as both resident and recruited discrete agents on the grid. Only one macrophage can occupy each grid cell and, independently of their nature (resident or recruited), and all macrophages have the following attributes: position, age and state (resting or activated). Such characteristics are updated at

every model time step. I_{rM} resident (initially resting) macrophages are seeded onto the grid at the start of the simulation. Macrophages are randomly assigned an age rM_{ls} or hM_{ls} for resident or helper macrophages, respectively. Once a macrophage reaches its assigned age, it is removed from the grid. If a resident macrophage is in the Moore neighbourhood (of order 2) of a bacterium, it is activated with probability rM_{Ap}. Once activated, $Ly6C^{+}$/helper macrophages are recruited into the domain with probability rM_{RhM}, and placed in the neighbourhood of the activated macrophage. As well as recruiting helper macrophages, activated macrophages also secrete a generic chemokine molecule, the dynamics of which are described in Section 2.2.4. Macrophages move along the gradient of this chemoattractant, directing the immune cells to the site of infection. When no chemokine is present in the spatial domain, the macrophages follow a random walk. The movement rates are described by rM_{RN} and hM_{RN} for resident and helper macrophages, respectively. $Ly6C^{+}$/helper macrophages are able to kill bacteria: once a bacterium is in the immediate neighbourhood (Moore neighbourhood of order 1) of an activated macrophage, this will kill said bacterium with probability hM_{phP}.

2.2.3.1 Neutrophils

Neutrophils are important in regulating the severity of the immune reaction. These are the first recruited immune cells to arrive at the site of infection and hence their role is crucial [99, 55, 71]. The lifespan of the neutrophils are set in the model as N_{ls}, see Table 2.1. The neutrophils move chemotactically in the same manner as all immune cells in the system, up the gradient of the chemoattractant, or as a random walk when no chemokine is present. They move at rate N_{RN}. Neutrophils can kill bacteria in their immediate neighbourhood with probability N_{phP}. Neutrophils are down-regulated by mast cells (see Section 2.2.3.2 for details).

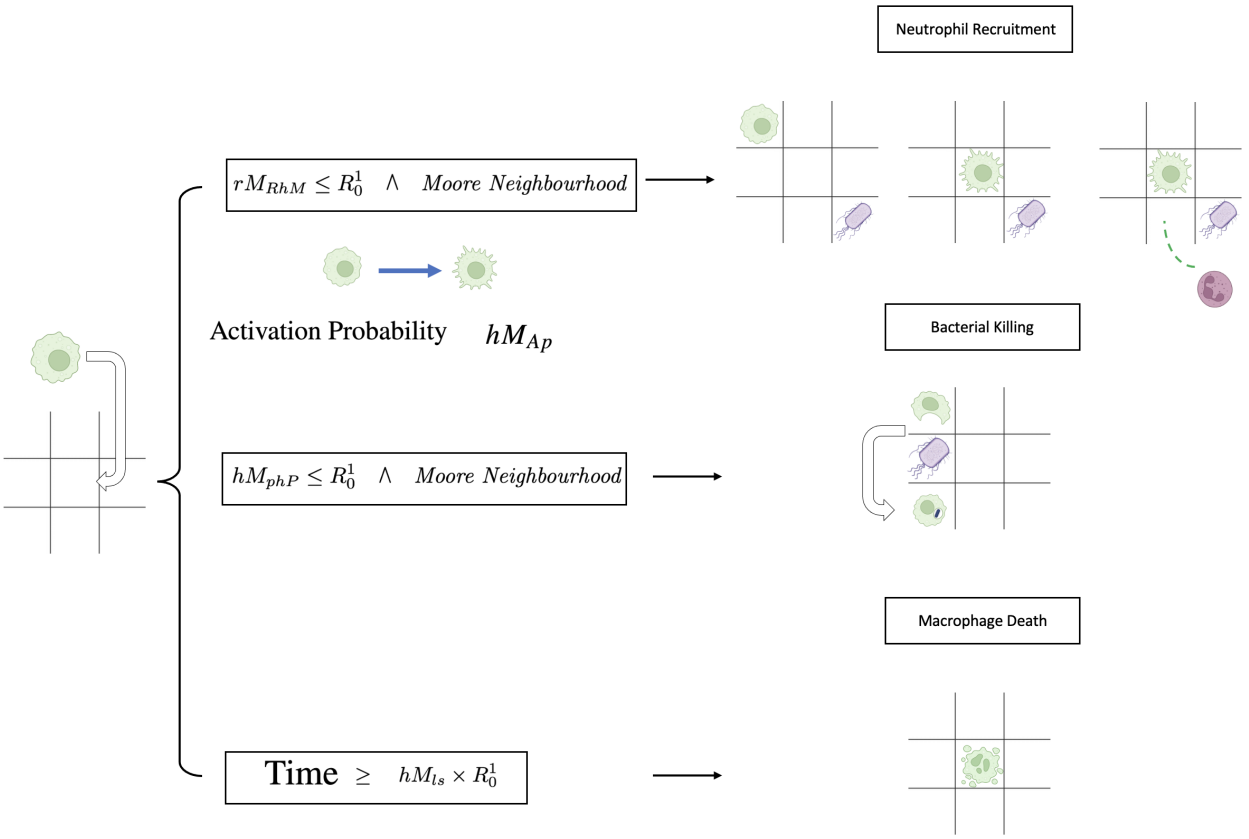

Figure 2.4: Schematic describing helper/recruited macrophage actions such as neutrophil recruitment, bacterial killing and death. R_0^1 is a randomly generated number using the uniform distribution on the interval $(0, 1]$.

2.2.3.2 Mast Cells

There are I_{MC} mast cells initially seeded on the grid. Their lifespan is set to MC_{ls}, they move at rate MC_{RN} and are recruited through the blood vessels with probability MC_{urM}. They are activated with probability MC_{Ap}. Mast cells are responsible for up-regulating helper macrophages, aiding with the clearance of bacterial infection. When there is a bacterium in the immediate neighbourhood (Moore neighbourhood of order 1) of a mast cell and no helper macrophages are present within this same neighbourhood, the mast cell recruits a helper macrophage to a random location within this neighbourhood.

Mast cells are also known to down-regulate the recruitment of neutrophils [110, 16]

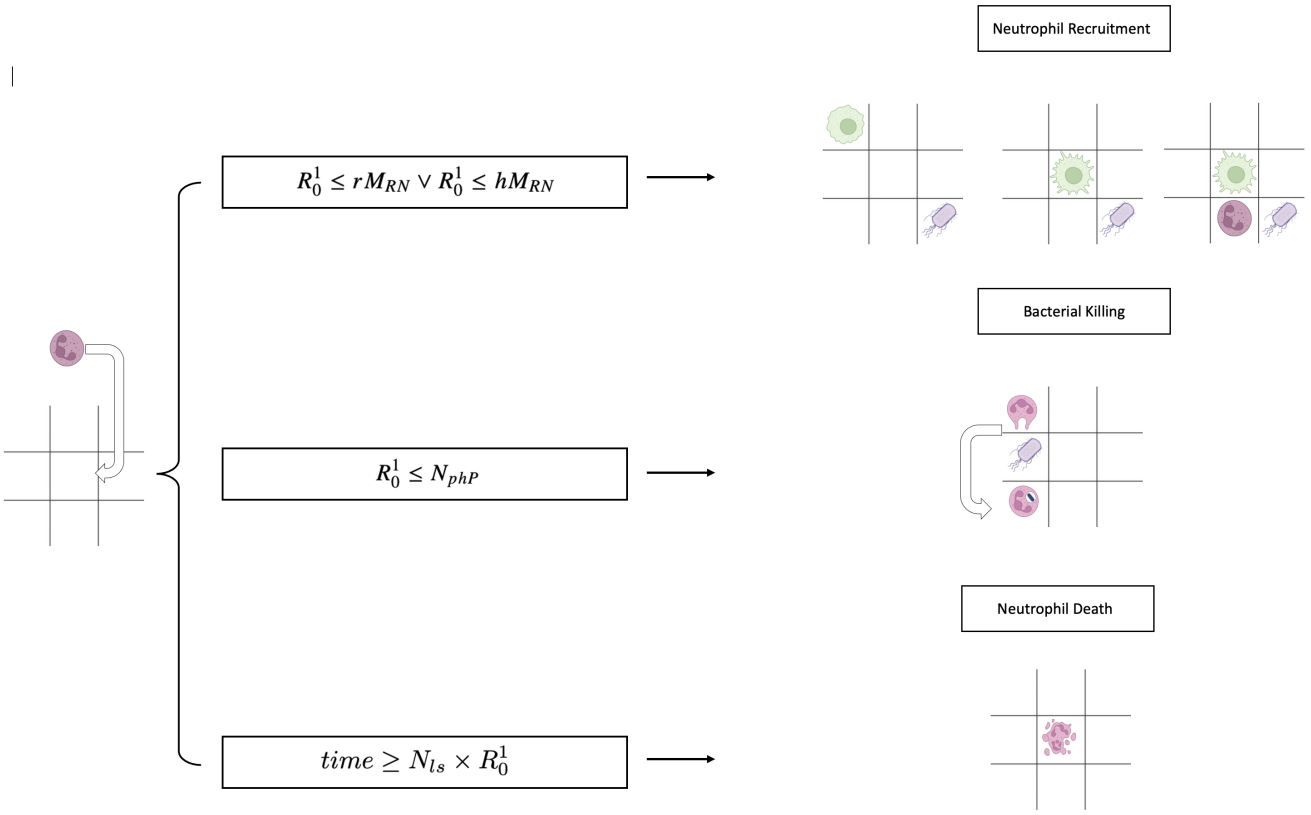

Figure 2.5: Schematic describing the actions of neutrophils such as recruitment, bacterial killing and neutrophil death. R_0^1 is a randomly generated number using the uniform distribution on the interval $(0, 1]$.

in order to limit excessive damage to the epithelial tissue [60]. When a mast cell is in an immediate neighbourhood of three or more neutrophils, it removes one (at random) from the grid.

2.2.3.3 Summary of rules

Summarising the rules for bacteria within our model we have:

- I_b represents the initial number of bacteria which is randomly seeded into the environment.
- Bacterial growth rate is B_{sp} while replication is set to a specific neighbourhood depth of $N_{db} = 2$.

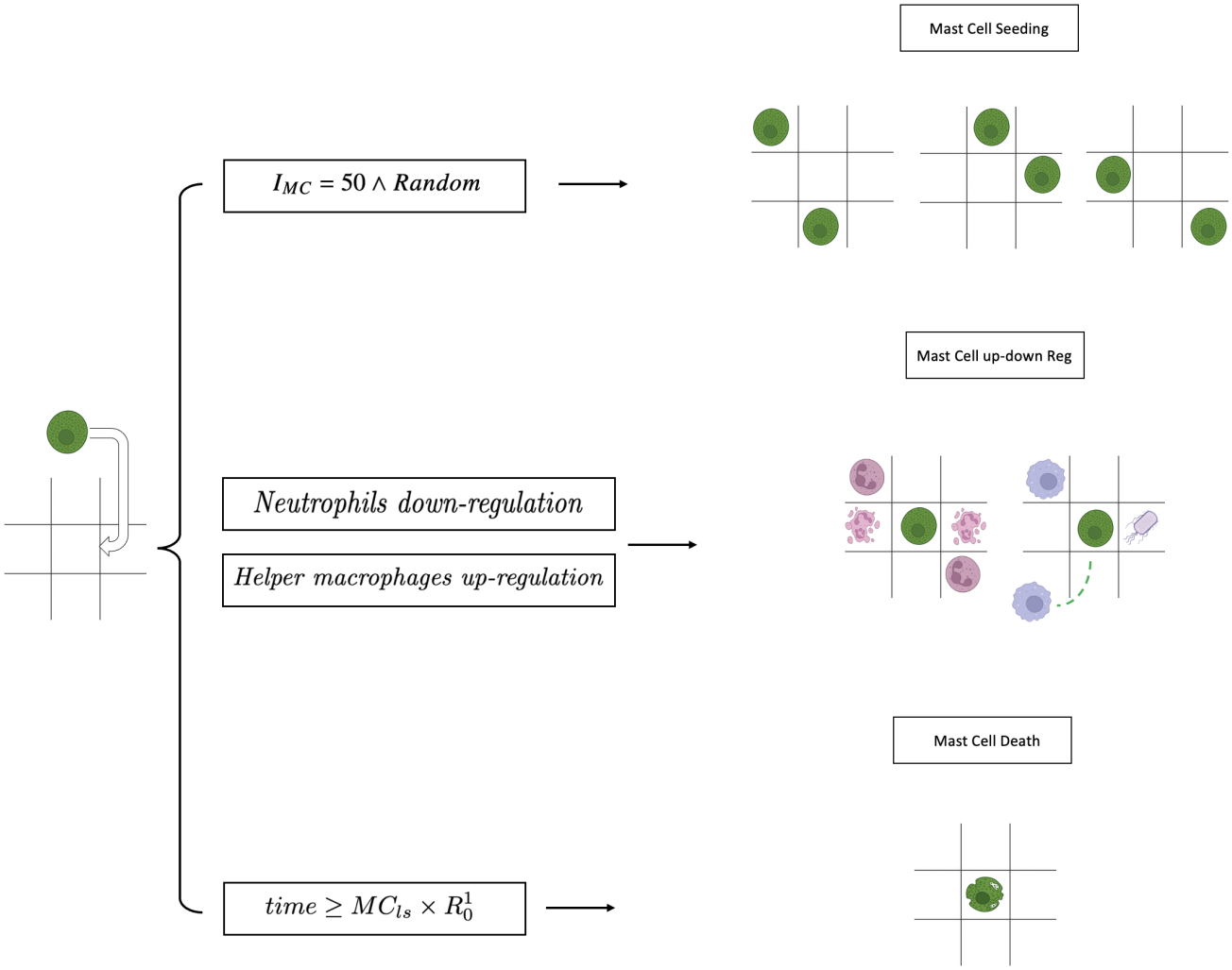

Figure 2.6: I_{MC} mast cells are initially seeded to our environment and assigned a random lifespan ($[0, MC_{ls}]$). When activated, mast cells are able to modulate the number of neutrophils and helper macrophages through up regulation and down regulation respectively.

- The number of bacteria needed for bacterial shedding to occur is $S_B = 6000$.
- When a bacteria escapes being killed, it is able to either proceed within the extracellular matrix, or with probability P_{Bp} it is cleared from the superficial layer but increasing the count of bacteria at deeper levels. Once shedding happens, this bacteria is again seeded within the environment along with all others able to successfully evade killing and penetrate to deeper levels of the urothelium.

The summarised rules for resident macrophages are:

- I_{rM} represents the initial number of resident macrophages which are randomly seeded into our environment.
- Each macrophage within this class is assigned a lifespan (measured in hours) upon creation, established through $R_0^1 \times rM_{ls}$, where R_0^1 is a randomly generated number using the uniform distribution on the interval $(0, 1]$. Once the age of the agent is greater than the established lifespan, the macrophage is removed from the grid.
- Resident macrophages follow a specified movement rate, rM_{RN}, see Table 2.1.
- When in the immediate neighbourhood of a bacterium, resident macrophages are activated with probability rM_{Ap}.
- Once activated, resident macrophages are able to recruit both helper macrophages and neutrophils to the site of infection.

For helper macrophages we have:

- Helper macrophages can be seeded within the immediate neighbourhood of the bacteria causing resident macrophage activation.
- Helper macrophages are recruited with probability hM_{RhM}
- Similarly to resident macrophages, each macrophage of this class has an associated lifespan (measured in hours) determined by $R_0^1 \times hM_{ls}$, where R_0^1 is a random number generated with the uniform distribution. Once the age of the agent is greater than the established lifespan, the macrophage is cleared.
- Helper macrophages are able to clear bacteria in their immediate Moore neighbourhood through killing with probability hM_{phP}.

- Helper macrophages are able to move within the grid with movement rate hM_{RN}, see Table 2.1. Helper macrophages move randomly to one of its empty neighbouring grid cells when the chemokine value for all its empty neighbours is 0, conversely, helper macrophages will follow chemotactic movement as explained in Section 2.2.4.

The rules followed by neutrophils are as follow:

- Similar to helper macrophages, neutrophils are recruited upon the detection of a bacteria in the immediate Moore neighbourhood of a resident macrophage or helper macrophage and are recruited with probability rM_{RN}.
- Neutrophils are activated with probability N_{Ap} once in the immediate neighbourhood of a bacterium.
- Each agent within this class will also have a lifespan attached to it (measured in minutes) determined by $R_0^1 \times N_{ls}$, where R_0^1 is a randomly generated number using the uniform distribution on the interval $(0, 1]$. Once the age of the agent is greater than the established lifespan, the neutrophil is removed from the grid.
- Neutrophils are able to kill bacteria present within their immediate Moore neighbourhood , which they do with probability N_{phP}.
- Neutrophils move within the grid with movement rate N_{RN}. In similar fashion to helper macrophages, Neutrophils follow random movement when the chemokine value for all neighbouring empty grid cells is 0, conversely, neutrophils will follow chemotactic movement as explained in Section 2.2.4.

Summarising the rules of action from mast cells we have the following:

- I_{MC}, represents the initial number of mast cells randomly seeded to the environment at the start of the simulation.

- MC_{ls} represents the mast cell lifespan which is individually assigned to each agent through calculating $R_0^1 \times MC_{ls}$, where again we have R_0^1 as a randomly generated number using the uniform distribution on the interval $(0, 1]$. If the lifespan is exceeded then the mast cell is cleared from the grid.

- Mast cells are responsible for up-regulation of helper macrophages which is done when there is no helper macrophage within the immediate neighbourhood of an activated mast cell. When this holds true, one is recruited at each time-step of the simulation during which the condition holds.

- Mast cells down regulate neutrophils; hence when activated, if there are more than three neutrophils within its immediate neighbourhood mast cells act by eliminating one neutrophil at random when the above condition holds for each time-step of the simulation.

- Similarly to helper macrophages and neutrophils, mast cells also follow random movement when the chemokine value for all neighbouring empty grid cells is 0, conversely, mast cells will follow chemotactic movement as explained in Section 2.2.4.

2.2.4 Chemokine dynamics

A generic chemokine is secreted by resident macrophages upon activation. This chemokine serves as a chemoattractant, directing all immune cells in the system to the site of infection. The spatiotemporal evolution of the chemokine concentration, $C(x, t)$, is described by the following PDE:

$$\frac{\partial C(x,t)}{\partial t} = \nabla \cdot (D(x)\nabla C(x,t)) + s(x,t) - (u(x,t) + d(x,t))C(x,t), \qquad (2.1)$$

which is subject to the initial condition $C(x, 0) = 0$. Here, D denotes the spatially-dependent diffusion coefficient, s denotes the source of chemokine from the activated macrophages, u denotes the uptake of chemokine by the host cells, and d denotes

the extracellular decay.

A reaction-diffusion equation, such as the one described in Eq. (2.1), provides a suitable framework for modeling the spatiotemporal evolution of the chemokine concentration ($C(x,t)$) in the context of immune cell recruitment to the site of infection. This choice is justified by several factors:

1. **Diffusion and Chemotaxis**: The equation includes a diffusion term ($\nabla \cdot (D(x)\nabla C(x,t))$), which accounts for the passive spread of the chemokine through tissue. This diffusion allows the chemokine to disperse away from its source, facilitating the recruitment of immune cells to distant areas of infection. Additionally, the chemokine serves as a chemoattractant, guiding immune cells towards higher concentrations, a process known as chemotaxis.

2. **Source from Activated Macrophages**: The term $s(x,t)$ represents the source of chemokine from activated macrophages. Upon activation, resident macrophages secrete chemokines to attract immune cells to the infection site. This source term captures the localized release of chemokine from discrete cells, effectively incorporating the discrete nature of macrophage activation into a continuum model.

3. **Uptake and Decay**: The terms $u(x,t)$ and $d(x,t)$ represent the uptake of chemokine by host cells and extracellular decay, respectively. These processes account for the removal of chemokine from the system, either through internalization by host cells or degradation in the extracellular environment.

4. **Mucus Barrier and 2D Dynamics**: In the context of urinary tract infections (UTIs), we assume diffusion of chemokines through the layer of mucus lining the bladder epithelium. This mucus layer acts as a barrier that limits the diffusion of chemokines into the third dimension, restricting their spread primarily within the two-dimensional plane of the bladder lining. By mod-

eling the dynamics in two dimensions (2D), we can effectively capture the spatial constraints imposed by the mucus barrier and the predominantly planar geometry of the bladder lining. This approach allows us to focus on the relevant dynamics occurring within the bladder epithelium while simplifying the computational complexity associated with modeling three-dimensional (3D) spatial dynamics.

To solve the presented PDE, we employed the finite difference method, a numerical technique commonly used to approximate solutions to partial differential equations. In this method, the spatial domain is discretized into a grid, and the derivatives in the PDE are approximated using finite difference approximations. The resulting system of algebraic equations is then solved iteratively to obtain the numerical solution at discrete points in space and time. For our specific case we note that we discretise our domain to a fixed computational grid matching the size and resolution of our ABM.

2.3 Bacterial Shedding

In addition to other roles played by the bladder epithelial cells (BECs), programmed death and shedding of these cells proves to be a powerful defense mechanism against heavy bacterial loads [22]. However, due to other functions served by BECs, such as acting as a physical barrier preventing potentially outside toxicity from reaching the underlying epithelial tissue, bacterial shedding cannot occur systematically [115]. Shedding is therefore regulated by the immune system, with studies showing a relation between the recruitment of mast cells and the activation of the shedding mechanism [22].

In *UTImodel* we assume shedding is dependant on the bacterial load and happens when the bacterial count goes over 6000 ($N_B > 6000$). Within our model, once a bacteria is in the immediate Moore neighbourhood of a neutrophil or helper

Symbol	Parameter description	Values	Units	Source
Bacteria (E. Coli)				
I_b	*minimal infectious dose*	1-1000	unitless	e
B_{sp}	*Bacterial replication speed*	0.37-0.97	hours	r [34, 108]
N_{db}	*neighbourhood replication depth*	2	unitless	e
S_B	*Bacterial load for shedding*	6000	unitless	e
P_{Bp}	*prob bacteria penetrates the bladder wall*	0.156332435	unitless	e
Macrophages ($Ly6C^-$)				
I_{rM}	*initial No. resident macrophages*	500	unitless	e
rM_{ls}	*resident macrophages lifespan*	30-32	hours	r [80]
rM_{RhM}	*resident macrophages recruitment prob.*	0.04-0.08	unitless	e
rM_{RN}	*resident macrophages movement rate*	0.17-0.26	hours	r [10]
rM_{Ap}	*resident macrophages activation prob.*	0.261	unitless	e
Macrophages ($Ly6C^+$)				
hM_{ls}	*helper macrophage lifespan*	30-32	hours	r [80]
hM_{RhM}	*helper macrophages recruitment prob.*	0.007-0.031	unitless	e
hM_{RN}	*helper macrophages movement rate*	0.13-0.18	hours	e
hM_{Ap}	*helper macrophages activation prob.*	0.129	unitless	e
hM_{Pp}	*helper macrophages killing prob.*	0.12-0.13	unitless	e
Neutrophils				
N_{ls}	*neutrophil lifespan*	30-32	hours	r [55]
N_{RN}	*neutrophil movement rate*	0.12-0.23	hours	e
N_{RhM}	*neutrophil recruitment prob.*	0.07-0.14	unitless	e
N_{Ap}	*neutrophil activation prob.*	0.148	unitless	e
N_{Php}	*neutrophil killing prob.*	0.11-0.17	unitless	e
Mast Cells				
I_{MC}	*initial No. mast cells*	50	unitless	e
MC_{ls}	*mast cell lifespan*	30-35	hours	e
MC_{RN}	*mast cell movement rate*	0.14-0.26	hours	e
MC_{urM}	*mast cell recruit. prob.*	0.003-0.033	unitless	e

Table 2.1: Parameter values for agents described in the model. *e* indicate estimated parameters. *r* indicate parameters which were set using values from available literature and data with their original references attached.

macrophage ($LY6C^{-}$), a number (z_1) is randomly generated from the interval $[0, 1)$ during each time-step, if $z_1 < hM_{phP}$ (for helper macrophages) or $z_1 < N_{phP}$ (for neutrophils), the bacteria is able to evade killing. In addition to this, a bacterial counter is updated once a new randomly generated number, z_2 satisfies $z_2 < P_{Bp}$. This counter, describes the bacteria within our model able to penetrate the superficial urothelium and form QIRs. However as bacterial shedding occur, eliminating the superficial layer of the bladder, underlying QIRs may potentially be re-exposed to the surface and play an important role in recurrence. Thus, understanding the progression of infection throughout multiple recurrence episodes is also key to devising an efficient antibiotic treatment strategy.

2.4 Design and Model Structure

The model is formed by five classes, each of which describes a different general instance of the model. Each class has been split into two documents. Header files (.h files) will contain the necessary declarations of variables and functions, while these same variables and functions will be fully characterised and manipulated in the cpp files. We will now provide a full overview of all classes within the model.

2.4.1 The Environment Class

In this class, we describe the environment upon which all agents will live, move and interact with each other. The environment is structured as a grid, defined as an array of size **grid_size**^{2}. Each one of these grid positions will hold a single instance of the Location class characterised below.

The Environment class is responsible for simulating a section of the bladder, which is then seeded with blood vessels, bacteria and immune cells. The functions controlling the creation and death of such agents are also found within the same class. This simulation of the bladder is then run through a ProcessTimestep function. This function iterates through all agents while first incrementing their age, then updating the model attribute values, while finally processing the agent-based model events leading to the next attribute state.

```
1
2  void Environment::initialiseBacterialCluster(int cluster_x, int
       cluster_y)
3  {
4    int bacteria_placed;
5    std::vector<std::pair<int,int>> cluster_locs, neighbours;
6    std::tuple<bool,int,int> space_finder;
7    Bacterium *bac;
8    bacteria_placed = 0;
9
10   int attempts = 0;
```

```
11
12  while (grid[cluster_x][cluster_y] -> getContents() !=
     LocationContents::empty && attempts < grid_size*grid_size)
13  {
14    neighbours = grid[cluster_x][cluster_y] -> immediate_moore;
15    space_finder = findSpace(neighbours);
16    if (std::get<0>(space_finder))
17    {
18      cluster_x = std::get<1>(space_finder);
19      cluster_y = std::get<2>(space_finder);
20    }
21    else
22    {
23      // No space at the coordinates or any neighbours, so pick a
     random location
24       cluster_x = distribution_0_grid_size(rng);
25       cluster_y = distribution_0_grid_size(rng);
26    }
27    attempts++;
28  }
29
30  if (attempts == grid_size*grid_size)
31  {
32    throw std::runtime_error("no empty spaces for cluster");
33  }
34
35  bac = addBacterium(cluster_x, cluster_y, false);
36  extracellular_bacteria.insert(bac);
37  bacteria_placed++;
38  cluster_locs.push_back(std::make_pair(cluster_x,cluster_y));
39
40  while (bacteria_placed < p->initial_number_bacteria)
41  {
42    neighbours = vonNeumannNeighbourhood(cluster_locs[0].first,
```

```
    cluster_locs[0].second,1,grid_size,rng);
43   space_finder = findSpace(neighbours);
44   if (std::get<0>(space_finder))
45   {
46     bac = addBacterium(std::get<1>(space_finder), std::get<2>(
    space_finder), false);
47     bacteria_placed++;
48     extracellular_bacteria.insert(bac);
49     cluster_locs.push_back(std::make_pair(std::get<1>(
    space_finder), std::get<2>(space_finder)));
50   }
51   else
52   {
53     cluster_locs.erase(cluster_locs.begin());
54   }
55  }
56 }
```

Listing 2.1: Part of the Environment class function responsible for initialising the bacterial cluster

As each grid position holds a location instance of the model, each position will then have several attribute values stored within it, such as age and agent characteristics. This can be further extended to include other variables such as chemokine dynamics within our two-dimensional grid.

For model clarity each event was contained within its own function. Where possible we grouped several events together, thus avoiding excess iterations through lists which can prove costly once attempting to run multiple or long-time simulations.

2.4.2 The Location Class

Each individual square within the grid built by the Environment class will constitute a Location instance. Any location based attributes can be handled within this class

and then made public throughout the model as they are used in further interactions.

Each location instance defines its contents. Hence, at each location we can have one of the following: “Agent", “Vessel", “Empty". Within our class, we have many functions that handle the adding and removing of agents and vessels following the agent-based model rules. Exceptions and error catchers are used to detect invalid actions such as adding agents to non-empty locations or deleting agents in empty locations. The main functions within the Location class include the **Location::setVessel()** function which adds a blood vessel to an empty Location instance. The blood vessel location instance is crucial in the model as it will represent the source of chemokines and antibiotic drug distribution at later stages of the model. Other similar functions in our Location class include the **Location::addAgent()** and **Location::removeAgent()** functions which, similarly to the previously mentioned function, handle Location contents when dealing with “Agent". The next class we will explore is responsible for the Location contents subset of an “Agent" type object.

2.4.3 The Agent Class

An instance of the Agent class will fully characterise the specific biological agent within the agent-based model. We hence do not consider blood vessels as an agent due to their fixed/static nature. All agents share global variables such as age, which is incremented in the model through time-steps and contain flags specifying different characteristics of the agent. Thus, eliminating the need to access single agents within the class to determine these factors. For example, to determine whether an agent can activate immune cells we can simply check the flag **can_activate_immunecells**.

The Agent class is further divided into subclasses, each of which describing a specific type of agent. Two subclasses (Bacterium, Immune cell), inherit from the Agent class while simultaneously containing their own specific individual subclass attributes. The Bacterium subclass is responsible for describing the cellular-automaton rules for bacteria. The Bacterial subclass includes two Boolean attributes. The first, **resting**,

indicates whether the bacteria has ceased replication due to unavailability of space. While the second, **moore_neighbourhood**, indicates which space finding algorithm (Von Neumann or Moore neighbourhood) is to be used in search of replication space. Many functions within the model will have access to manipulate and change these boolean values.

The Immune cell subclass is responsible for defining all the functions representing macrophage actions in our agent-based model. We have different macrophage categories depending on their interaction with the bacterial pathogen. Using **enum** on **MacrophageState** we access these different categories: “resting", “active".

2.4.4 The Parameters Class

The Parameters class is where all the model parameters are declared and set. We use a data-serialisation language, YAML, to handle dynamical parameter integration to C++ by parsing a generated $M \times N$ matrix to produce M parameter sets. We can hence generate a high number of parameter sets by parsing a table with all possible values for all parameters. This allows quick analysis of the model and is essential for uncertainty and sensitivity analysis, shown in Section 2.5.

2.4.5 The main model file

Our main compilation file, with the name **UTImodel.cpp** is where we define our simulation along with our temporal domain. Here, we use all the functions defined in all other classes to simulate a time-step of our agent-based model. After setting our initial conditions, we loop through all the events, recording at each step all the relevant variables. This data is then written to text files which are then saved in an output folder in the model path.

2.5 Uncertainty and Sensitivity Analysis: Theory and Verification

2.5.1 Introduction

With the increase in data availability and computational power, mathematical models are becoming key aspects in numerous fields including disease research.

This increase in availability of models and data prompts us to devise and explore techniques that allow us to analyse the underlying uncertainty in mathematical models describing complex biological systems.

As seen in Section 2.3, the model built to study infections in the bladder is relatively complex and involves a diverse range of parameters, many of which are initially unknown to us. It is hence important to understand how uncertainty related to the parameter values propagates through to affect the model outputs.

During this chapter we explore several techniques that will aid us to apportion variance in the model output to specific individual parameters. We also describe the creation of a YAML framework dedicated to creating model input files and a Python framework that allows the techniques described further below to be applied.

2.5.2 Uncertainty and Sensitivity Analysis

- Uncertainty Analysis (UA) involves evaluating and quantifying uncertainty stemming from input variability or imprecise parameters. It assesses the reliability of model predictions and identifies sources of uncertainty using techniques like sensitivity analysis and Monte Carlo simulation. This process aids decision-making by providing insights into the model's limitations and variability.

- Sensitivity Analysis (SA) intends to assign the uncertainty in model outputs to uncertainty in specific individual model inputs.

Ideally UA and SA should be run in tandem. UA is performed first, thus quantifying

the uncertainty of the model, which can then be apportioned to specific inputs using SA.

2.5.3 Uncertainty Analysis

Developing a mathematical model that is capable of appropriately capturing real-world systems is a complex process that often requires the combination and cohesion of numerous parts [94], some examples follow:

- Mechanics - Here we describe the events which are at the heart of the real world system.
- Model Parameters - The variables with a range of possible values defines the full model output.
- Initial Conditions - The state at which the model finds itself during the beginning stage.
- Resolution - The granularity with which the model operates.

This non-exhaustive list of model components is ideal to examine the nature of uncertainty attached to the model. Each one of these components will come with a level of uncertainty attached to it. In addition to this, further uncertainty can be introduced in the model through the consideration of computational costs and coding errors. The use of UA to better improve and understand our biological model is however restricted by the impossibility of varying all factors. As an example, varying the mechanics of a model would most likely lead to the development of a new model, which would be impractical in most cases. However, we can still analyse the mechanics of the model through the variation input factors. In the case of mechanistic models, these are the model parameters and the initial conditions. The uncertainty in these factors arises from a variety of possible reasons such as natural variation of the measured object, measurement errors and in some cases,

simply the inability to measure certain objects. The term 'epistemic uncertainty' is used to describe the uncertainty in the model that arises from the uncertainty in the input factors. On the other hand, 'aleatory uncertainty', is used to describe all uncertainty related to inherent randomness within the model. Consequently, deterministic models will be free of 'aleatory uncertainty', while the uncertainty output from stochastic models presents both epistemic and aleatory uncertainty. In order to perform UA, it is crucial to explore the full k(number of factors)-dimensional parameter space. Considering the cross product of all parameter values, especially when k is a large number, proves that carrying out an analysis of the full range is impractical due to the computational cost assigned to running the complete range of simulations. This leads to the need of sampling methods which are used to generate a manageable number of samples while sufficiently capturing the entire parameter space.

2.5.4 Sampling Methods

To draw valid conclusions from model outputs, we make sure the sample space we apply to our mathematical model is representative of the full rank sample space. In general, we identify two sampling approaches which we can see in Figure 2.7. The first approach, probability sampling, provides different methods and algorithms for sampling techniques where random selection is used. This allows for statistical inferences to be made on the entire group.

During our work, we will focus on the probability based random sampling method Latin Hypercube Sampling (LHS). This method allows us to investigate large parameter sets while cuting down on computational cost when combined with sensitivity analysis methods.

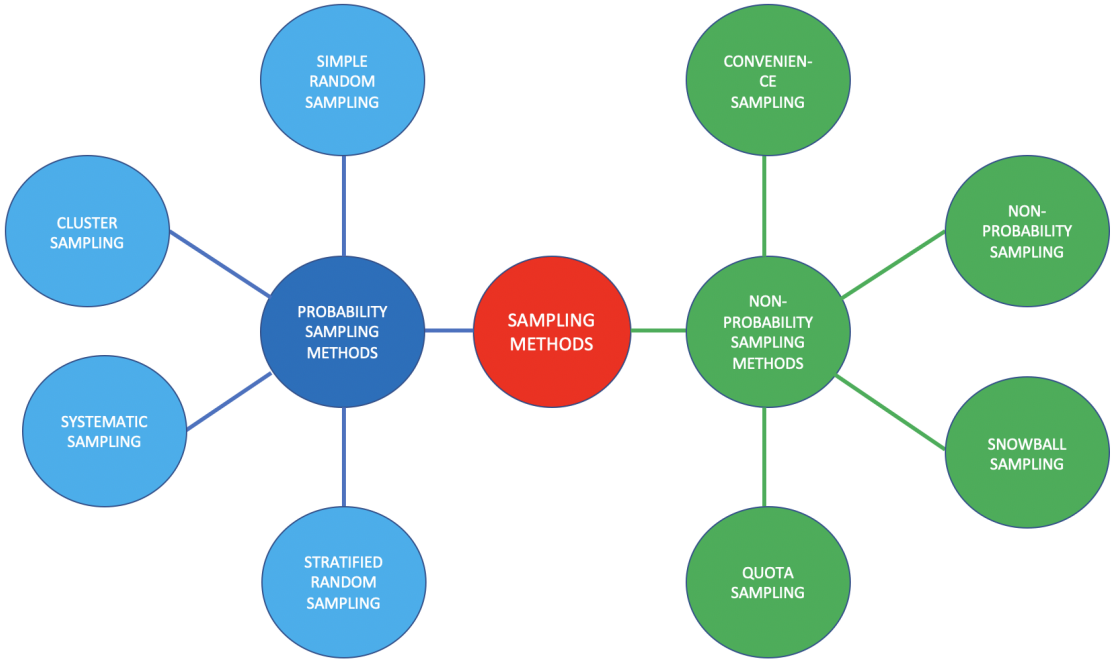

Figure 2.7: This schematic representes the various methodologies available in sampling. Sampling techniques can be divided in two groups based on whether a probabilistic approach (probability sampling methods) was used or not (non-probability sampling methods) to generate the sample.

2.5.4.1 Latin Hypercube Sampling

Latin Hypercube Sampling (LHS) is a Monte Carlo (MC) derived sampling method that relies on attaching probability density functions (pdfs) to each of the uncertain parameters. This assumed distribution is usually either normal where we have prior knowledge of the parameter, or uniform where no prior knowledge of the parameter is available. This use of probability distributions to generate samples is the core idea behind Monte Carlo methods, which are known for their efficiency. LHS, goes one step further, with improved efficiency due to the sample points being spread more evenly across all possible values. The algorithm for LHS is described and can be seen in Figure 2.8.

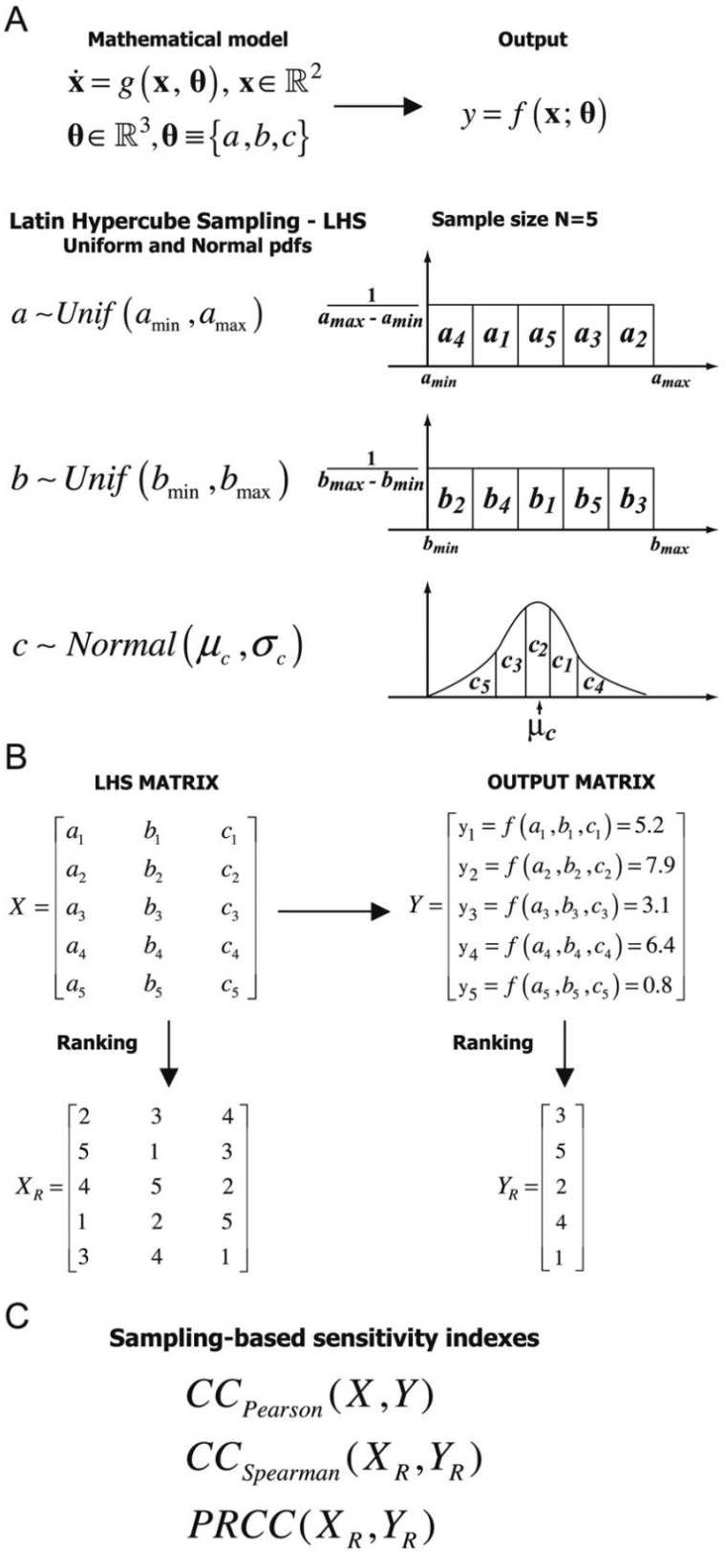

Figure 2.8: The LHS process illustrated. [70]

1. We begin by defining a sample number, N_s. N_s will represent the number of unique parameter samples generated by our algorithm.

2. As opposed to most Monte Carlo methods, we now stratify each input range into N_s parts each of which containing equal probability. This extra stratification step is key to the efficiency that LHS is known for.

3. We now create an LHS matrix of size N_s rows by K columns, where K is the number of uncertain inputs. The entries of the matrix are given by selecting one stratification without replacement randomly for each one of the K uncertain inputs.

4. Each row of the matrix generated during the previous step will now correspond to an input sample set that could be used to generate a simulation. We hence use the LHS matrix to parametrise the model resulting for us in an output matrix consisting of N_s rows.

2.5.4.2 Sensitivity Analysis

Once we are finished with UA, we can proceed by apportioning the uncertainty evaluated to each of the uncertain model inputs. This will allow us to better understand the effects of our parameters on the behaviour of the model, thus, helping us identify critical input parameters and also identify parameters that carry little effect on our model and hence can be fixed. Depending on the number of input parameters that are varied, we can recognise two groups of SA techniques:

- Local SA: Here we determine the sensitivity of the model output to a single varying input. We begin by fixing all inputs to their specific values while only varying the parameter of intere

- Global SA: When carrying out this process, all input parameters are varied. This is done with the aim of understanding the emerging influence in model's output variance of a certain set of input parameters and their interactions.

Local SA is a very efficient and computationally non-expensive, especially when dealing with smaller models that do not require the analysis of a large number of parameters. However, due to the limited exploratory capability associated with this method, particularly when a large number of input parameters is present, local SA methods become limited and are replaced by the Global SA methods.

2.5.4.3 Partial Rank Correlation Coefficient

Correlation provides us with a measure of the strength of a linear relationship between an input and an output. A simple correlation coefficient between x_j and y can be represented as follows:

$$r_{x_j y} = \frac{\mathrm{Cov}(x_j, y)}{\sqrt{\mathrm{Var}(x_j)\mathrm{Var}(y)}} = \frac{\sum_{i=1}^{N}(x_{ij} - \bar{x})(y_i - \bar{y})}{\sqrt{\sum_{i=1}^{N}(x_{ij} - \bar{x})^2 \sum_{i=1}^{N}(y_i - \bar{y})^2}}, \quad j = 1, 2, \ldots, k.$$

One of the global SA techniques we will explore utilises the above concept of correlation in order to produce a coefficient known as the Partial Rank Correlation Coefficient (PRCC) which works by establishing nonlinear but monotonic relationships between x_j and y. This method is combined with LHS in the following way:

1. Using the previously defined sampling method, LHS, we generate the parameter samples which are then used to run the model generating the output Y.

2. Each input X_i ($i = 1, \ldots, K$) is rank transformed within X. The same procedure is carried out with each result Y_j ($j = 1, \ldots, R$). The highest value is given rank N_s, while the lowest is given rank 1.

3. Linear regression is applied to each input ($\hat{x}_i$) and output ($\hat{y}_j$) in the following form:

$$\hat{x}_i = c_0 + \sum_{p=1, p\neq j}^{K} c_p x_p,$$

$$\hat{y}_j = b_0 + \sum_{p=1, p\neq j}^{K} b_p y_p.$$

4. The PRCC value corresponding to input x_i and output y_j is evaluated by using the above correlation equation between both residuals:

$$\begin{cases} r_i = x_i - \hat{x}_i, \\ q_j = y_j - \hat{y}_j. \end{cases} \tag{2.2}$$

Let us represent the respective means of r_i and q_j as $\bar{r}_i$ and $\bar{q}_j$; this leads to the final equation for the PRCC value:

$$PRCC_{x_i, y_j} = \frac{\sum_{v=1}^{N_s} (r_{iv} - \bar{r}_i)(q_{iv} - \bar{q}_j)}{\sqrt{\sum_{v=1}^{N_s} (r_{iv} - \bar{r}_i)^2 \sum_{v=1}^{N_s} (q_{iv} - \bar{q}_j)^2}}, \tag{2.3}$$

2.5.4.4 Extended Fourier amplitude sensitivity test

Another method that exists to analyse sensitivity is Extended Fourier Amplitude Sensitivity Test (eFAST). eFAST is a variance-based method which outperforms PRCC in input-output trends with non-linear, non-monotonic nature. This method relies on varying the inputs at different frequencies. The strength of such input frequency on the model output frequency is evaluated using Fourier analysis techniques. The eFAST algorithm is implemented by following the steps outlined below:

1. As previously, each of the uncertain inputs must be assigned a probability distribution and its appropriate defining values. In a similar way to before, we use the uniform distribution when no prior knowledge is available, and the normal distribution if prior knowledge on the parameter is available.

2. We add an additional dummy parameter to the original K model parameters, which distribution will be irrelevant. The number of input parameters is now K+1. To generate the input samples, each input x_i is analysed in turn.

3. Input parameter x_i is assigned a high frequency, ω_i, which is calculated using the equation below, where N_s and M represent the number of samples required per run and the number interference factor, which is the maximum number of Fourier coefficients kept following partial variances calculations (usually 4) respectively. The rest of the inputs are assigned low frequencies, evaluated using a maximum complimentary frequency (ω_{-i}), where

$$\begin{aligned} \omega_i &= \frac{N_s - 1}{2M}, \\ \omega_{-i} &= \frac{1/M}{\omega_i/2}. \end{aligned} \tag{2.4}$$

4. Frequencies to be used are now chosen to satisfy the following: 1) The step between frequencies must be maximised and 2) The number of inputs with non unique frequency must be minimised.

5. As each input parameter, x_q, is now associated with a frequency, we use the equation below to calculate g_q, a vector of values all within the range (0, 1):

$$g_q = \frac{1}{2} + \frac{1}{\pi} \arcsin(\sin \omega_w s + \phi_w),$$

where ω_q represents the respective frequency, s is a vector of length, N_s, that varies between $-\frac{\pi}{2}$ and $\frac{\pi}{2}$, while ϕ_w is a random phase shift operator in the range $(0, 2\pi]$.

6. We now have each parameter generating N_s values. This is repeated N_R (number of re-samples) times. Each time a new re-sampling is underway a new ϕ_w is created, allowing us to explore more of the parameter space.

7. Steps 3 to 6 are repeated, each time changing the input of intere Once all parameters have been processed, all samples ($N_s * N_R * (K + 1)$) are passed through the model to produce the output required.

After generating the full sample and producing the output, we are now ready to analyse the results of the model.

For each input of interest and re-sample curve, we obtain output that is then Fourier transformed while the variance is calculated from the Fourier coefficients considering each frequency of intere S_i (First order variance) will represent the fraction of the variance of the model output that can be apportioned to the input x_i. The total variance, S_{T_i} will take into account both the first-order variance whilst also accounting for the variance resulting from higher order interactions between different inputs.

2.5.5 Implementation of Uncertainty and Sensitivity Analysis

In order to carry out the uncertainty and sensitivity analysis techniques, we need to construct a framework capable of handling the computational requirements for the simulations while also maintaining accuracy. To do this, we elect to divide the process of UASA (uncertainty analysis/sensitivity analysis) into three stages. In addition to the reduction of computational power, it gives us the opportunity to check the output at each stage. A brief description of each stage of implementation:

1. Data preparation: In order to carry out accurate uncertainty analysis, it is vital for the parameters used to be previously examined, and for the values appointed to these parameters to be cross-referenced with any existing literature on the subject. As we elect to generate our samples using LHS (see Section 2.5.4.1), the output of this first stage will be a data matrix consisting of all the data samples to be fed into our model. One limitation here is the lack of existing literature and limited existing libraries within `C++` that allow the creation of either simulation loops or clusters. In order to overcome this, we introduced `YAML`.

   `YAML` (Yet Another Markup Language) is a data serialisation language that allows us to develop a framework using `python`, `C++` and `Rstudio`. We

use `Rstudio` to generate our LHS samples which are then imported through `python`. `Python` is then responsible for taking in a data frame and outputting N_s `YAML` files, each containing a separate parameter set which, through a newly developed `python` module, we are able to feed to the `C++` model.

2. Simulation Output: The second stage includes sorting simulation output and plotting simulation results. At this stage, SA is not carried out. We simply visualise the output through multiple plots in order to ensure expected results.

3. Sensitivity Analysis: This step is carried out in `Rstudio`. We use the flexibility of this program to deal with complex data frames to be able to better analyse the simulation output while also implementing the sensitivity analyses. Therefore PRCC and eFAST algorithms were developed in RStudio.

2.5.6 Efficiency vs Flexibility tradeoff

Due to the model being implemented in a compiled language (`C++`), we can expect our simulation run-time to be noticeably shorter than that of a model using an interpreted language such as `python` or `Rstudio`. However, this boost in efficiency creates certain restrictions in terms of flexibility of parameter input. Due to this, the parameters are expected to be available at compilation time to the model. This, however, is disadvantageous in terms of UASA as we are essentially required to carry out a great number of simulations while using multiple parameter variations. In order to avoid being restricted to `C++`, we devise a framework that allows us to only invoke `C++` when a simulation of the model is taking place, all other aspects of our analysis will be carried out by `python` and `Rstudio` as outlined in the Methodology section above.

2.5.7 Result Aggregation

As we produce multiple simulations of our model, the results from each simulation are saved in separate `text` files. Using `Rstudio` we are able to efficiently aggregate all the results needed by importing them into a data frame that can subsequently be manipulated to calculate sensitivity values. In addition to this, the data frame of outputs can be further used to generate plots, calculate average simulation values and perform exploratory data analysis on the model.

2.5.8 Verification

There exist several papers [70, 54, 94] which provide UASA methodology and results of the sensitivity analyses. Here we follow a similar method to test our UASA framework. In order to validate our UASA framework, prior to utilising on our model, we tested it on a model whose behavior and sensitivity analysis results were available. In order to do this, we choose a simple Lotka-Volterra model as the verification model.

Parameter	Mean	Standard Deviation	Distribution
α	1.5	0.01	Normal
β	1	0.2	Normal
ω	3	0.2	Normal
δ	1	0.01	Normal

Table 2.2: Summary of parameter means, standard deviations, and distributions.

As with our original model, we implement the differential equation model in C++, data and parameter passing using YAML. The analysis is then implemented using Rstudio both for efficiency and visualisation purposes. Lotka-Volterra models, also known as predator-prey models are a set of linear ordinary differential equations used to describe biological phenomena where species of predatory nature interact with other species labelled prey. The model is characterised using the following set

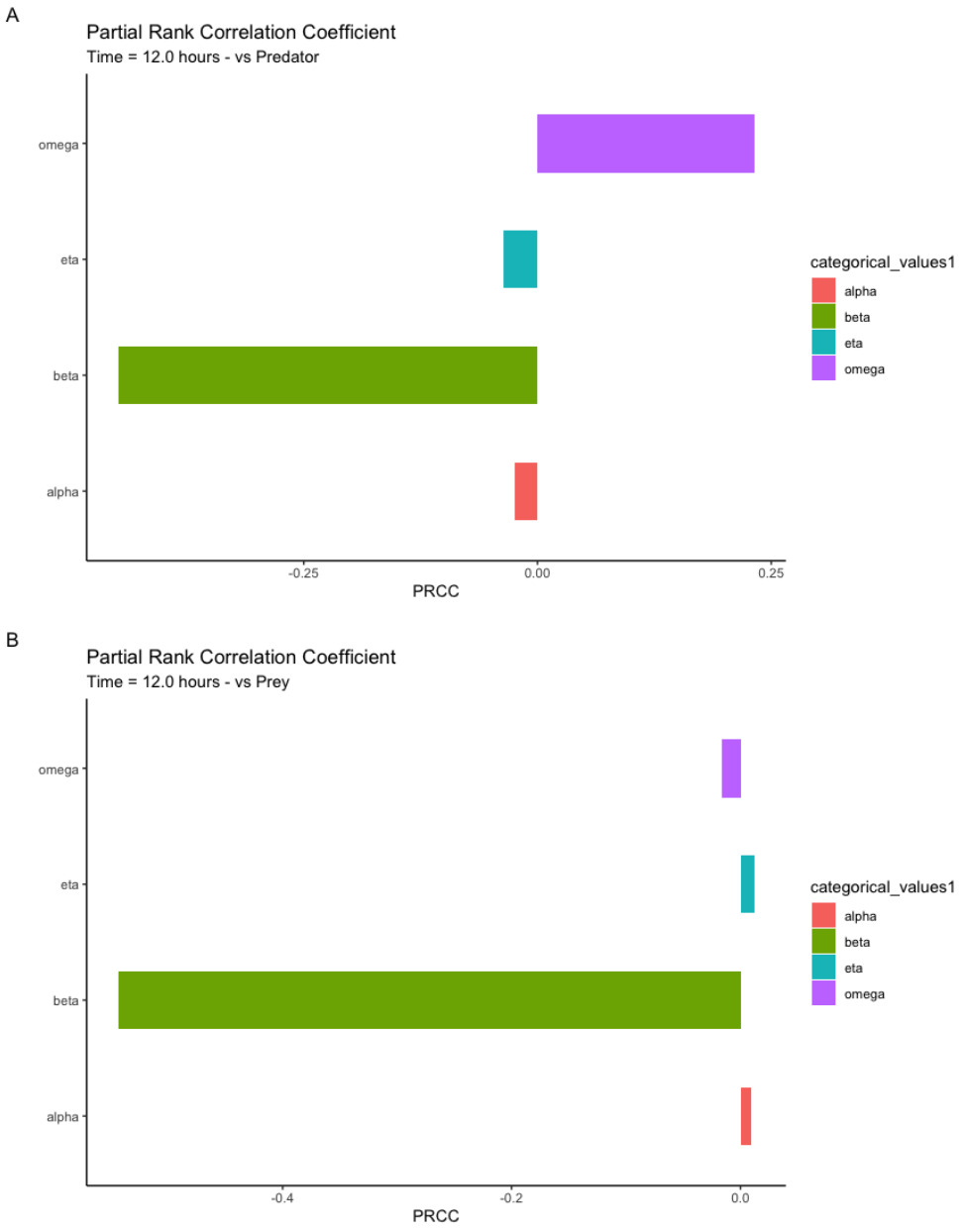

Parameter	PRCC	P-value	Significant?
α	-0.0247	$4.34e-01$	No
β	-0.4483	$1.49e-50$	Yes
η	-0.0365	$2.47e-01$	No
ω	0.2316	$1.21e-13$	Yes

Parameter	PRCC	P-value	Significant?
α	0.0097	$7.58e-01$	No
β	-0.5434	$7.47e-78$	Yes
η	0.0118	$7.08e-01$	No
ω	-0.0165	$6.02e-13$	No

Figure 2.9: PRCC results for T = 12.0 hours. Figure A is a histogram of the PRCC values for each parameter in relation to y (predators). Figure B is a histogram of the PRCC values for each parameter in relation to x (prey). These PRCC values are shown in the attached tables where we indicate the significance of each parameter according to its p-value.

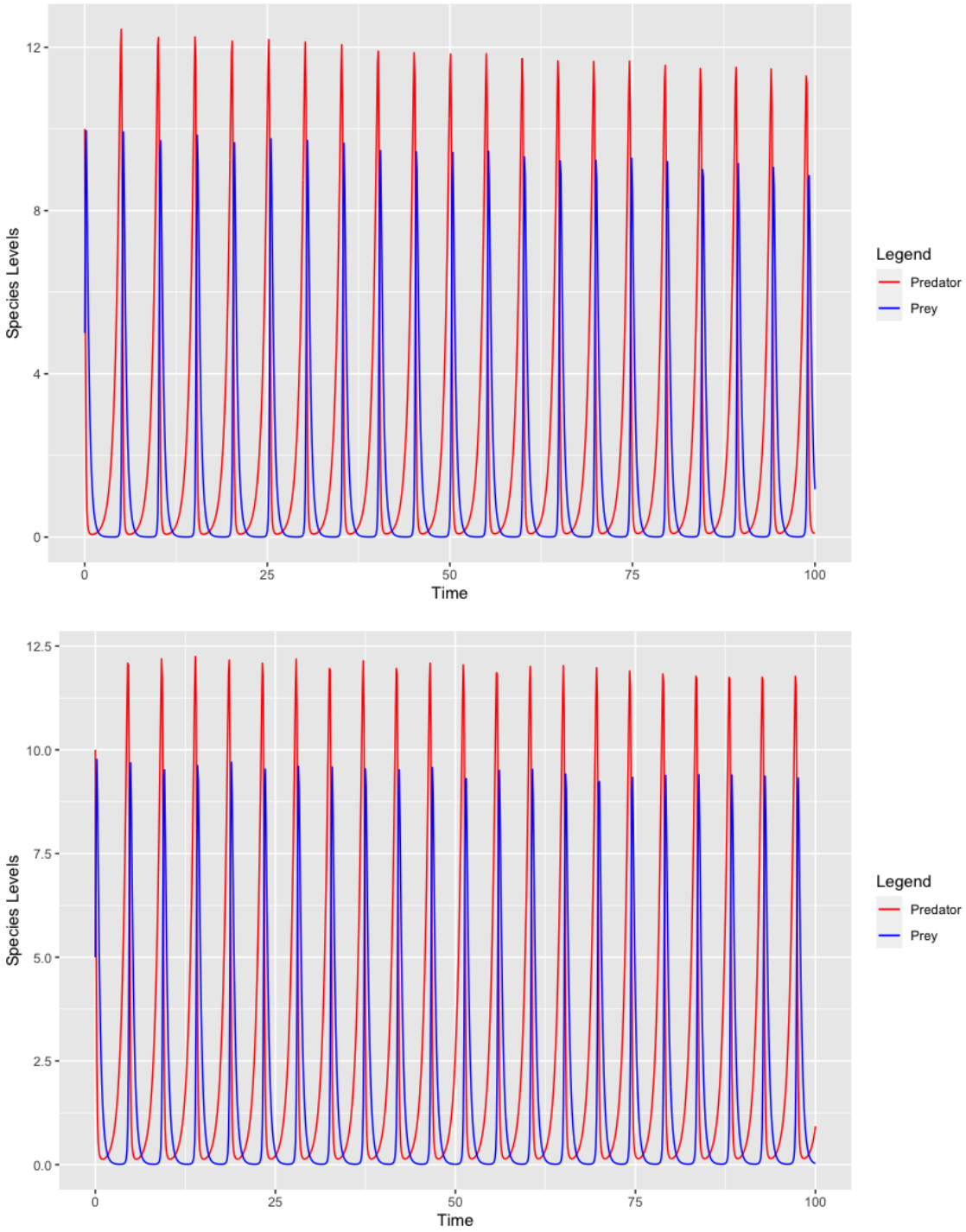

Figure 2.10: The following results represent two separate simulation runs using a Lotka-Volterra model. These simulations were produced using a parameter space generated by LHS, which in turn allows us to use PRCC previously described to assess the uncertainty of the model.

of equations:

$$\frac{dx}{dt} = \alpha x - \beta xy,$$
$$\frac{dy}{dt} = \delta xy - \omega y.$$

where x is the number of prey, y, the number of predators. α, β, δ and ω are real parameters describing the interaction rates between the two species. In order to move forward with verification, let us first do some exploratory data analysis. Plotting the results for several runs of the model is usually a good indicative of the relationship between the parameters and the uncertainty in the model output. The output resulting of each model run is a **text** file, in which each row specifies the x, y and t value. In order to easily analyse and explore this data, we simply aggregate all these **text** files to generate a multidimensional data-frame. After the data-frame is defined, we follow the steps outlined previously to calculate the PRCC values. Looking at Figure 2.10, we can clearly see what the expected behaviour of the model is, however, we can also see how differences between simulations arise especially if we compare the far right end of the time axis. Here we are able to note how different parameters resulted in different final model states. We are now ready to apply the PRCC algorithm with the results fully characterised in Figures 3.8, 3.10 and 3.11. We take $N_s = 200$ (see Section 2.5.4.1), although the original results used for verification [70] were conducted with $N_s = 1000$. As discussed in the verification study cited above, a minimal value can be defined as $N_s = K + 1$, where K is the number of model parameters (4 in the Lotka-Volterra model). However, as there is no a-priori systematic way to define the size of an LHS sample, I carried out various PRCC analyses using different LHS sample sizes ($N_s = 10, 25, 50, 75, 100, 200$) and noticed the consistency of the results with the verification study when sample sizes are $N_s > 50$. As can be seen in Figures 3.8, 3.10, 3.11 we can see high PRCC values for β showing high similar to Marino et al. 2008. Similarly, at $T = 9$ three significant parameters are identified: β, ω and η. Having replicated the results

presented in Marino et al. 2008, we have confirmed that our implementation of the UASA framework is accurate.

We choose to focus our analysis on the PRCC values as opposed to the eFAST method as the latter proves to be much more computationally expensive. Keeping in mind that our model will be used to produce longer simulations and also additional model developments may also be implemented in the future as described in Section 6.4.

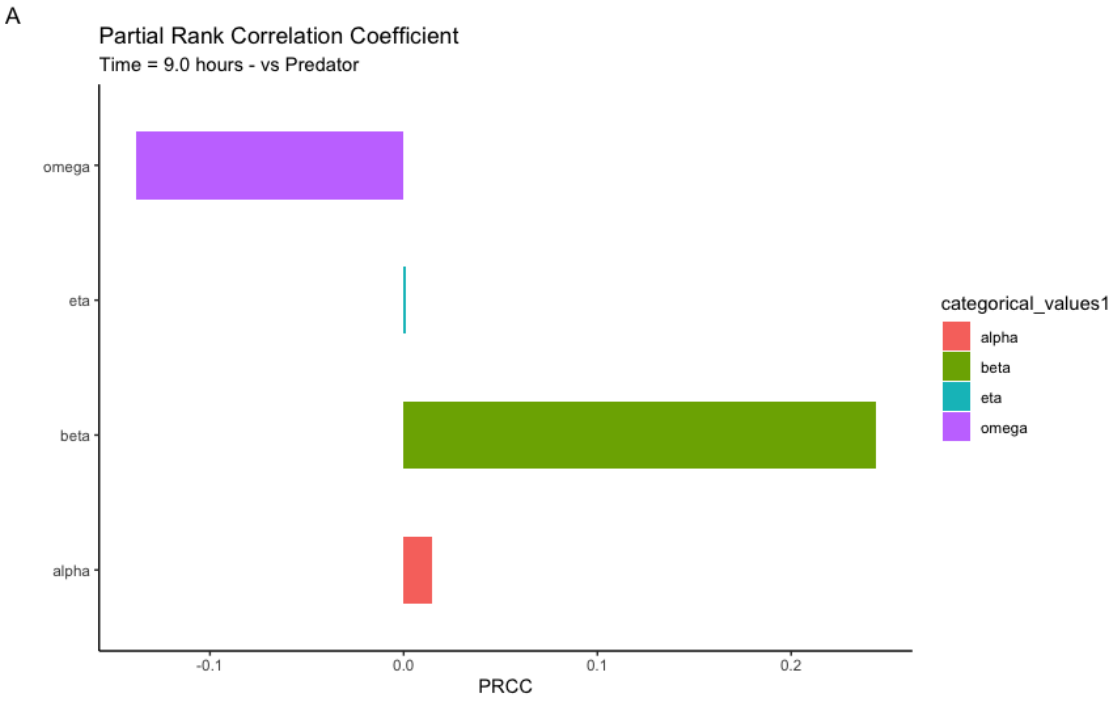

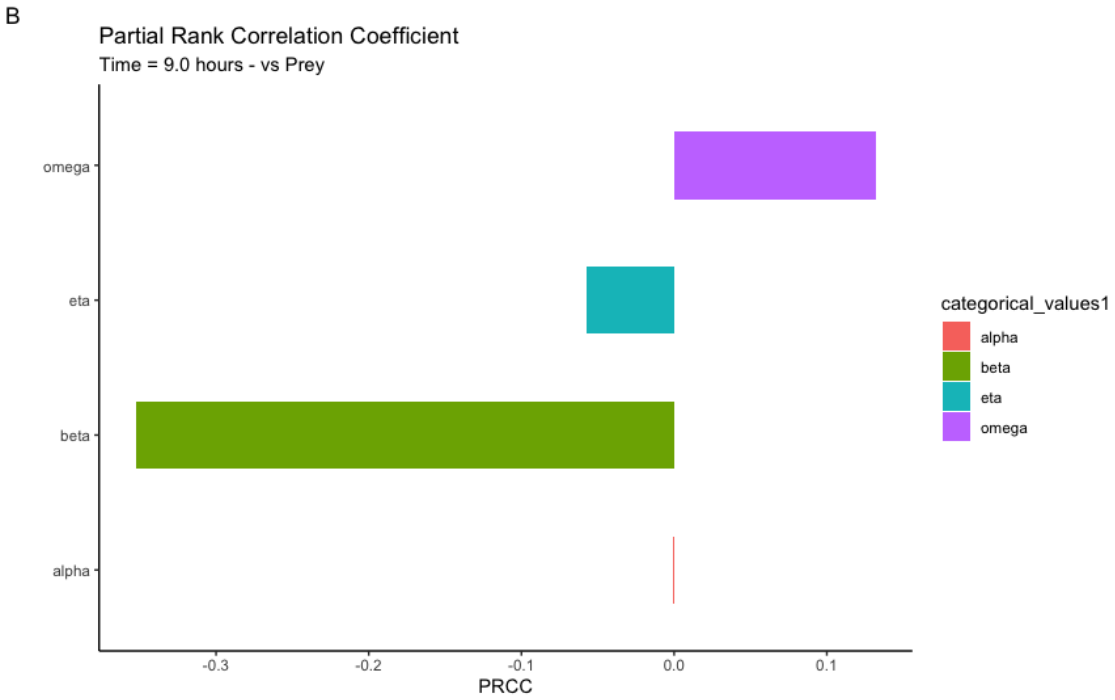

Parameter	PRCC	P-value	Significant?
α	0.0147	$6.42e-01$	No
β	0.2435	$5.94e10-15$	Yes
η	0.0012	$9.68e10-01$	No
ω	-0.1381	$1.17e10-05$	Yes

Parameter	PRCC	P-value	Significant?
α	-0.0004	$9.88e-01$	No
β	-0.3524	$1.39e-30$	Yes
η	-0.0569	$7.20e-02$	Yes
ω	0.1318	$2.91e-05$	Yes

Figure 2.11: PRCC results for T = 9.0 hours. Figure A is a histogram of the PRCC values for each parameter in relation to y (predators). Figure B is a histogram of the PRCC values for each parameter in relation to x (prey). These PRCC values are shown in the attached tables where we indicate the significance of each parameter according to its p-value.

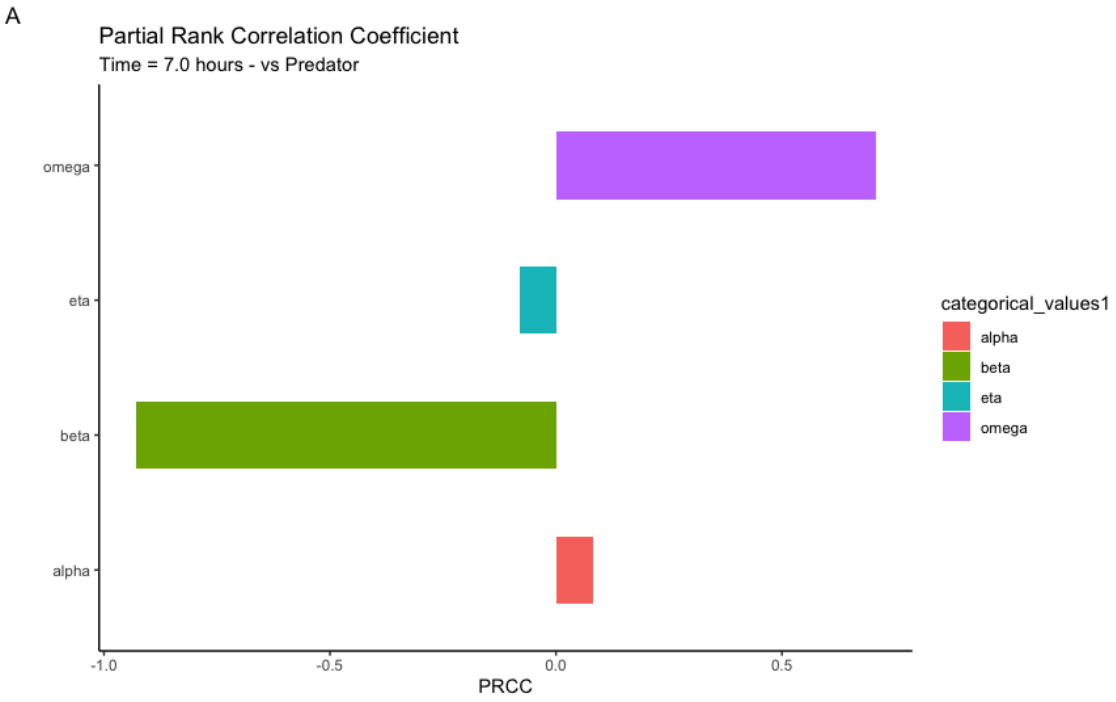

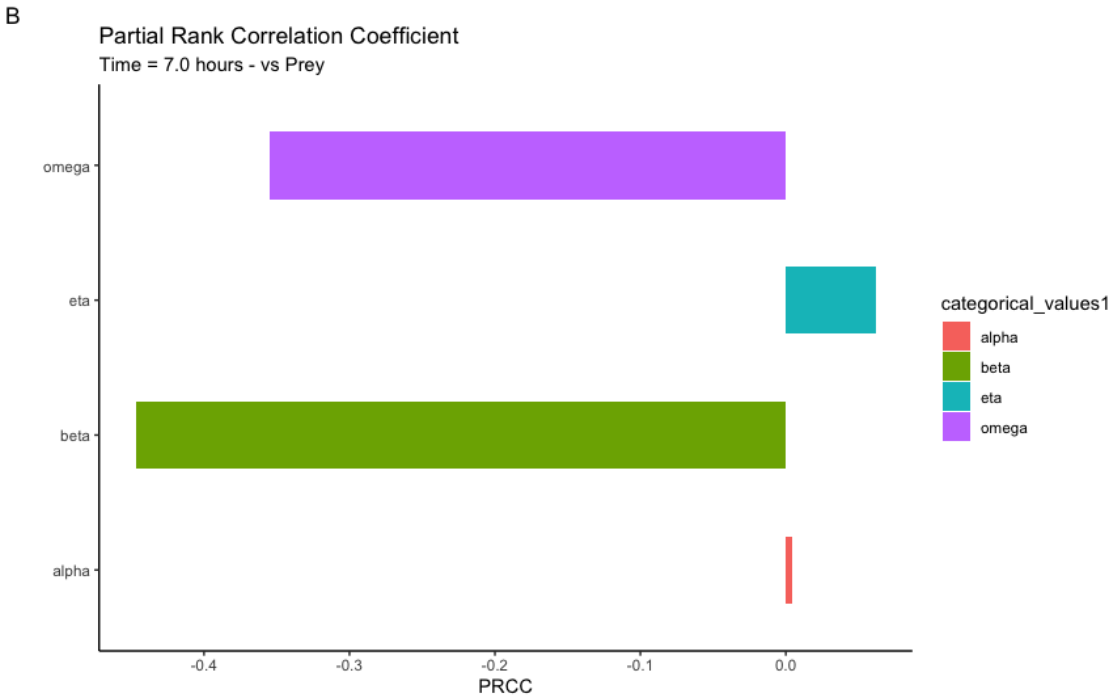

Parameter	PRCC	P-value	Significant?
α	0.0826	$3.92e-01$	No
β	-0.9290	$1.39e-350$	Yes
η	-0.0809	$1.04e-02$	Yes
ω	0.7068	$2.91e-152$	No

Parameter	PRCC	P-value	Significant?
α	0.0040	$8.98e-01$	No
β	-0.4467	$3.64e-50$	Yes
η	0.0615	$5.16e-02$	No
ω	-0.3545	$2.91e-31$	Yes

Figure 2.12: PRCC results for T = 7.0 hours. Figure A is a histogram of the PRCC values for each parameter in relation to y (predators). Figure B is a histogram of the PRCC values for each parameter in relation to x (prey). These PRCC values are shown in the attached tables where we indicate the significance of each parameter according to its p-value.

2.6 *UTImodel*: Sensitivity Analysis

2.6.1 Introduction

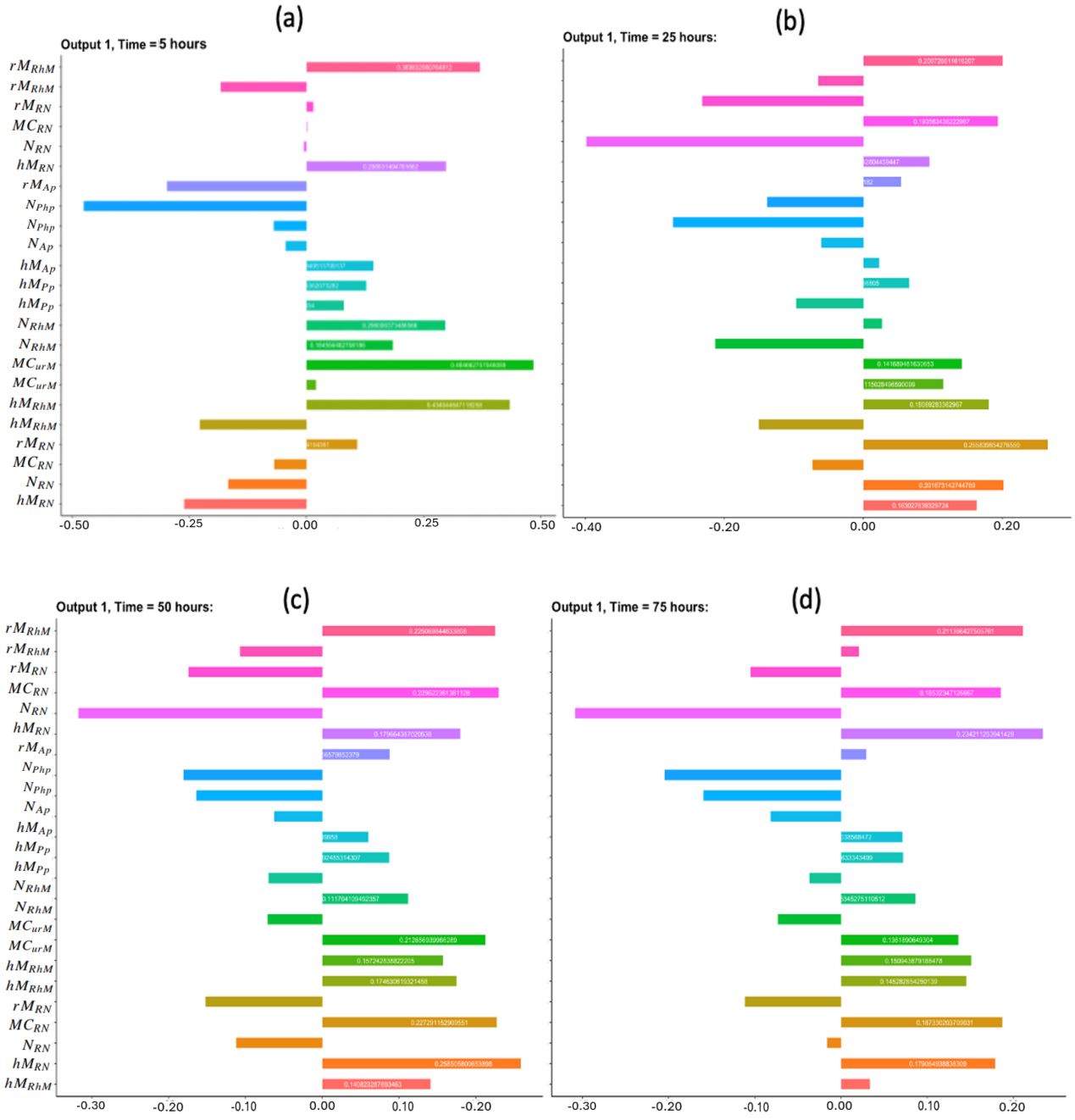

Figure 2.13: UASA- Output 1 (Bacterial Load): PRCC values for all parameters involved in UA.

In this section, we explore the sensitivity analysis results. As with the verification

performed with the Lotka-Voltera model, we must first start by defining our parameter space. As very little a-priori information is given about the parameters, we opt to use a uniform distribution with specific ranges for each parameter. Some of these ranges have been collected from literature, while others are simply baseline estimates. Once our LHS sample has been generated using the parameter probability distribution in Table 2.4 below, we proceed to evaluate the PRCC values of the parameter sets for each output. This is done by applying the same methodology followed in Section 2.5.4.3. In order to analyse our simulation thoroughly, we collect the output values for various time points into separate data frames and perform sensitivity analysis for each model output separately. This is a crucial step as the model output consists of many variables. Hence, in order to perform full UASA, we specify first the model outputs and perform the previously implemented techniques for each output separately. We choose to focus our sensitivity analysis on the following outputs:

- Output 1: Number of **bacteria**.
- Output 2: Number of **bacteria** killed by **neutrophils**.

Variables such as bacterial load, immune load and number of cleared bacteria by any specific immune cell are important to analyse. As shown in the literature, the neutrophil load during initial stages of infection can be essential to the infection outcome of UTIs. Hence, the variability introduced from our parameters to these outputs must be explored further in order to eventually better tune our model.

2.6.2 Output 1 - Bacterial Load

While conducting sensitivity analysis for bacterial load we choose to generate histograms containing the PRCC values of all parameters at the following time-points: $T = 25, 50, 75$ hours. As can be seen from Figure 2.13, variability of neutrophil parameters can lead to significant changes in the bacterial load output, shown by the

Parameter	PRCC	P-value	Significant?
rM_{RN}	0.2550	$9.05e10-3$	**Yes**
hM_{RN}	−0.1655	0.2919	No
rM_{AP}	0.1520	0.2919	No
hM_{AP}	−0.0494	0.7329	No
MC_{UrM}	0.2157	0.13295	No
MC_{RN}	0.0799	0.6921	No
N_{RhM}	0.0788	0.58628	No
N_{AP}	−0.1374	0.3411	No
N_{RN}	0.2908	$4.05e10-3$	**Yes**
rM_{RhM}	−0.0969	0.50289	No
hM_{RhM}	0.19323	0.17878	No

Table 2.3: Output 1: PRCC values of parameters responsible for recruitment, movement and activation of immune cells at T = 5 hours. Significance is established when $p-value < 0.01$.

PRCC values. Neutrophil parameters such as movement rate, activation probability and ability to kill bacteria carry a significant[1] PRCC value. This represents the importance of neutrophils during the initial stages of infection for bacterial clearance. Recruitment of resident macrophages from the blood vessels, along with their movement rate, is shown to carry significance to bacterial clearance through PRCC values.

In order to further investigate PRCC values from parameters of relevance, we also produce a figure showing PRCC values throughout the model simulation time for a range of selected parameters. We choose to focus on N_{AP} (neutrophil activation probability), N_{phP} (probability of bacterial killing by neutrophil) and N_{RN} (neutrophil movement rate) as they have shown significance in Figure 2.13. As illustrated in Figure 2.13, N_{AP} and N_{RN} achieve high PRCC values at early stages

[1]The PRCC value of a parameter is considered significant when the attached p-value satisfies $p < 0.01$

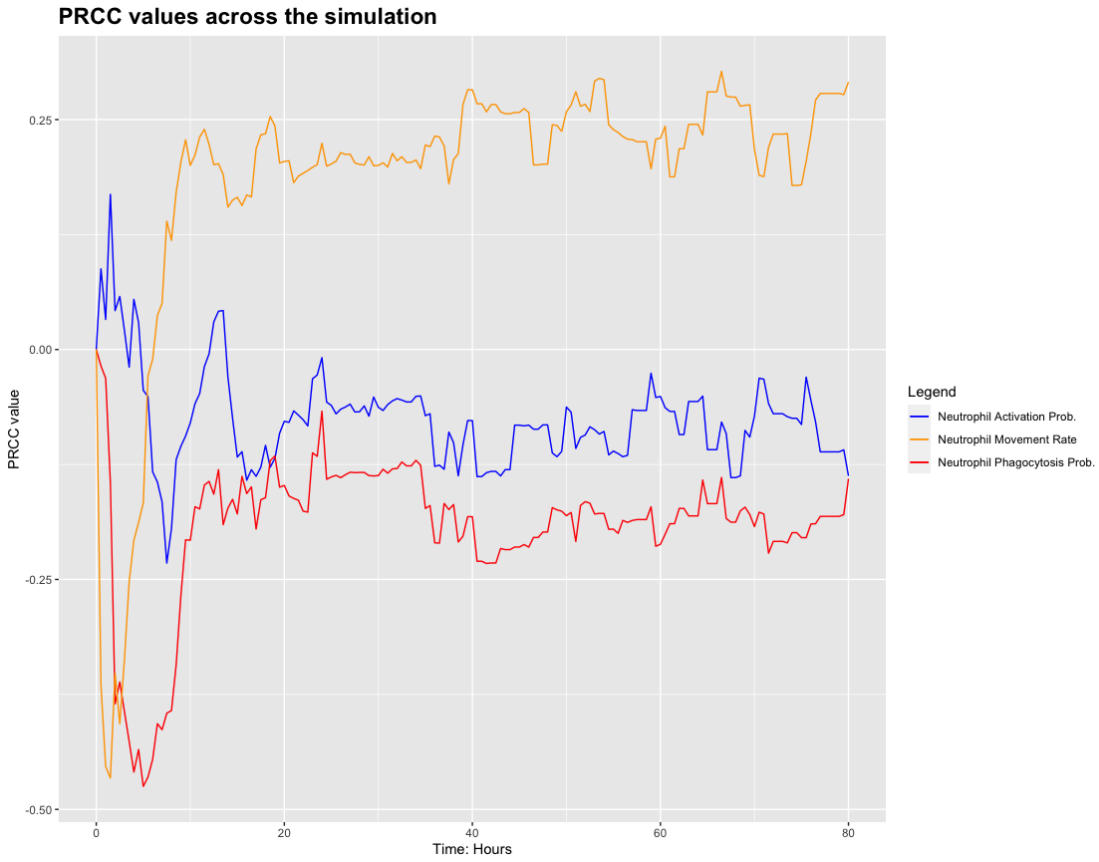

Figure 2.14: Plots of the PRCC curves for 3 model parameters: N_{AP}, N_{RN} and N_{phP}.

of the model (T = 2-4 hours) due to involvement in actions such as neutrophil activation and movement. The PRCC curve for N_{phP} follows a similar pattern to both parameters mentioned prior, however, as this parameter is responsible for the ability of neutrophils to kill bacteria (which happens after recruitment and activation of the neutrophil), maximal PRCC values are achieved at $T = 6$ hours. Figure **??** shows how significance of the parameters listed above evolved over time within our simulation. This work highlights how important it is to correctly estimate neutrophil parameters. Future experimental work to this effect has been suggested to our collaborators working in the field of UTI immunology.

Distribution	Parameter	min-value	max-value
Uniform	rM_{RN}	0.01	0.1233 – 0.1982
	hM_{AP}	0.01	0.14902
	rM_{AP}	0.01	0.133300
	N_{RhM}	0.001	0.07179 – 0.140252
	N_{AP}	0.01	0.1488802
	N_{phP}	0.01	0.114296 – 0.171797
	N_{RN}	0.1	0.12445 – 0.238014
	rM_{RhM}	0.001	0.031795 – 0.101217
	hM_{RhM}	0.001	0.00717 – 0.051795
	MC_{RN}	0.01	0.14314 – 0.26691
	MC_{UrM}	0.001	0.0033 – 0.03236
	hM_{Pp}	0.01	0.12429 – 0.137977

Table 2.4: Parameters used to conduct UASA.

2.6.3 Output 2 - Bacterial Clearance due to Neutrophils

In a similar fashion to the previous section, we now investigate the sensitivity analysis results on the output representing the number of bacteria killed by neutrophils. In doing so, we look at the model parameters responsible for the variability in bacterial clearance.

As mentioned during the literature review, many models both *in vivo* and *in vitro*, point towards the importance of neutrophils during the early stages of infection for bacterial clearance. As can be seen in Figure 2.16, the movement rate for activated neutrophils has a maximal PRCC value of 0.4. Other significant parameters include the neutrophil movement rate, killing and recruitment probability. As we look at later times in the model, we see how the significance of recruited immune cell related parameters declines. As expected from our model, after an initial stage of recruitment rush due to bacterial detection by resident immune cells (such as resident macrophages and mast cells) during which recruited immune cells carry high significance due to bacterial clearing, we expect resident immune cells such as

resident macrophages to present high significance at later stages of the simulation through their associated parameters. In Figure 2.16, we can clearly see the contrast in behaviour previously described in relation to resident and recruited immune cells, and their significance profile throughout the simulation. In addition to these plots, we also reproduce tables with additional statistical tests as we did during our verification step (see Table 2.3 and Table 2.5). This includes the p-value attached to each PRCC value, the exact PRCC value and whether such a parameter is deemed significant.

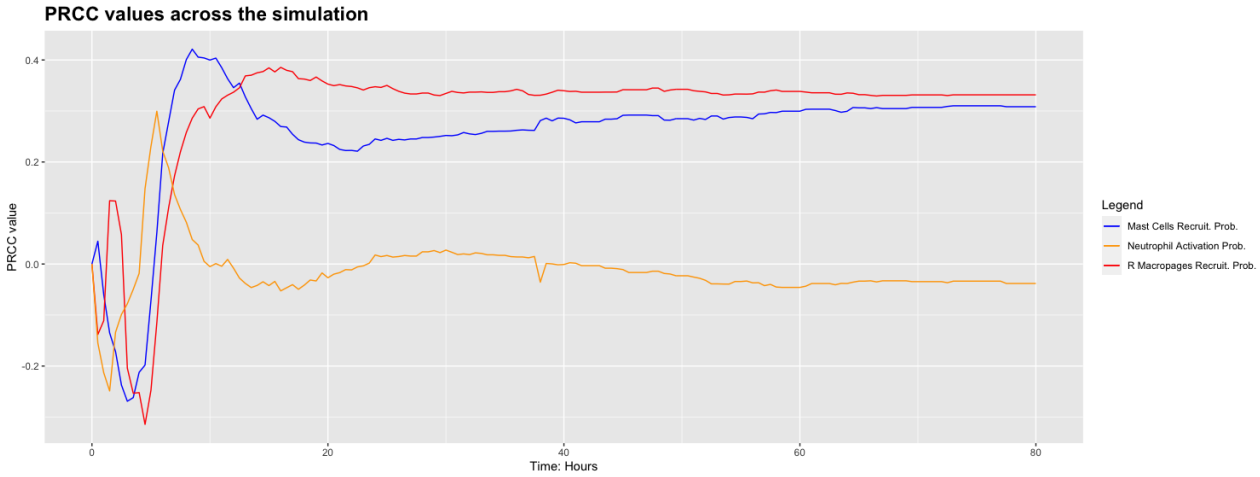

Figure 2.15: UASA- Output 2 (Bacterial Clearance - Neutrophils): PRCC values for all parameters involved in UA.

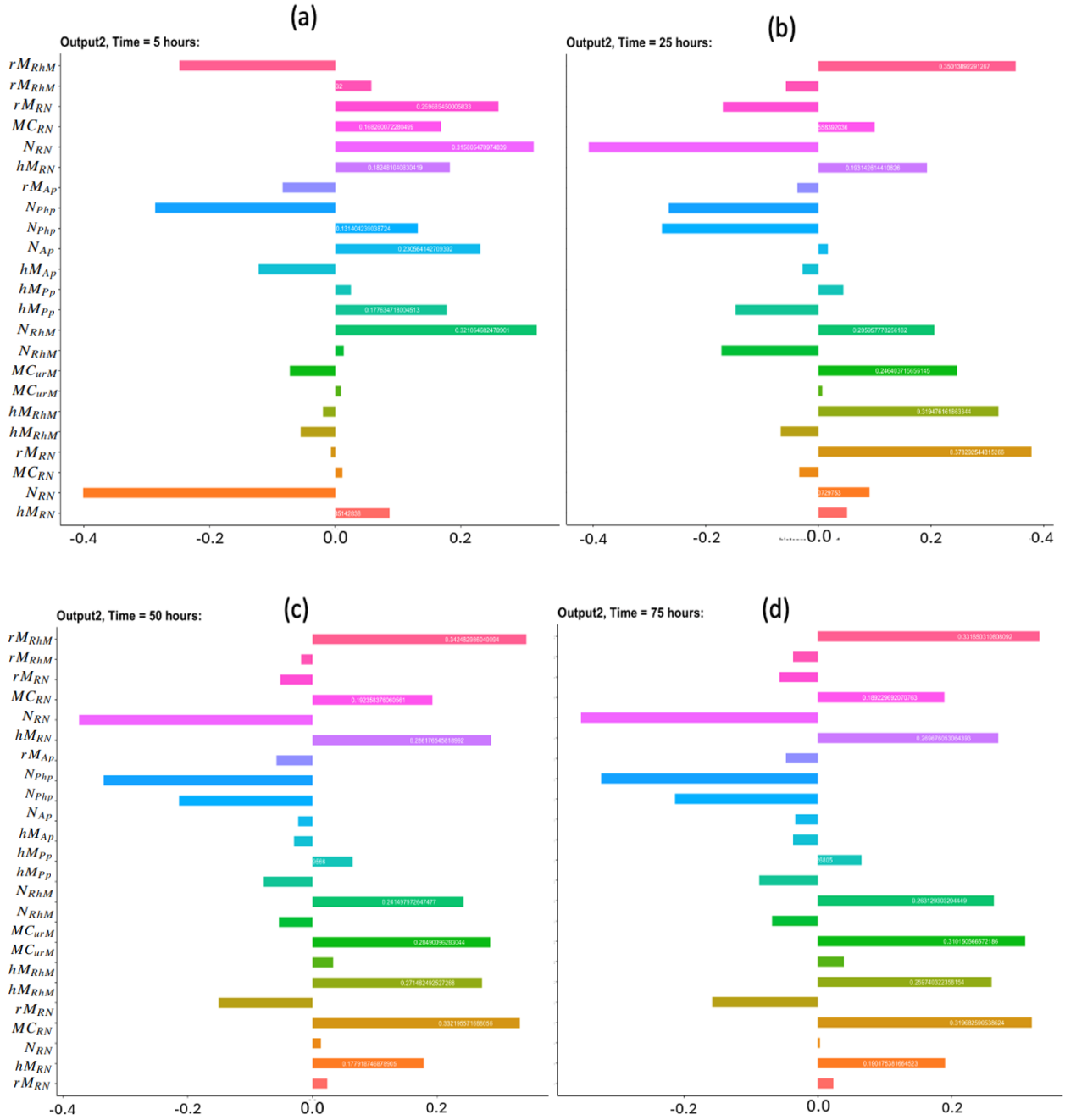

Figure 2.16: UASA- Output 2 (Bacterial Clearance - Neutrophils): PRCC values for all parameters involved in UA at times $T = 5, 25, 50, 75$ from (a)-(d) respectively.

Parameter	PRCC	P-value	Significant?
rM_{RN}	0.1142	0.4295	No
hM_{RN}	−0.0988	0.49456	No
rM_{AP}	0.05774	0.6903	No
hM_{AP}	0.1763	0.1504	No
MC_{UrM}	−0.2372	0.0971	No
MC_{RN}	0.11332	0.4332	No
N_{RhM}	0.2953	0.00897	**Yes**
N_{AP}	−0.16856	0.2419	No
N_{RN}	0.115220	0.4255	No
rM_{RhM}	−0.10703	0.4594	No
hM_{RhM}	−0.4250	0.00209	**Yes**

Table 2.5: Output 2: PRCC values of parameters responsible for recruitment, movement and activation of immune cells at T = 5 hours. Significance is established when $p - value < 0.01$.

2.7 Conclusion

In this chapter we introduced the framework for our agent-based model by first looking at an overview of the bacteria, immune agents, the environment and the rules governing the interactions between all these agents. In doing so we built a table of all the model parameters. In Table 2.1 we can see all the model parameters and their values along with the origin of these values. We also introduce the integrated chemokine dynamics, in which our immune cells move along the gradient of a chemokine secreted by resident macrophages, allowing immune cells to move towards the infection. We introduce the model mechanism for bacterial shedding to simulate the process of bladder wall shedding and the subsequent reduction of the bacterial burden. We do this by voiding the environment in our model of bacteria and repopulating it with the bacteria that was able to earlier penetrate the bladder wall when it came into contact with immune cells such as neutrophils or helper macrophages.

Once the model is presented we described the uncertainty and sensitivity analysis framework that allowed us to study the effects our model parameters have on the

outputs. The UASA framework is tested on the Lotka-Volterra predator prey model, which allows us to compare the results from our UASA framework against those publicly available, thus validating this framework.

In the next step, we used our UASA framework to study the effects of parameters on the model output. We find that the parameters associated with neutrophils and macrophages, such as movement rate, recruitment probability and activation probability are significant parameters affecting the bacterial load output of our model, especially during the early stages of the infection. This is consistent with the literature, as recruitment of macrophages and neutrophils is known to be crucial during the early stages of infection for detection and clearance. After the early stages of the infection, the parameters carrying high significance are those responsible for recruitment of immune cells such as resident macrophages, helper macrophages and neutrophils in particular.

In the next chapter we will focus our analysis of this model, focusing on the initial bacterial load and how it affects the infection outcome, along with analysing the effects of bacterial shedding. This will allow us to use our model in order to study aspects of bladder infections that prove difficult to study through experimental means. This will allow us to answer critical questions such as the importance of initial bacterial load on the development of infection, and the possible growth profiles arising from different initial bacterial loads.

Chapter 3

ANALYSIS OF THE EFFECTS OF INITIAL BACTERIAL LOAD AND BACTERIAL SHEDDING ON INFECTION OUTCOME

3.1 Introduction

Currently, our model describes bladder infections by being able to capture a number of possible outcomes. Individual simulations may resolve in a variety of ways; bacteria may colonise the modelled bladder section, immune cells may be able to fight back and completely eradicate bacterial infection with the combination of immune agents and periodic bacterial clearance through shedding of the bladder wall or an infection may persist in small numbers without having the ability to successfully evade the immune system. Within our model, we characterise the behaviour of each bacteria through a series of rules and parameters. Initially, I_B bacteria are seeded, each following a specific replication rate, B_{sp} (within a determined neighbourhood depth, $N_{db} \in \mathbb{Z}_{>0}$).

Symbol	Parameter description	Values	Units	Source
Bacteria (E. Coli)				
I_B	*minimal infectious dose*	1-1000	unitless	e
B_{sp}	*Bacterial replication speed*	0.52-0.84	hours	e
N_{db}	*neighbourhood replication depth*	2	unitless	e
S_B	*Bacterial load for shedding*	6000	unitless	e
P_{Bp}	*prob bacteria penetrates the bladder wall*	0.156332435	unitless	e

Table 3.1: Parameters for bacterial action within *UTImodel*

We will now investigate the effect that I_B can have on the infection outcome which will allow us to gain better insight on how heavy initial bacterial loads compare to lighter bacterial presence at initial stages of bladder infection and how this can affect the initial outcome and the recurrence profile. We must first establish a baseline for all the parameters within our model, for which we use the values outlined in Chapter

2. We also note that as described in the Introduction our model output frequency is 0.5 hours, thus, all plots representing model simulations are created through these discrete datapoints. Next, our analysis will focus on the parameters responsible for bacterial seeding and growth.

Symbol	Parameter description	Values	Units	Source
Macrophages ($Ly6C^{-}$)				
I_{rM}	*initial No. resident macrophages*	500	unitless	e
rM_{ls}	*resident macrophages lifespan*	30-32	hours	r
rM_{RhM}	*resident macrophages recruitment prob.*	0.04-0.08	unitless	e
rM_{RN}	*resident macrophages movement rate*	0.17-0.26	hours	e
rM_{Ap}	*resident macrophages activation prob.*	0.261	unitless	e
Macrophages ($Ly6C^{+}$)				
hM_{ls}	*helper macrophage lifespan*	30-32	hours	r
hM_{RhM}	*helper macrophages recruitment prob.*	0.007-0.031	unitless	e
hM_{RN}	*helper macrophages movement rate*	0.13-0.18	hours	e
hM_{Ap}	*helper macrophages activation prob.*	0.129	unitless	e
hM_{Pp}	*helper macrophages killing prob.*	0.12-0.13	unitless	e
Neutrophils				
N_{ls}	*neutrophil lifespan*	30-32	hours	r
N_{RN}	*neutrophil movement rate*	0.12-0.23	hours	e
N_{RhM}	*neutrophil recruitment prob.*	0.07-0.14	unitless	e
N_{Ap}	*neutrophil activation prob.*	0.148	unitless	e
N_{Php}	*neutrophil killing prob.*	0.11-0.17	unitless	e
Mast Cells				
I_{MC}	*initial No. mast cells*	50	unitless	e
MC_{ls}	*mast cell lifespan*	30-35	hours	e
MC_{RN}	*mast cell movement rate*	0.14-0.26	hours	e
MC_{urM}	*mast cell recruit. prob.*	0.003-0.033	unitless	e

Table 3.2: Immune agent parameters in *UTImodel*

3.2 Initial Bacterial Load

Here we investigate the effect that the initial bacteria load, I_B, can have on the infection dynamics. We first fix all model parameters, with the exception of I_B. Subsequently, we generate 200 simulations through each variation of I_B. It's important to note that for very small numbers of cells, continuum models may not be applicable due to their inherent assumption of large populations and steady-state conditions.

As we simulate 80 hours, we will refer to an infection as being in the early stages when $t \in [0, 15)$ hours. We refer to $t \in [15, 30)$ hours as the middle stage of infection, which in the literature is identified as the stage when recruited immune cells are heavily involved in bacterial clearing. Finally, we refer to $t \in [30, 80]$ hours as the late stage of the infection. Bacterial shedding occurs within the model when $N_B > 6000$, which usually occurs during the late stages of infection. Throughout this analysis, we will use the following notation $N_B^{T=y}$ to refer to the bacterial load at time y hours.

3.2.1 Case where $I_B = 1$

When choosing $I_B = 1$, there is a large amount of variation in infection outcomes. Progression profiles of UPEC can be observed, each resulting in a different final outcome. Figure 3.1 shows the number of bacteria from $T = 0$ to $T = 15$, for 4 simulations that highlight the extremes of infection progression outcomes. In Figure 3.1 (a), bacterial replication within the initial hours is slow; however, UPEC manages to evade the efforts of clearance by the immune cells and is able to replicate at higher rates towards the end of the early stage, reaching a final bacterial load of $N_B^{T=15} = 120$. In Figure 3.1 (b) however, the infection progresses initially at a higher rate reaching a bacterial load of $N_B^{T=6} = 420$. Following this, the immune response manages to achieve good partial clearance outpacing replication at $T = 7.5$ hours. Towards the end of the early stage, the bacterial load is $N_B^{T=15} = 218$. In Figure

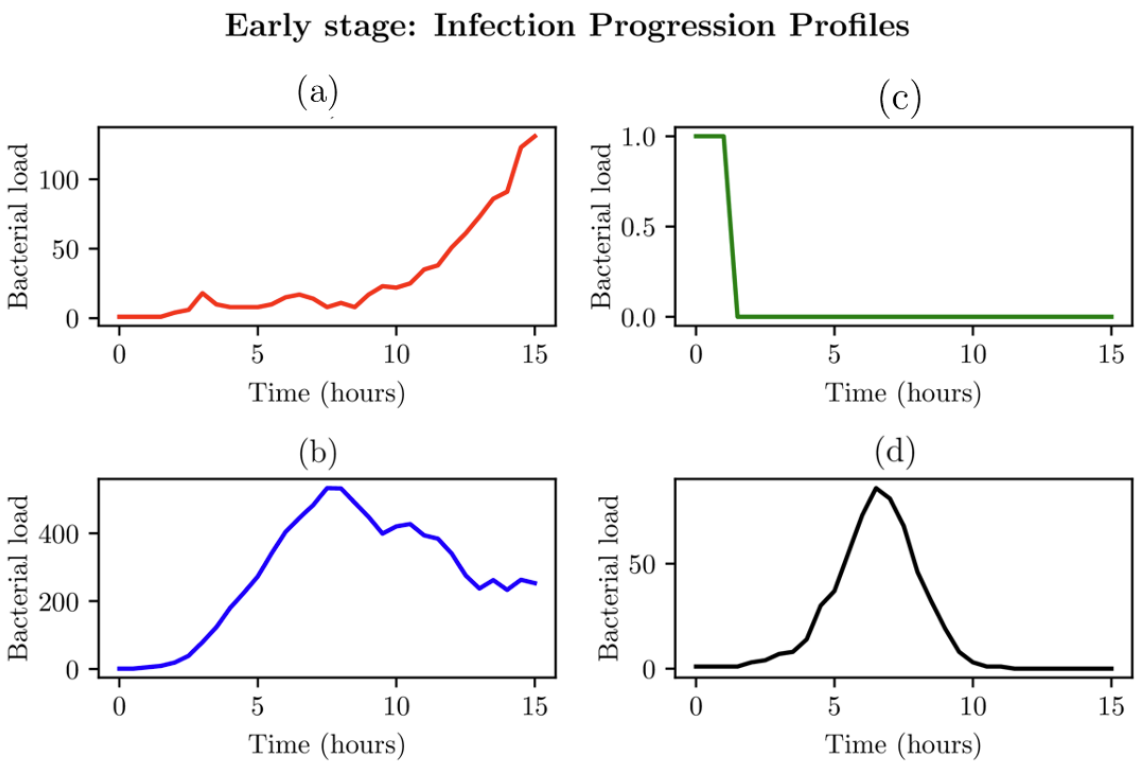

Figure 3.1: Simulations (a)-(d) represent 4 different bacterial growth profiles arising with $I_B = 1$. We can see from a) slow initial growth until approximately the 10 hour mark when replication becomes exponential. From b) we can see an almost immediate clearance of bacteria by the immune cells without allowing replication. While the other 2 profiles b) and d) describe average replication in the initial stages almost unhindered by immune activity. In both we can see how after 7 hours approximately the immune action begins to take effect completely clearing bacteria in d)

3.1 (c), bacteria is almost instantly cleared prior to being able to replicate, where immune cells successfully kill the bacteria. As immune cells are initially randomly placed within our grid, it is possible for an individual simulation to have immune cells within the immediate vicinity of I_B, which, in addition to having a low initial bacterial load ($I_B = 1$), leads to fast and total clearance of bacteria. In Figure 3.1 (d), the infection progresses quickly, reaching $N_B^{T=6} = 100$. The bacterial increase however, although steady throughout the early stage of the infection, halts and the immune system manages to successfully clear all bacteria with $N_B^{T=15} = 0$. To gain a better insight into the immune clearance process we also present Figure 3.2

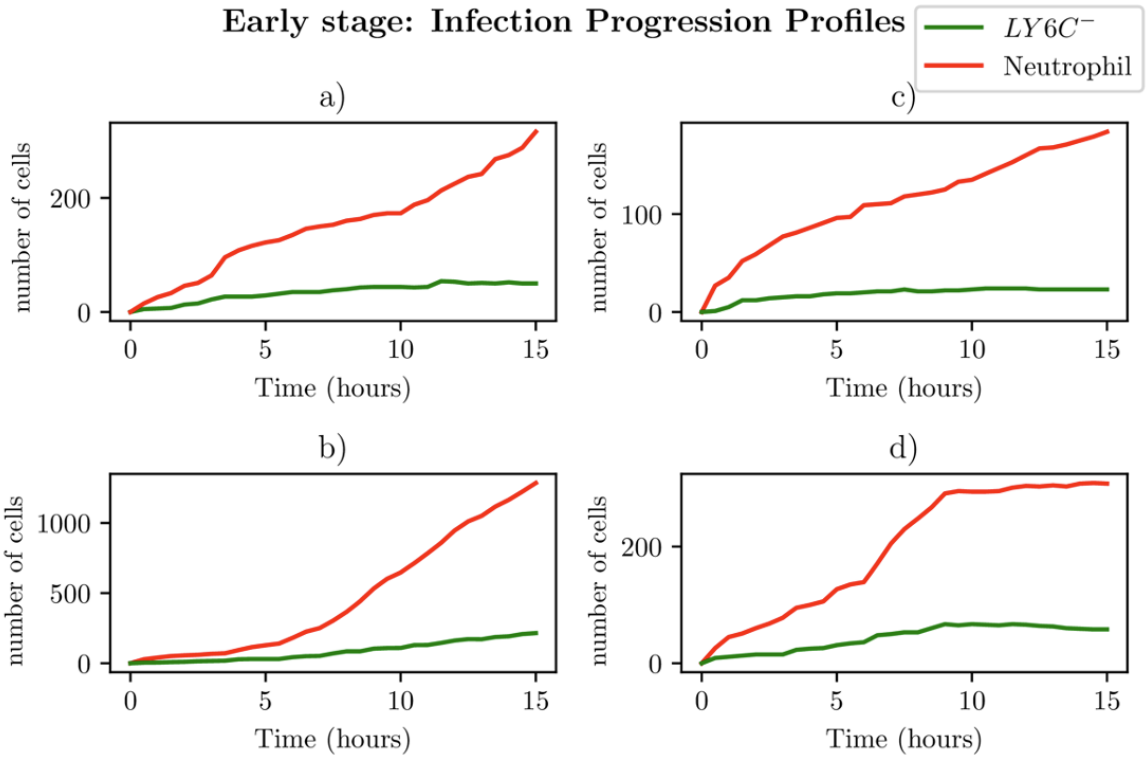

Figure 3.2: Simulations (a)-(d) represent the neutrophil and helper macrophages ($LY6C^-$) profiles arising from the case $I_B = 1$. The specific simulations correspond to those shown in Figure 3.1.

which describes the immune cell dynamics for the same 4 simulations as shown in Figure 3.1. As expected, we see here higher recruitment of both macrophages and neutrophils in simulations with higher bacterial loads. Figure 3.3 shows spatial plots of the simulation shown in Figures 3.1(a) and 3.2(a) at timepoints $t = 0, 5, 10, 15$ hours. We see here as the infection progresses, there is a large influx of immune cells through the blood vessels that are subsequently directed by the chemokine signal to the site of infection at the centre of the domain. We see that, at $t = 15$ hours, the immune response has not been successful in containing the infection spread.

While analysis of these individual simulations for the first 15 hours is useful, we also look at the aggregate[1] behaviour resulting from our simulations with $I_B = 1$. With a total of 200 simulations, run for a total of 80 hours, clearance was achieved

[1]This is done by looking at the totality of simulations and calculating various standard statistics to determine the normal behaviour of the outputs of intere

in 76.7% of instances. Within these, the vast majority (65.8%) was due to early clearance, i.e. before 15 hours, with mid and late clearance accounting collectively for the remaining 10.9% of clearance cases.

Thus, our model indicates that a low initial bacteria load usually leads to total bacterial clearance within the initial stages of infection, with the majority of instances achieving total clearance within 6 hours. However we see in this work that when only a single bacterium can lead to significant infection spread, as in 23.3% of simulations, clearance was never achieved. Here the bacteria were able to further colonise bladder epithelial tissue, bypassing immune cell action and bacterial shedding.

3.2.2 Case where $I_B = 100$

We now investigate an initial bacterial load of $I_B = 100$, by examining the different possible infection progression profiles. As can be seen in Figure 3.4, total clearance here does not occur at any time before $T = 6$ hours, with the simulations in Figure 3.4 (a)-(d) showing early periods of considerable bacterial growth before halting due to immune cell intervention. Simulation (a) presents an individual infection simulation where the bacterial load reaches a maximum of $N_B^{t=4.5} = 280$, after which, the immune response achieves successful total clearance. Simulation (b) on the other hand presents a relatively steady bacterial load until $T = 9.50$ hours, reaching $N_B^{T=9.5} = 327$, after which the immune cells are only able to achieve partial clearance of the bacteria, with $N_B^{T=15} = 107$. In simulations (c) and (d) we see the bacterial load decline occurring earlier in the simulations, with successful immune responses to the infection.

In looking at the aggregate of the 200 simulations where $I_B = 100$, we can see that bacteria persist in 30.8% of simulations (as opposed to 23.3% when $I_B = 1$). Early clearance accounted for 45.8% of simulations while mid stage clearance accounted for 21.9% of instances. Late clearance was achieved in 3 simulations (1.5%). See Figure 3.5 for pie charts summarising this.

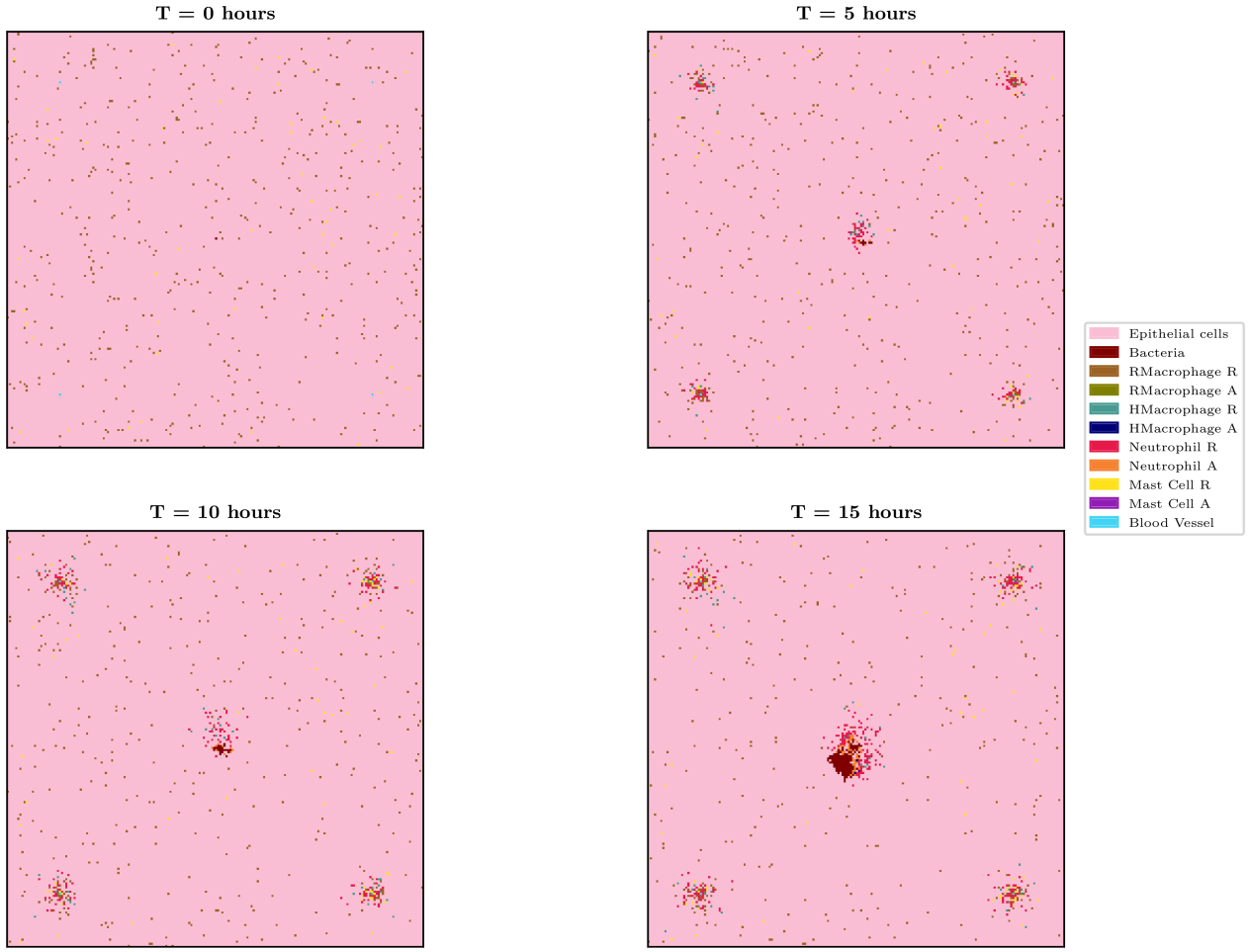

Figure 3.3: Spatial plot showing the agents in the system for simulation (a) from Figures 3.1 and 3.2 at times $T = 0, 5, 10$ and 15 hours. Agents and blood vessels indicated by the key in the plot.

Although an increased I_B causes recruitment of immune cells at earlier times to the site of infection in comparison with lower I_B, bacteria are able to replicate and reach higher loads, typically having reached a maximum within the initial 5 hours. As can be seen in Figure 3.4, both (b)-(c) instances attained bacterial loads $N_B > 300$.

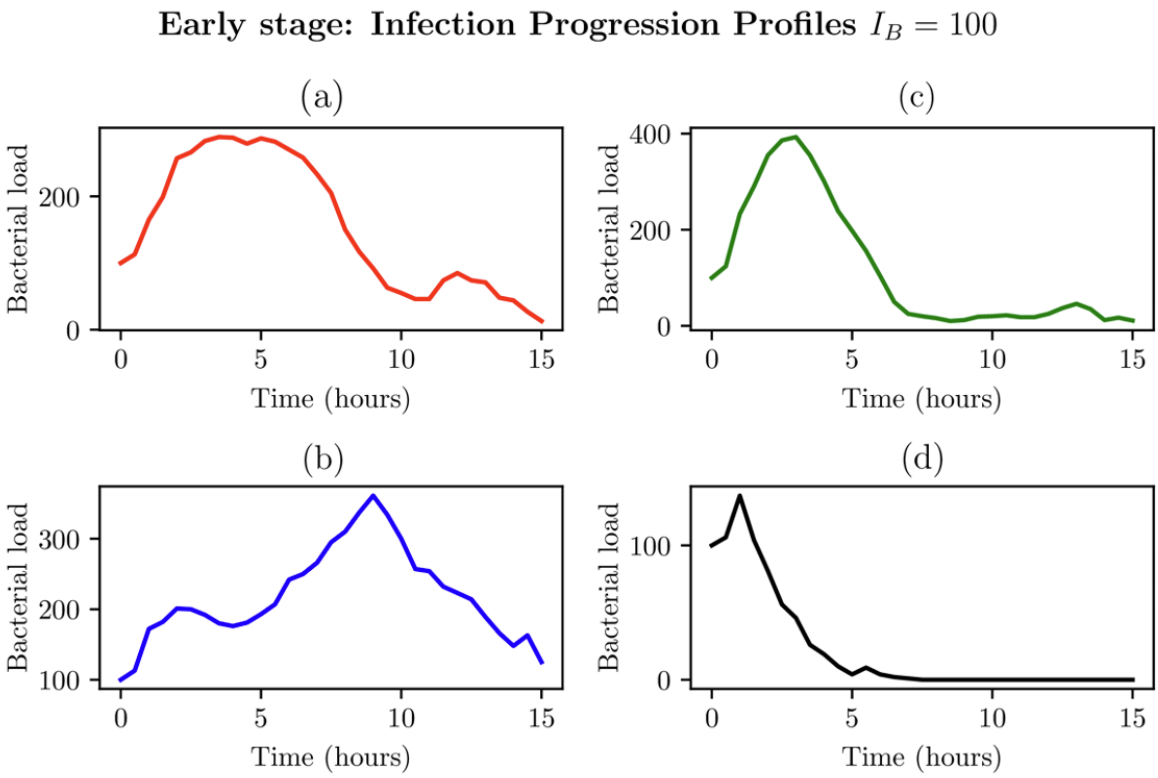

Figure 3.4: Simulations (a)-(d) represent the bacterial growth profiles arising from 4 simulations chosen to represent different possible outcomes for I_B = 100.

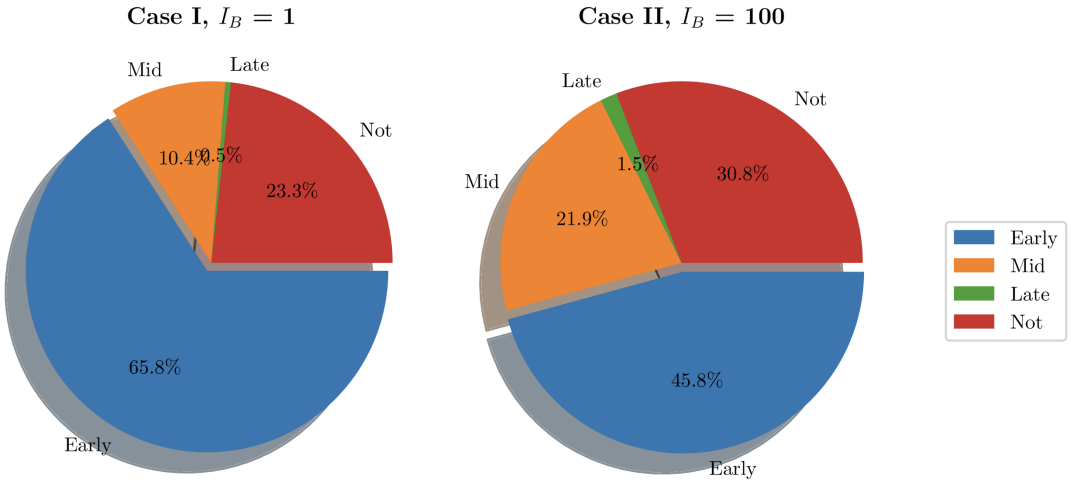

Figure 3.5: Pie charts summarising bacterial clearance status for simulations with I_B = 1 and I_B = 100.

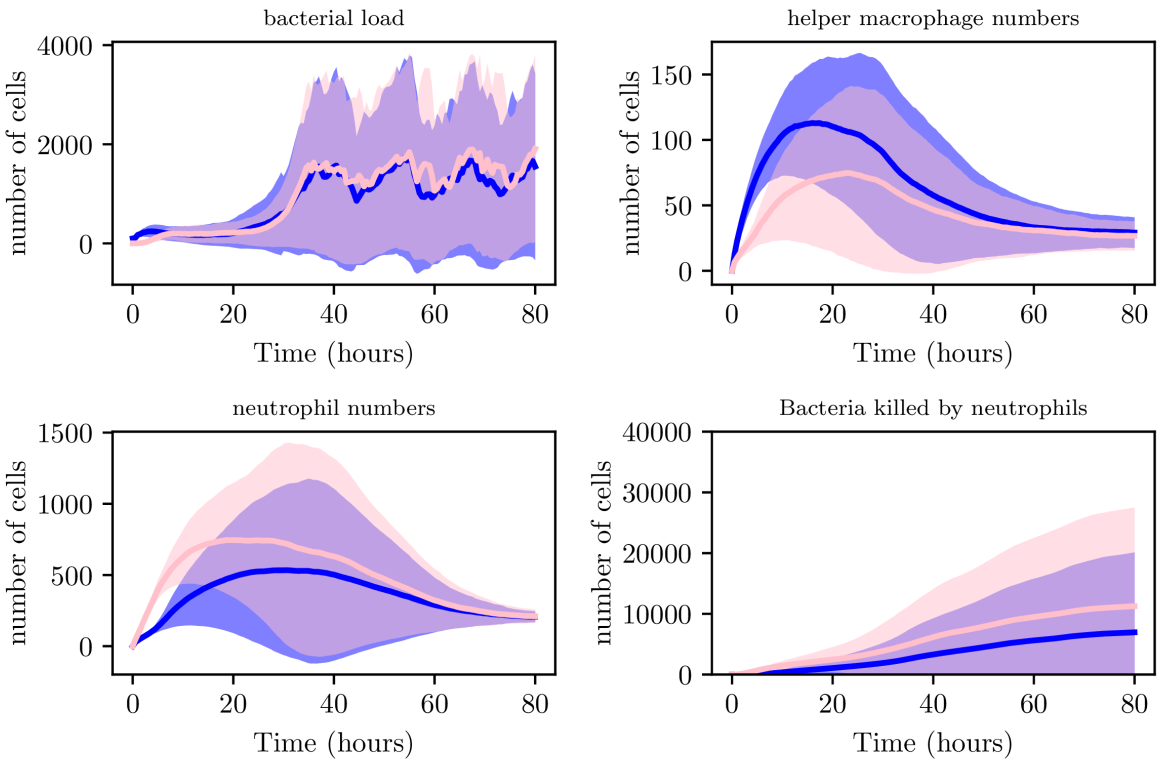

Figure 3.6: Average values for bacterial load, helper macrophage load, neutrophil load and neutrophil clearance for simulations with $I_B = 1$ (shown in blue) and for simulations with $I_B = 100$ (shown in pink), with 95% confidence intervals (shown by the shaded regions).

Reaching these stable numbers allows the bacterial population to persist despite attempted clearing by neutrophils and helper macrophages. Through analysis of spatial plots we can see that earlier immune cell intervention in simulations with $I_B = 100$, as opposed to simulations with $I_B = 1$, is due to the closer proximity of the boundary of the bacterial population to recruited immune cells. As can be seen from Figure 3.6, the aggregate profiles and patterns of bacterial growth in the $I_B = 1$ simulations are similar to those with $I_B = 100$. The differences in the profiles of helper macrophages, neutrophil and bacterial clearance are due to the higher intensity of immune action due to the increased initial bacterial count.

3.3 Bacterial Replication Rate

Studies have shown that UPEC presents different replication profiles [18, 15]. At early stages of the infection, *E. coli* replicates with an average doubling time of 20-45 minutes [98, 90]. As the infection progresses however, research has shown that UPEC adopts a relatively lower replication rate, estimated with a doubling time of 40-60 minutes [41, 15]. We now include this to our model and investigate the effects on bacterial clearance and immune presence. In order to do this, we include two parameters describing the replication rate. $B_{earlysp}$ describes the replication rate during the earlier stages of the model (when $t < 10$ hours). On the other hand, B_{latesp} is then used after 10 hours. Hence, we set

$$B_{sp} = \begin{cases} B_{earlysp}, & t < 10 \text{ hours} \\ B_{latesp}, & t \geq 10 \text{ hours} \end{cases} \tag{3.1}$$

Here we analyse the output resulting from 1000 individual simulations of our model. We allow UPEC to adopt two replication profiles as detailed above, whilst also varying the initial bacterial load, $I_B \in \{1, 100, 500, 1000\}$, with 200 simulations performed for each case.

This will allow us to investigate the effects I_B can have on the progression of the infection. As can be seen from Figure 3.7, during the initial 2 hours, lower I_B present a relatively slower growth rate while high I_B will initially present with a much higher growth rate. These differences however are less noticeable when looking at $2 < T < 9$ hours, as the bacterial count of high I_B begins to decline due to clearance by neutrophils and helper macrophages that have arrived at the site of infection. While in contrast, a low I_B allows bacteria to maintain a steady growth within the interval $2 < T < 6$ hours. Once $9 < T < 14$ hours, all simulations converge closely. The final bacterial load of the early stage, $N_B^{T=15}$, matches in order of initial bacterial count except for $I_B = 1$ which has managed to overtake $I_B = 100$.

Although the trend appearing from the early stages of infection seems to indicate possible bacterial clearance, once we look at the later stages of the simulation we realise the importance bacterial shedding plays, where we see the periodic nature of the bacterial profiles.

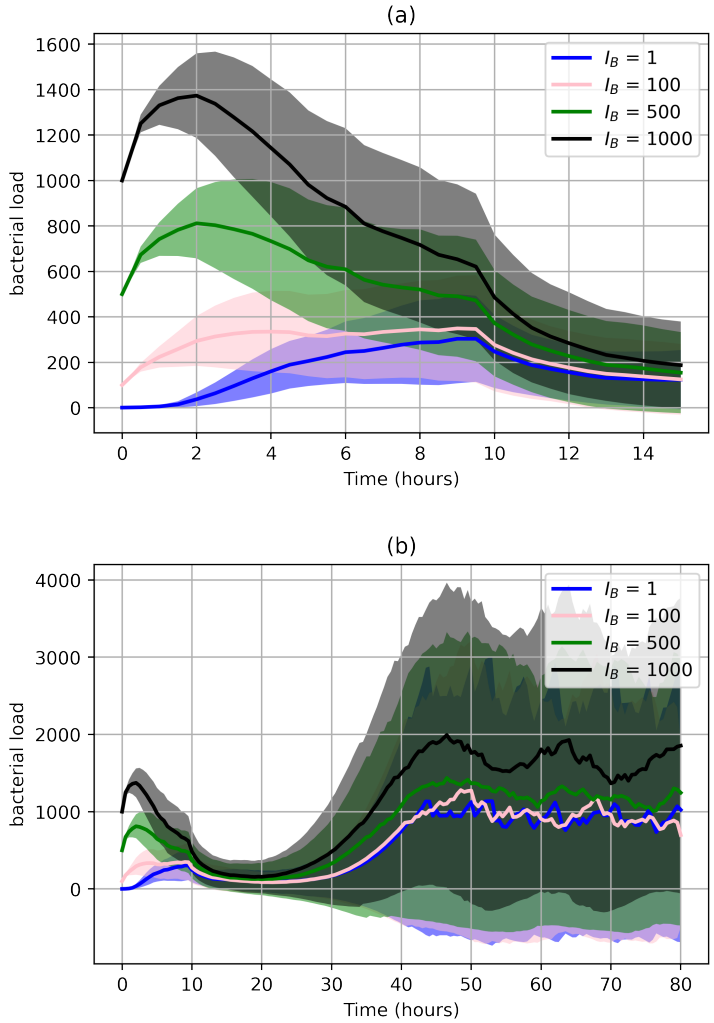

Figure 3.7: Average values for bacterial load. (a) The early stage with initial bacterial loads $I_B \in \{1, 100, 500, 1000\}$. (b) The average loads throughout the entire simulation ($0 < T < 80$). 95% confidence intervals are shown by the shaded regions.

As illustrated in Figure 3.7, although the growth of UPEC during the early stages can be slow and heavily hindered by neutrophils, at later stages bacterial growth increases significantly. Consequently, bacterial shedding can be a crucial mechanism

to control infection within the superficial urothelium and prevent full colonisation of the bladder wall.

Similarly to Figure 3.5, we show the pie charts of these simulations where we have taken the following initial bacterial loads: $I_B = 500$ and $I_B = 1000$. In contrast to the earlier analysis shown in Figure 3.5 where we looked at relatively low initial bacterial loads, Figure 3.8 presents the clearance in the case of high initial bacterial loads. As we can see, with higher initial bacterial loads, clearance is not achieved in 40.6% of instances (when $I_B = 500$) and 61.9% when ($I_B = 1000$). In addition to this, total bacterial clearance is now achieved generally during the middle stages of infection rather than early stages as was shown with $I_B = 1$ and $I_B = 100$. This signals towards the ability of higher I_B to establish more severe infections.

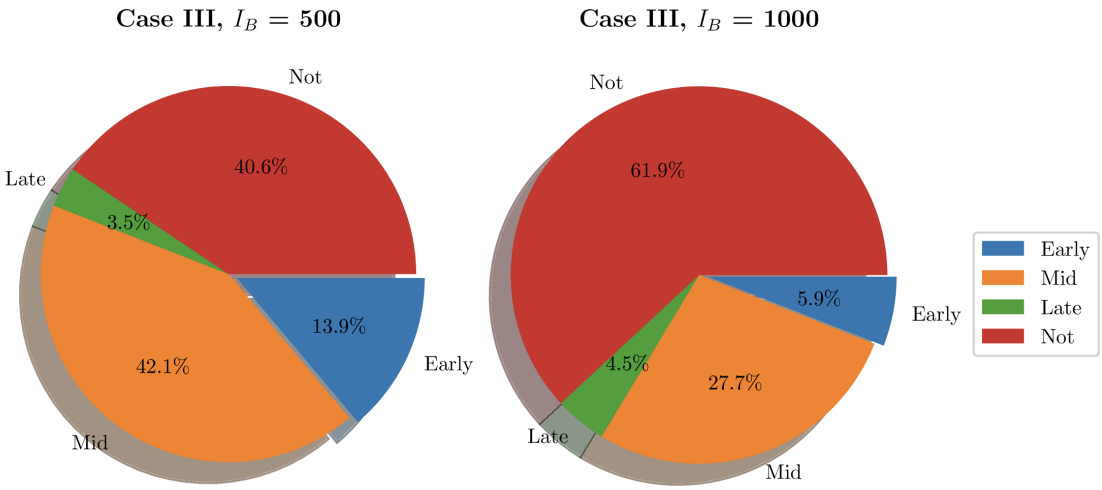

Figure 3.8: Pie charts summarising bacterial clearance status for simulations with $I_B = 500$ and $I_B = 1000$.

3.4 Simulating an Immunocompromised Environment

We now generate 200 simulations with $I_B = 1$, however, we change the number of resident immune cells to reflect an immunocompromised environment. We set $I_{rM} = 300$, and $I_{MC} = 30$ (as opposed to all previous simulations where $I_{rM} = 500$ and $I_{MC} = 50$). As can be seen in Figure 3.9, in an immunocompromised environment with low initial loads of resident immune cells, our model indicates that bacteria are able to establish larger infections.

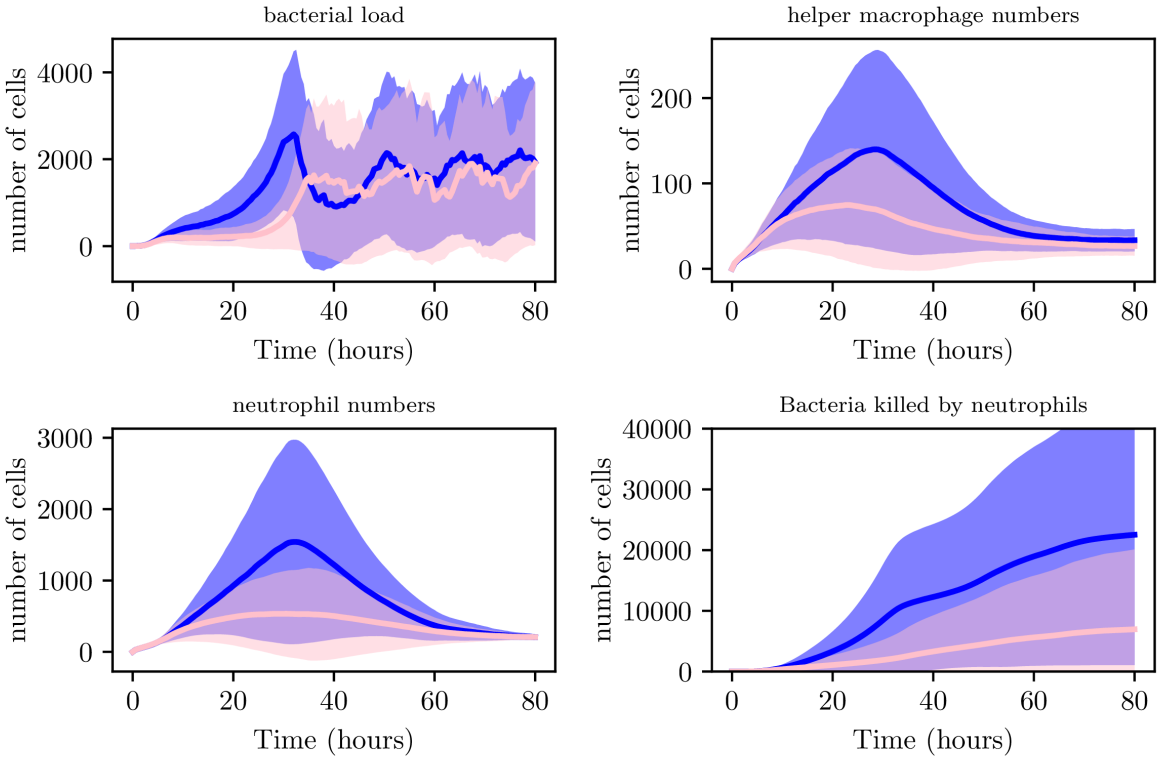

Figure 3.9: Average values for bacterial load, helper macrophage load, neutrophil load and bacteria killed by neutrophils. Simulations for the immunocompromised environment in pink and the non-immunocompromised environment in blue, with 95% confidence intervals shown by the shaded regions.

Furthermore, an aggregate analysis of the 200 simulations (see Figure 3.10) indicates that our model does not achieve clearance in 51% of instances, in contrast with the non-immunocompromised environment (also $I_B = 1$), only 23.3% of simulations

do not achieve clearance. Our model produced late clearance in 6.7% of instances, which allows more time for the bacteria to penetrate the umbrella cells and potentially form more QIRs. This in turn would lead to greater bacterial loads and growth post shedding, thus increasing the likelihood of recurrence.

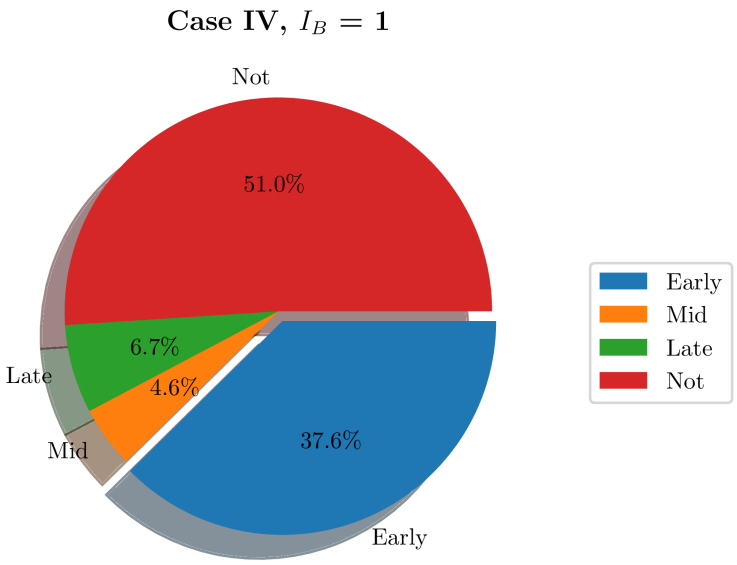

Figure 3.10: Pie charts summarising bacterial clearance status for simulations with and immunocompromised environment, $I_B = 1$.

3.5 Conclusion

In a 2-dimensional 16 mm^2 section of the bladder, we use our hybrid agent-based model to simulate Uropathogenic *E. coli* as individual elements, as well as immune cells. In particular, we model resident and helper macrophages, neutrophils and mast cells. In addition to these discrete elements, we also model a generic chemokine in order to act as a chemoattractant. This is molecule directs the immune cells to the site of infection, diffusing into the spatial domain via a PDE.

We have outlined the basic framework for the model in Chapter 2. Here we include a gradual decrease in the speed of bacteria, as evidenced in the literature, and also model bacterial shedding as a mechanism for reducing bacterial burden in the bladder. We investigate several initial bacterial loads and show that even with one bacterium at the start of the simulation it is possible for infection to spread with colonisation of the bladder epithelial tissue. This finding is consistent with recent work in the porcine model of UTI, in which an initial inoculum of $\leq$10 bacteria was sufficient to seed a productive infection in vivo [103]. Not surprisingly, as the initial bacterial burden increases, the time taken for the infection to clear increases. The number of simulations not cleared within the 80 hours of the simulated infection also increases as the initial bacterial load increases. Interestingly, the average number of bacteria present in the cases where the infection is not cleared, is not too dissimilar for $I_B = 100$, and we only see a big difference when $I_B = 1000$. At this initial bacterial load, the average number of bacteria during the late stage of infection is significantly larger than for smaller initial bacterial loads. In Section 3.4 we investigate an immunocompromised environment with smaller numbers of immune cells acting against the infection. Here we see, as expected, that for immunocompromised simulations, more cases resulted in infection persisting at the end of the simulation than in the non-immunocompromised simulations. These results are consistent with clinical scenarios. For example, UTI occurs in up to 72% of immunocompromised donor kidney recipients, usually within the first few

months post-transplant [72].

We have shown that the modelling framework that we have developed is able to simulate various scenarios in order to analyse the resulting impact of particular parameters, helping to aid understanding of these infections. Although we have only modelled the first 80 hours of an infection course, as we keep a count in the model of the bacteria that manage to penetrate into the epithelial bladder wall and evade bacterial shedding, in future work we will run longer simulations to investigate the growth of these bacteria and their role in recurrent infections. In Chapter 5 we integrate a treatment model of the most commonly used antibiotics in order to simulate treatment effects. To our knowledge, integrating a treatment model into a spatial model has not been done before to study bladder infections, and the spatio-temporal framework we present here is the crucial starting point. We acknowledge the limitations of the model parameterisation of our framework and also plan to conduct a number of simulations to more rigorously test the effects of varying the neutrophil parameters, as these were highlighted in the sensitivity analysis as the most sensitive quantities.

Chapter 4

LABORATORY EXPERIMENTS

4.1 Introduction

To complement the outcomes of our model, a series of laboratory experiments were undertaken under my supervision at the School of Medicine laboratory, overseen by Dr. Rob Hammond. These experiments aimed to provide further understanding of E. coli replication rates. Additionally, we investigated the effects of antibiotic treatment, specifically Trimethoprim, to inform the parameterization of our model.

4.2 Bacterial growth for *E. Coli*

Our first experiment looked at the determination of bacterial numbers paired with absorbance measurements. Absorbance, the measure of light absorbed by a suspension of bacterial cells or an organic molecule solution using a colorimeter or spectrophotometer, provides insights into the concentration of bacterial cells. When paired with absorbance measurements, the determination of bacterial numbers offers an insight into the trend line of E. Coli. This involves direct plate counting, a standard technique in microbiology used to estimate bacterial population density. In this method, a small and diluted portion of the initial sample is plated onto agar plates and incubated for 24 hours under optimal growth conditions. After incubation, bacterial colonies visible on the agar plates are counted. Each colony represents a viable bacterial cell originally present in the sample. By correlating these colony counts with absorbance readings, an estimation of cell concentration can be achieved, producing a bacterial trend line based on both measurements.

To begin the process of standard plate counting, we used serial dilutions to create decreasing concentrations of the initial sample. These dilutions are then placed on agar plates (a petri dish containing growth medium) where we allow for the bacteria

to replicate and form colonies. We aim to have a plate with a low enough initial dilution allowing us to count the individual colonies once they form. Agar plates are countable when presenting with 50-250 individual bacterial colonies and where the original bacterial count in our concentration is unknown to us. The number of dilutions required in order to be able to individually count forming colonies on a plate is not known either, and so, we proceed by creating a dilution series hoping to produce a countable result.

In order to appropriately classify the subgroups of specific bacteria we use the Anatomical Therapeutic Chemical Classification System, a system of alphanumeric codes developed by the World Health Organization (WHO) for the classification of drugs and other medical products. The bacterium used for these experiments is *E. Coli* belonging to the subgroup with the ATC classification 25922. We begin by creating a first dilution in a test tube containing $10\mu mL$ of our initial sample and $90\mu mL$ of growth medium for the bacteria. This first dilution gives us a sample with a 10^{-1} dilution factor. Similarly, a second dilution is created through the dilution of the first by a factor of 10^{-1}, thus leaving us with a total dilution factor of 10^{-2} in relation to the initial sample. We repeat this process until we achieve a final sample with a total dilution factor of 10^{-9}. Each one of these diluted samples is placed in turn onto an agar plate and left for a period of 24 hours when we then determined their colony forming unit (CFU) count. The CFU describes a unit which estimates the number of bacteria in a sample that are viable and able to replicate via binary fission under the controlled conditions of the experiment. Next we calculated the number of colony forming units CFU/mL values:

1. We first determined the concentration (measured in CFU) of cells in the diluted sample:

$$CFU_D = \frac{x}{y},$$

where x is the number of colonies counted, y is the dilution factor added

initially to the current agar plate and CFU_D is the CFU count in cells/mL within the diluted sample.

2. We can now determine the concentration of cells within the original sample which we define as CFU_I:

$$CFU_I = \frac{CFU_D}{z},$$

where z is the dilution factor within the current agar plate, CFU_D is the concentration within the diluted sample determined in the previous step.

For additional verification, during each dilution we create three samples. This allows us to get a more precise result by taking averages of the countable colonies. After allowing time for the colonies to form we get the results seen in Figure 4.1:

- **Plate I** (10^0 dilution factor): We are able to count the colonies resulting from the 10^{-3} dilution test tubes. The average count from the three colony growths is $(31 + 25 + 33)/3 = 27.77$ and when taking into account the dilution factor this results in 2.77×10^6 CFU/mL.

- **Plate II** (10^{-2} dilution factor): We are able to count the colonies forming from the 10^{-2} dilution. The average count is $(23+21+11)/3 = 18.33$. When accounting for the current agar plate and the dilution factor within the final count is 1.83×10^5 CFU/ml.

- **Plate III** (10^{-3} dilution factor): We are able to count the colonies forming from the 10^{-1} dilution with the average being $(33+35+36)/3 = 34.6$. Taking into account the dilution factors we get 3.46×10^4 CFU/mL.

We now use spectophotometry in order to obtain readings for our dilution samples that we will pair along with the CFU values to produce the trend line graph for *E. Coli*. To do this, we use a spectophotometer in order to measure the photons (light

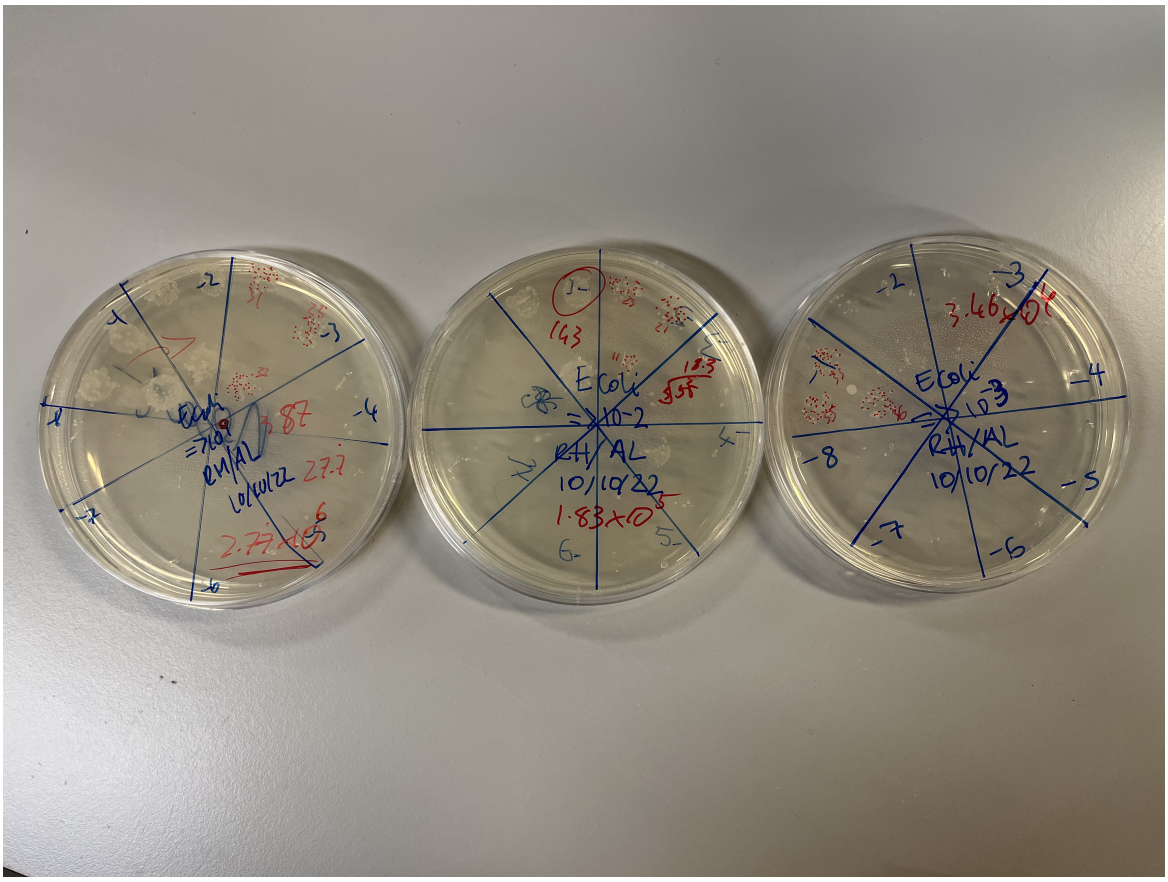

Figure 4.1: Plate I-III from left to right. The colony count and dilution factors can be seen inscribed within the agar plates during the experiment.

intensity) that passes through our test tube. Hence, spectophotometric analysis allows us to determine the amount of cells in a sample based on the amount of light that is absorbed by the sample. Therefore, when taking measurements using the spectophotometer, an increased turbidity (cloudiness), indicates bacterial growth. Although this method is effective in measuring the cell density, it can lead to results that can be different from plate counts, as it indirectly measures all bacteria dead and alive as opposed to the standard cell count which focuses on live bacteria. The reading received by the spectophotometre is termed absorbance or optical density and for our purposes it will indirectly reflect the number of bacteria.

Using results from these experiments, shown in Figure 4.2 and Figure 4.4, we set

Dilution	Turbidity	CFU count
Plate I	0.43	2.77×10^6
Plate II	0.05	1.83×10^5
Plate III	0.01	3.46×10^4

Table 4.1: Pairing CFU and spectophotometry values.

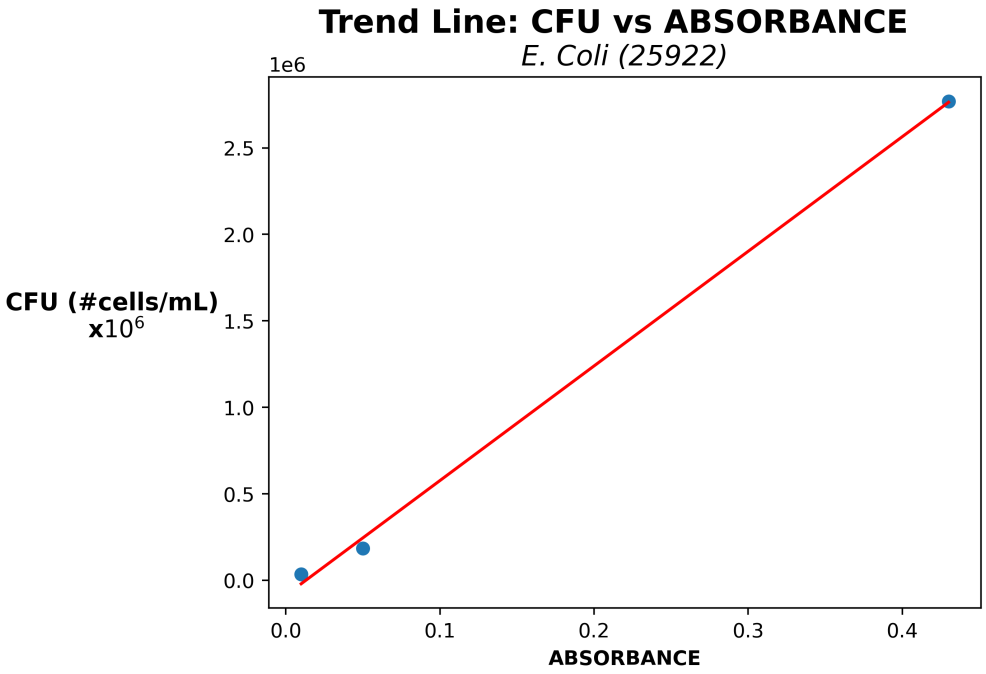

Figure 4.2: The blue dots represent the values shown in Table 4.2. The red line is the result of a simple linear regression through our blue data points. This line allows us to predict the concentration in CFU cells/mL through the use of the absorbance property without the need to directly count the agar plate for other concentrations.

the replication speed of *E. Coli* in our model as 0.31 hours.

4.3 Antimicrobial Susceptibility Testing of Trimethoprim

Our aim is to be able to use our developed framework in order to further investigate the nature and progression profiles of recurrent UTIs. To do this, we need to fully parameterise all parts of the model. Thus, for our second laboratory experiment, we chose to investigate the effects of Trimethoprim on the growth of *E. Coli*. This will allow us to further parameterise our antibiotic treatment framework by comparing it to *in vitro* results.

To do this, we use the SLIC (Scattered Light Integrated Collector) machine developed by Dr. Robert Hammond [47]. When investigating bacterial growth and antimicrobial susceptibility using photonic energy, we take into account the limit of detection (LoD) which is around 10^5 cells/mL, however, when utilizing a SLIC machine we are able to detect changes with a LoD of 25 cells/mL. This allows us to rapidly detect population changes and bacterial growth.

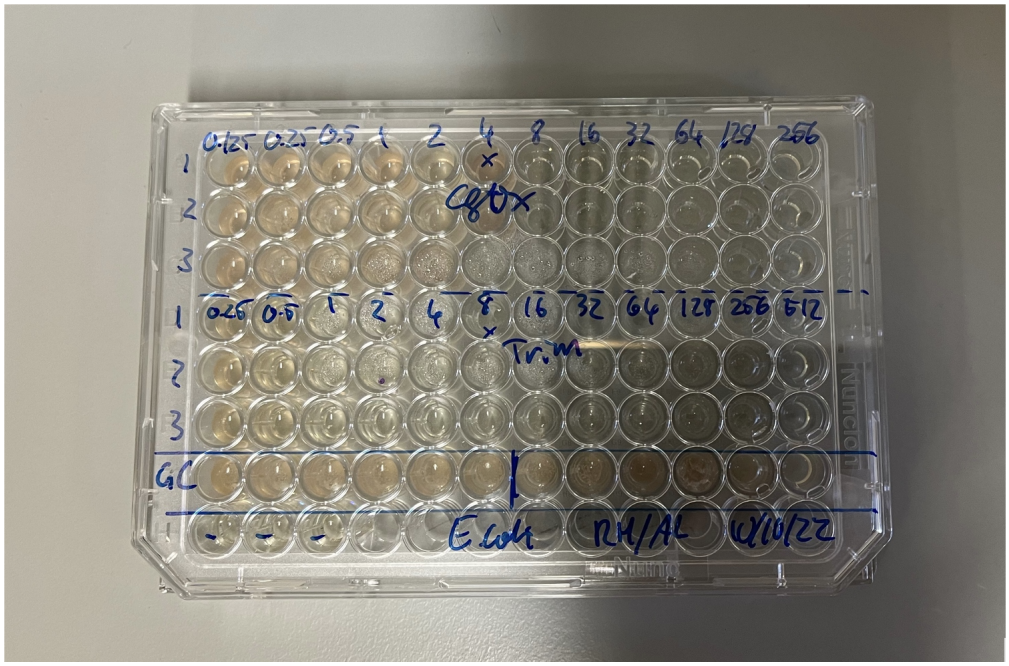

Figure 4.3: This picture was taken after preparing the microtiter plate for the antimicrobial susceptibility test conducted for Trimethoprim and leaving the plate in the SLIC machine for data collection shown in Figure 4.4.

For our experiment, we prepare test tubes containing different dilutions of *E. Coli*, to which we add specific concentrations of Trimethoprim, These dilutions are placed in a microtiter plate as can be seen in Figure 4.3. In addition to the dilutions containing the mixes of bacteria and antibiotic we also have a row of control for the bacteria, allowing us to get information about the growth rate without the effect of Trimethoprim. We conduct the same experiment for control using another antimicrobial agent used for UTIs, Cephalexin.

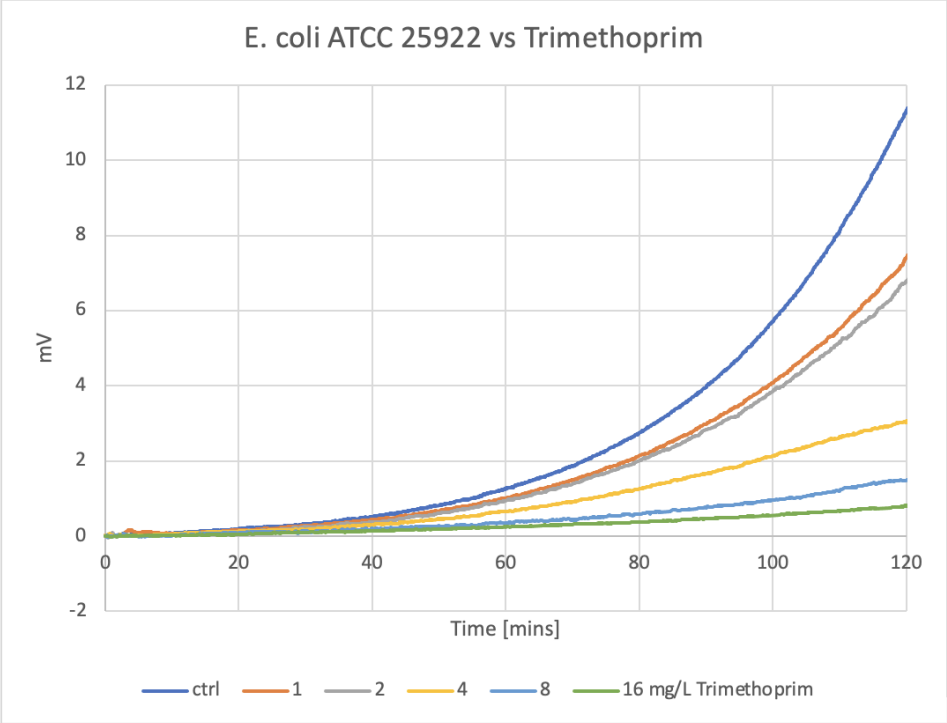

Figure 4.4: SLIC machine results for *E. Coli* ATC 25922 with Trimethoprim. Control growth curve is in blue

The microtiter plate in Figure 4.3 contains different Cephalexin concentrations in the first 3 rows, while along the columns, we have the different concentrations of antimicrobial agent within the growth medium along with the bacteria. Rows 3-6 contain the different concentrations of *E. Coli*.

After the preparation of the microtiter plate, we placed it in the SLIC machine where it collected concentration data for *E. Coli* allowing us to observe the growth profiles of the bacteria with different concentrations of Trimethoprim. In addition to the data presented by the SLIC machine, a simple visual analysis of the microtiter plate after 24 hours gave an indication of the susceptibility of the bacteria to the antibiotic. As we can see from Figure 4.3, the solutions to the left of 4 mg/L of Trimethoprim show bacterial growth, which is identifiable by the cloudiness of the solutions. While, the solutions to the right of 4 mg/L appear clearer with no signs of bacterial growth.

The control line, final row within the microtiter plate, helps to identify uninhibited *E. Coli* bacterial growth. We therefore estimate the MIC of Trimethoprim to be used in our model as 4 mg/L.

Due to the ability of the SLIC machine to capture results at very high sensitivities, we are able to analyse the rapid growth profiles of *E. Coli* for short period of time. As we can see in Figure 4.4, the blue curve denotes the control line for our experiment, hence, it shows the growth profile for *E. Coli* in from $T = 0$ min to $T = 120$ min. We can see the initial lag period which concluded roughly at $T = 40$ min, after which, the exponential growth phase begins.

We can see how for concentrations of Trimethoprim above the MIC value of 4 mg/L, such as the case of the green and blue lines in Figure 4.4, bacterial growth is almost completely inhibited. The yellow line, which uses 4 mg/L, consistently describes the growth behaviour expected for the MIC value concentration.

Chapter 5

SIMULATING ANTIBIOTIC TREATMENT OF BLADDER INFECTIONS

5.1 Introduction

Having introduced our hybrid agent-based model designed to capture the host-pathogen interactions involved in bladder infections, we proceeded by conducting several analyses of the model and its outputs. We conducted an in-depth global uncertainty and sensitivity analysis to identify how variation in model parameters propagates to our outputs, especially bacterial and immune cell number outputs. Additionally, we also conducted an analysis on specific parameters such as the initial bacterial load (I_B) and replication rates for bacteria. We found that higher initial bacterial burden leads to poorer outcomes, however, a single bacteria may be sufficient to establish an infection. Studies show how very low initial levels of bacteria (fewer than than 10^6 colony forming units per milliliter of urine) are associated with symptoms of acute bladder infection [57]. Other review articles discuss how low initial bacterial loads may persist and establish infection, this may be due to factors such as the virulence (or strength) of the bacteria involved, the immune response of the individual, or other underlying health conditions that can make an individual more susceptible to infection [104]. Our model is parameterised to capture the behavior of *E. Coli*, known for its fast replication rates which, under optimal conditions allow each individual bacteria to replicate each $20-30$ minutes and we also found in our model simulations that very small bacterial numbers can lead to an established infection. In addition to investigating the effects of initial bacterial load, we used our model to simulate immuno-compromised environments (characterised by deficient initial numbers of immune cells such as resident macrophages and mast cells) confirming what is shown in the literature; bacterial spread typically progresses at

a higher rate in such environments typically leading to more severe disease. The effects of bladder infection specific processes such as bacterial shedding were also examined, as seen in Chapter 3 .

Having conducted the aforementioned analyses we see that our model is able to accurately capture essential processes that happen during infections of the bladder. Hence, with additional developments and parametrisation, our framework will be capable of providing new clinical insight into bladder infections. In this chapter we will explore the effect of antibiotic treatment on the bladder infection dynamics. This will allow us to inform clinicians in tailoring individualised treatment options leading to improved outcomes for patients, while also minimising the risk of antimicrobial resistance emergence.

5.2 Using Trimethoprim to treat bladder infections

In order to be able to use our framework to inform treatment and provide clinical insight, we focus in this chapter on simulating treatment for patients presenting with bladder infections. We introduce to our framework a model capable of capturing the treatment process which we will parameterise through *in vitro* experiments performed and reported on in Chapter 4, and additional experimental data available in the literature.

Trimethoprim is the most commonly used antibiotic for the treatment of UTIs caused by bacteria such as *E. Coli*. It has a broad spectrum of activity and works by inhibiting the bacterial enzyme dihydrofolate reductase, which is essential for the synthesis of DNA and RNA. Trimethoprim is often used in combination with sulfamethoxazole, a sulfa drug that also targets dihydrofolate reductase, to enhance its efficacy and prevent the development of antibiotic resistance.

Several studies have evaluated the efficacy of Trimethoprim in the treatment of UTIs. A randomized, double-blind trial published in the Annals of Internal Medicine compared a single dose of norfloxacin, another antibiotic commonly used for UTIs, with a 3-day course of Trimethoprim for the treatment of uncomplicated UTIs in women. The study found that both treatments were similarly effective, with cure rates of 88% for norfloxacin and 84% for Trimethoprim [82].

In addition to its antibiotic properties, the pharmacokinetics and pharmacodynamics of Trimethoprim have also been studied. A study published in Antimicrobial Agents and Chemotherapy investigated the pharmacodynamics of Trimethoprim alone and in combination with sulfamethoxazole in a murine model of UTI caused by *E. Coli*. The study found that the combination of Trimethoprim and sulfamethoxazole was more effective than Trimethoprim alone in reducing bacterial load and preventing the development of resistance [37].

Despite its effectiveness, the use of Trimethoprim has also been associated with

the development of antibiotic resistance. A review published in Biomolecules discusses the mechanism of action of Trimethoprim and its role in the development of resistance. The review also explores new developments in the field of antibiotic research, including the identification of new targets for antibiotic therapy and the use of alternative approaches such as phage therapy and immunotherapy [9].
Another review published in Clinical Microbiology and Infection discusses the challenges and opportunities in the antibiotic pipeline, including the need for the development of new antibiotics to address the rising incidence of antibiotic-resistant infections. The review highlights the importance of antimicrobial stewardship programs in promoting the appropriate use of antibiotics and preventing the development of resistance [84].

Together, these studies provide valuable insights into the efficacy, pharmacology, and resistance of Trimethoprim, and underscore the importance of responsible antibiotic use and the development of new antibiotics to combat antibiotic-resistant infections. Due to the recurrent profile of UTIs and subsequent treatment through antibiotic administration, many antimicrobial agents aimed at the treatment of UTIs are related to growing rates of resistance, hence, making them unreliable for use in severe recurrent UTIs. Of the antibiotics used against bladder infections, cited within the treatment guidelines for the vast majority of UK NHS departmental prescribing committees, Trimethoprim is clearly the usual choice as a first line of treatment [45]. When patients present with a recurrent UTI, usually characterised by the occurrence of 2 or more episodes within 6 months, or alternatively, 3 or more episodes within 12 months, a daily dose of Trimethoprim is prescribed of 100 mg, or a one-time 200 mg dose when the patient is known to have been exposed to triggers [45]. As we have seen, covering the available guidelines and literature on the use of Trimethoprim will be fundamental to appropriately parameterise the antibiotic treatment within our model.

5.2.1 Integrating antibiotic treatment into our model

Similarly to the generic chemokine we introduced in Section 2.2.4 our antibiotics are secreted two-dimensionally with the source in this case being the blood vessels within our computational environment. The antibiotic will be responsible for:

1. Halting bacterial growth during the intensive phase of antibiotic treatment. Within our bacterial replication module in our model, a bacterium is considered to be in the intensive phase whenever its location's concentration value for Trimethoprim exceeds $Trim_{MIC}$. The minimum inhibitionary concentration (MIC) value is defined as the lowest concentration of antibiotic which will stop bacterial growth. In the case of Trimethoprim, different sources within the literature estimate the MIC value for Trimethoprim to be $1-4mg/L$, with the EUCAST (which is the european organization that deals with breakpoints and technical aspects of phenotypic *in vitro* antimicrobial susceptibility testing) estimating this value at $4mg/L$.

2. Bacteria is also killed when it replicates to a neighbouring grid cell within the environment where the value of the antibiotic exceeds $Trim_{Kill}$. *In vitro* experiments performed in Chapter 4 also confirm this.

Treatment is modelled through the following PDE which is solved following the finite difference method and to ensure numerical convergence, finite difference scheme step size refinement is employed. This involves iteratively refining the grid spacing (Δx and/or Δt) to increase the resolution of the discretised domain. By decreasing the grid spacing, the approximation becomes more accurate, leading to a more precise solution. In our case :

$$\begin{aligned}\frac{\partial Trim(\boldsymbol{x},t)}{\partial t} &= \nabla\cdot(D_{Trim}(\boldsymbol{x})\nabla Trim(\boldsymbol{x},t)) + r_{Trim}m(\boldsymbol{x}) \\ &\quad - \phi_{Trim}Trim(\boldsymbol{x},t)cell(\boldsymbol{x},t) - \eta_{Trim}Trim(\boldsymbol{x},t),\end{aligned} \tag{5.1}$$

where $D_{Trim}(\boldsymbol{x})$ is the diffusion coefficient of the chosen treatment option, in our case, Trimethoprim. ϕ_{Trim_b} is the uptake rate of the drug by the bacteria, with $cell(\boldsymbol{x}, t) = 1$ if position $\boldsymbol{x}$ is occupied by a bacteria at time t and $cell(\boldsymbol{x}, t) = 0$ otherwise. η_{Trim} is the drug decay rate for Trimethoprim and r_{Trim} the supply rate for Trimethoprim through the blood vessels. Additional parameters also include t_{Trim} which denotes the time at which Trimethoprim is administered. T_I is the drug administration interval, which mimicking current treatment guidelines, we set at 24 hours to simulate a daily treatment dose of Trimethoprim.

$$Trim_{Kill} = \begin{cases} Trim_{Killrep}, & \text{for replicating bacteria} \\ Trim_{Killnonrep}, & \text{for non-replicating bacteria} \end{cases} \tag{5.2}$$

As mentioned previously the antibiotic will also be responsible for killing bacteria within the environment. The Minimum Bactericidal Concentration (MBC) is defined as the lowest concentration of an antimicrobial agent required to kill a bacterium over a fixed period of time. Within our model we define the MBC for Trimethoprim acting on *E. Coli* as $Trim_{Killrep}$. Thus, whenever the concentration of Trimethoprim concentration within the cell occupied by a replicating bacterium goes above $Trim_{Killrep}$, the bacterium is removed, otherwise, when the bacterium is not replicating the bacterium is killed if the antibiotic value is above $Trim_{Killnonrep}$ (see Equation 5.2). For our model, we set these values to be the same, however, in future experimental work this can be further investigated. Trimethoprim when used alone however, is know to be a primarily bacteriostatic agent, hence the MBC value is estimated to multiple times higher than the MIC value. We set this in our model as $3 \times$ MIC value.

For the simulations shown in the next section, we use the values from Table 5.1. for the last 3 parameters in Table 5.1, the units are shown in percentages as we evaluate the concentration of the drug in our environment by scaling it over the total

	Parameter value	units	source
D_{Trim}	1.7×10^{-6}	$cm^2 s^{-1}$	e
ϕ_{Trim}	2.1×10^{-11}	$\mu moles/cell/hour$	e
η_{Trim}	0.1	hr^{-1}	e
t_{Trim}	24	$hours$	treatment guidelines
T_I	24	$hours$	treatment guidelines
$Trim_{Killrep}$	12	%	lit. [112, 116]
$Trim_{Killnonrep}$	12	%	lit. [112, 116]
$Trim_{MIC}$	4	%	exp., lit. [116, 61]

Table 5.1: This table shows the parameters of our treatment framework and the values adopted for each parameter. The source, whether the parameter was collected from the literature (lit.), experiments (exp.) or estimated (e), is also included.

concentration, thus allowing us to implement thresholds in percentages[1]. These will represent simulations of a full course of treatment for a patient presenting with recurrent bladder infections, where the parameters involved in bacterial growth and clearance are parameterised from the experiments shown in Chapter 4. Note that the MIC value for Trimethoprim on *E. Coli* bacteria provided within the EUCAST break-point tables was verified during our experiments in Chapter 4, where we tested the susceptibility of *E. Coli* to Trimethoprim and used the literature MIC value as a baseline to determine such susceptibility.

[1]We estimate these percentages to approximately mimic the effect of specified doses acting within the bladder. In future work we plan to incorporate a full Pharmacokinectic/Pharmacodynamic model of Trimethoprim to more accurately model particular doses and their effects in the bladder.

5.3 Simulating treatment in *UTImodel*

Having further parameterised our model to account for our *in vitro* experiments detailed in Chapter 4, we proceed by utilising our model by analysing the results resulting from treatment protocol simulations for recurrent UTIs. To do this we run our model for a total simulation time of 240 hours. We begin treatment at $T_I = 24$ hours and follow the general treatment protocols seen in Section 5.2. When dealing with recurrent uncomplicated UTIs, patients are usually advised to follow a treatment regimen of Trimethoprim lasting a week in order to clear the infection, other instances, where the infection presents a more aggressive profile, the treatment length or may be extended or dose may be increased. Treatment is halted after $T = 192$ hours, representing the point of completion for a 1 week treatment regimen. We choose to start by simulating 50 instances of our model where the antibiotic dose approximately equates to values around the MIC, and 50 instances where the dose equates to values above the MIC, as parameterised by our experiments and the literature in Chapter 4 and Section 5.2. In addition to this, we run our simulations for varying initial bacterial loads, $I_B = 1, 100, 500, 1000$.

5.3.1 Low initial dose

Using parameter values from Tables 5.1, 3.1, 3.2, and an initial dose of Trimethoprim of 20 mg, we first analyse the outputs resulting by varying the initial bacterial load. We choose to simulate *UTImodel* for $I_B = 1, 100, 500, 1000$, as was done previously in Chapter 3 as this will give us a good insight into the bacterial replication rate and infection outcome. Additionally, as we have already performed a similar analysis for our model without the treatment framework, we will be able to use the aggregate results to analyse how treatment effects the outcome of infections depending on the initial bacterial load. Consequently, this will helps us gain an understanding of the treatment response. As explained in Section 2.3, our model includes the process of bacterial shedding, which in turn, will allow us to investigate concepts such as

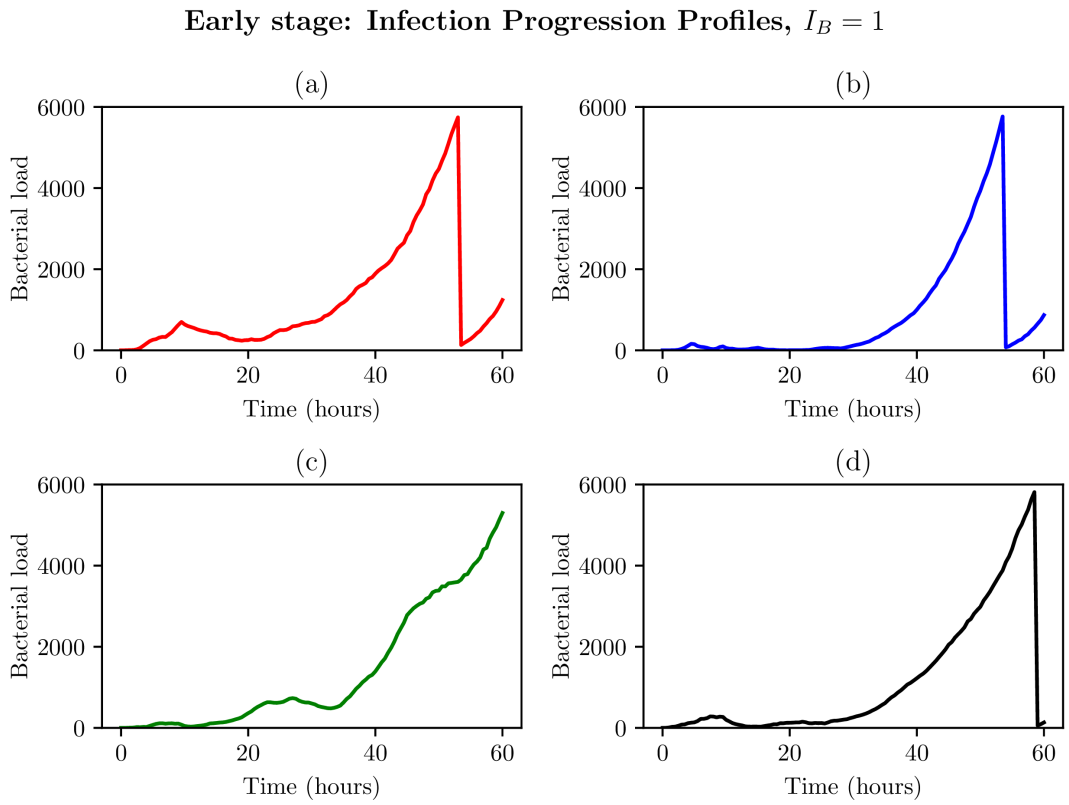

Figure 5.1: Simulations (a)-(d) represent the bacterial growth profiles arising from 4 representative example simulations with $I_B = 1$ where bacteria was not cleared during the early stage of the infection. Antibiotic diffusion enters the environment at $T = 24$ hours. Bacterial shedding happens when $N_B = 6000$.

quiescent bacterial reservoirs. Several studies have provided evidence for the existence of such reservoirs within the bladder's epithelium in patients with recurrent bladder infections. These studies have shown that bacterial DNA can be detected in the bladder epithelial cells of patients with recurrent UTIs even after successful antibiotic treatment. Furthermore, bacterial strains isolated from these patients have been found to have similar virulence factors and invasion mechanisms as those that form bacterial reservoirs. The presence of these reservoirs has important implications for the treatment of recurrent UTIs. Traditional antibiotic treatment is often ineffective against such bacteria due to their dormancy and reduced susceptibility to antibiotics. Thus, the relationship between bladder infections and quiescent bacte-

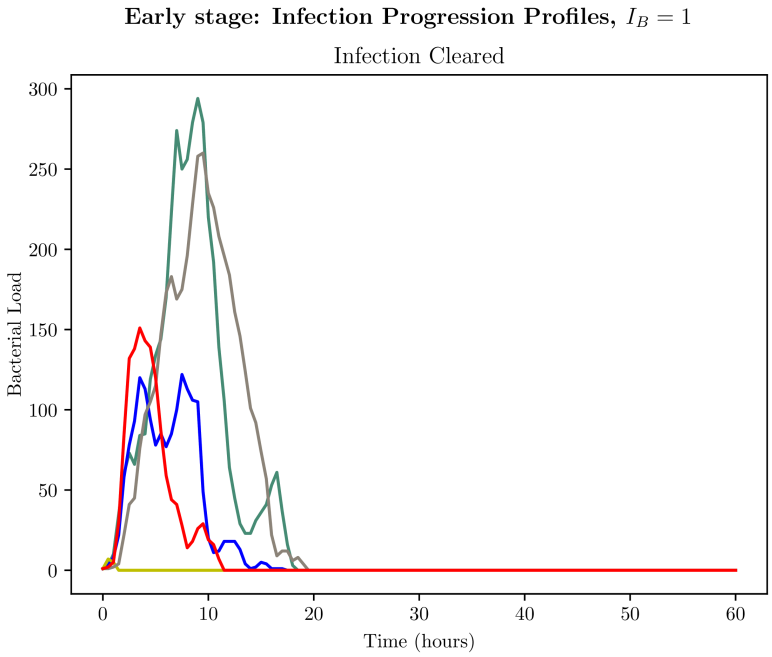

Figure 5.2: Bacterial growth profiles arising from 5 simulations with $I_B = 1$ where the bacteria was successfully cleared. Each colour refers to a different simulation, treatment is introduced to our environment at $T = 24$ hours.

rial reservoirs is a significant area of research that could have important implications for the management of recurrent UTIs.

5.3.1.1 Case where $I_B = 1$

Looking at the profiles arising from $I_B = 1$ in Figure 5.1 and Figure 5.2, we can see how from very low initial bacterial loads, *E. Coli* still manages to establish infection due to its high replication rate. In Figure 5.1(a) we can see how initial replication of the bacteria is contained by the immune system however as time progresses the infection manages to reach the bacterial shedding threshold ($N_B = 6000$) at $T = 53$ hours. Figure 5.1(b) shows a similar outcome as seen in Figure 5.1(a), however, we can clearly see how in this case the first dose of treatment kept the infection contained for a longer period of time than Figure 5.1(a), resulting in shedding at a slightly later time of $T = 55$ hours. Other progression profiles, such as Figure 5.1(c) show how the combination of the immune system and antibiotic treatment

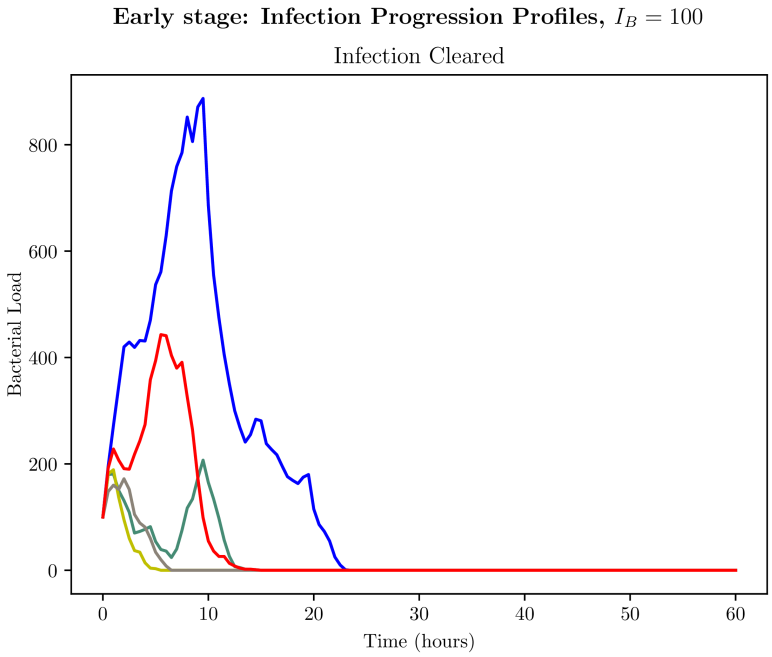

Figure 5.3: Bacterial growth profiles arising from 5 simulations with $I_B = 100$ where the bacteria was successfully cleared. Each colour refers to a different simulation, treatment is introduced to our environment at $T = 24$ hours.

can prevent the need for bacterial shedding during the early stages of the infection. Looking at figure Figure 5.2 however, which shows examples of when the infection is cleared, we can see how quickly the immune system can eliminate all bacteria when the initial bacterial load is low, without the need for antibiotic treatment.

5.3.1.2 Case where $I_B = 100$

In the case of $I_B = 100$ we can observe a range of behaviours. As can be seen from our analyses, the bacteria may be completely cleared, which happens through the intervention of the immune cells such as helper macrophages and neutrophils during the early stages of the infection. This can be seen in Figure 5.3, where we show 5 example simulations and how $N_B = 0$ within $T = 24$ hours. This infection profile is interesting as it describes the subset of infections that were cleared solely through the immune system similar to Figure 5.2 for I_B. The antibiotic had no effect on the bacterial load in these infections as the treatment is set to begin within our model

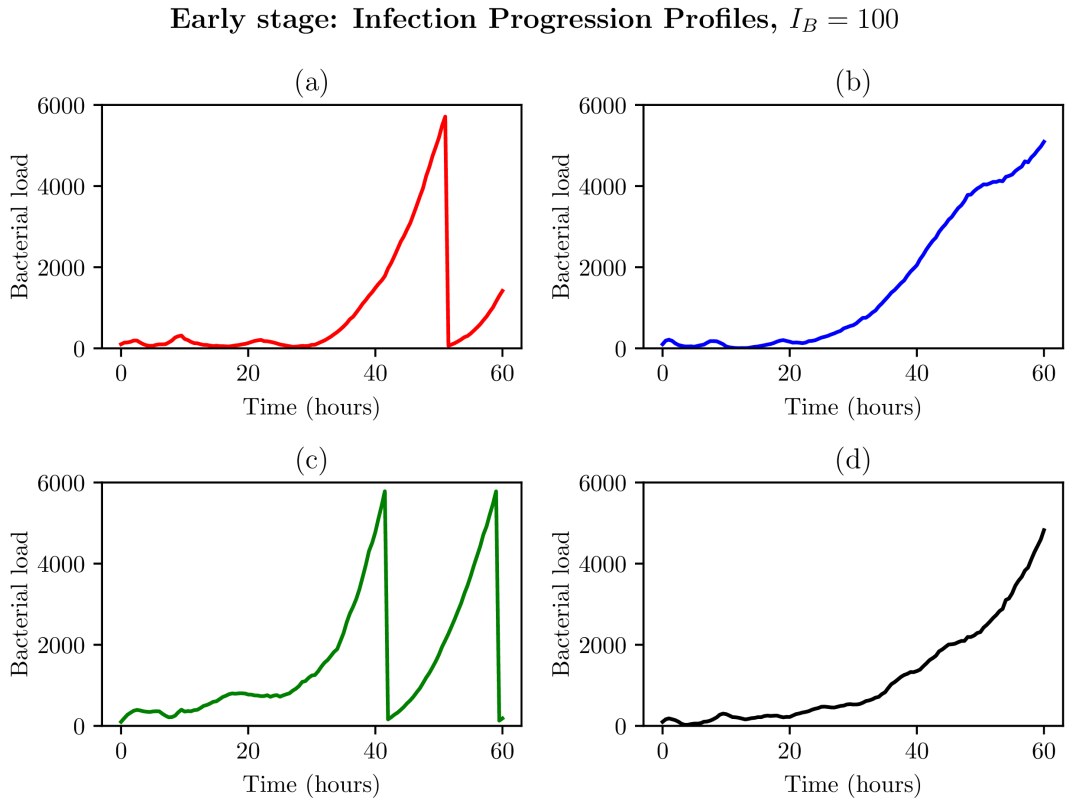

Figure 5.4: Simulations (a)-(d) represent the bacterial growth profiles arising from 4 representative examples with $I_B = 100$ that were not cleared during the early stages of the infection. Again, treatment is administered at $T = 24$ hours, and bacterial shedding occurs if N_B reaches 6000.

at $T = 24$ hours. In cases where infection was not cleared, we observe different progression profiles, as shown in Figure 5.4.

Figure 5.4 (a) shows a subdued infection profile where bacteria manages to overcome both the immune system and the antibiotic diffusion. As shown, initially the bacterial load increases slightly reaching $N_B = 397$ by $T = 8$ hours, however, as the immune system catches up with the bacteria at $T = 16$ hours, we have $N_B = 61$. The bacteria manage to overcome the immune system and increase in numbers which is interrupted once the treatment is introduced at $T = 24$ hours allowing for greater bacterial clearance, however, eventually the bacteria manage to begin a fast replication period at $T = 32$ hours which eventually triggers bacterial shedding once

N_B = 6000.

While Figure 5.4 (c) tells a similar story to (a) during the initial stages of infection,

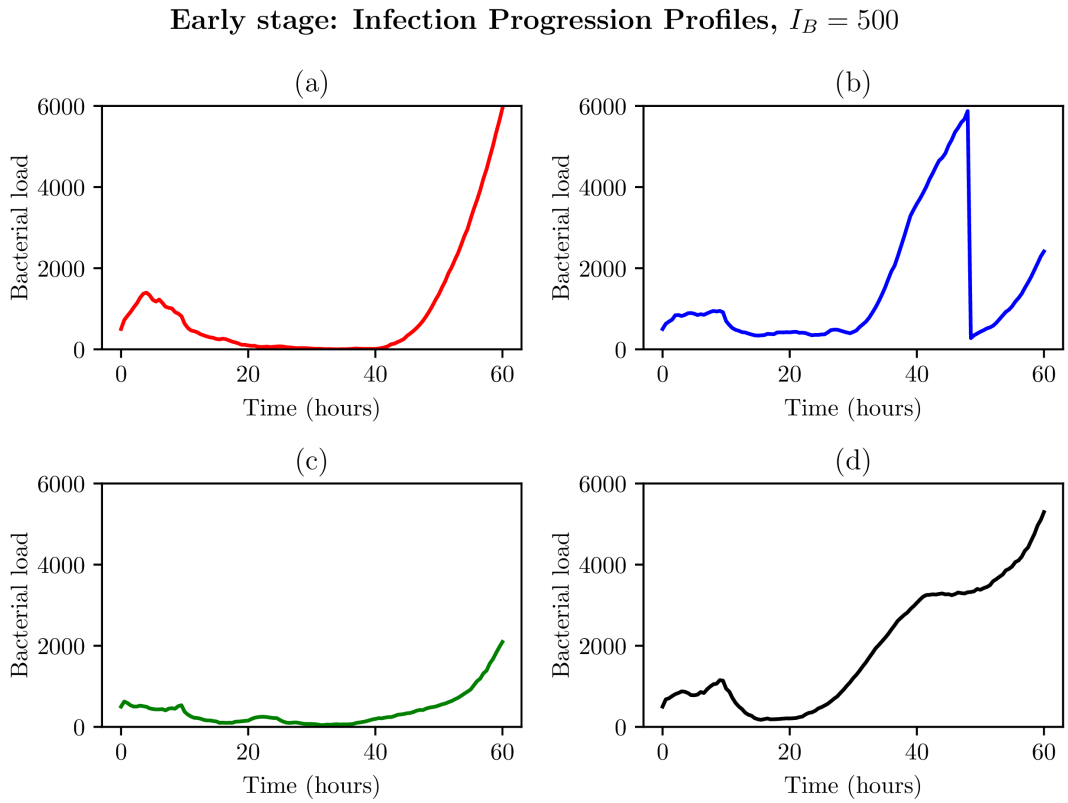

Figure 5.5: Simulations (a)-(d) represent the bacterial growth profiles arising from 4 representative example simulations with I_B = 500 where bacterial clearance is not achieved during the early stages of infection. Treatment is administered at T = 24 hours and bacterial shedding occurs if N_B exceeds 6000.

the fast replication rate of bacteria shown in Figure 5.4 (c) managed to trigger two episodes of bacterial shedding prior to T = 60 hours. The progression profiles of Figure 5.4 (b) and (d) show how treatment in these instances along with the action of immune cells manages to subdue the infection to the extent of not reaching the bacterial load needed for bacterial shedding. This is important, as the process of bacterial shedding, as well as assisting in clearing bacteria when numbers reach high levels within the superficial urothelium may also lead to negative consequences, as discussed previously.

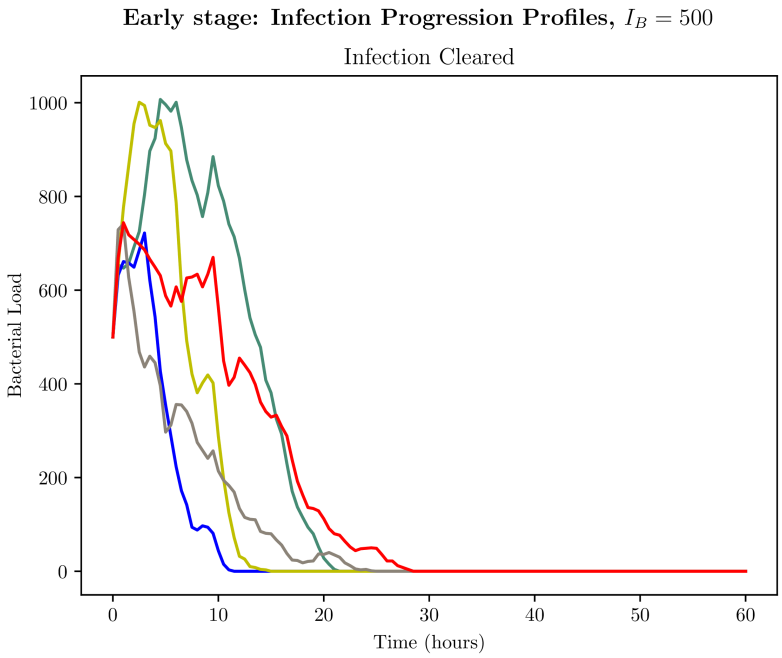

Figure 5.6: The bacterial growth profiles arising from 5 simulations where $I_B = 500$ where the infections were cleared during the early stages. Again, each colour refers to a different simulation, treatment is introduced to our environment at $T = 24$.

5.3.1.3 Case where $I_B = 500$

Similarly to Figure 5.3 and Figure 5.2, Figure 5.6 shows progression profiles that resulted in early bacterial clearance. We note how the immune cells are able to stop bacterial replication while clearing all the bacteria. A notable difference between $I_B = 100$ and $I_B = 500$, however, is that initial bacterial clearance takes longer, as one might expect. While early stage clearance for $I_B = 100$ happened usually around $T = 12$ hours, in the case of $I_B = 500$, bacterial clearance usually happens around $T = 20$ hours. Looking at Figure 5.5 we can see how infections that are not cleared during the early stage usually achieve a bacterial load of $N_B = 6000$. In Figure 5.5 (a) we can see how the infection is completely subdued after an initial interval of fast bacterial replication. The infection, however, manages to overcome the immune system and the Trimethoprim and increase exponentially at $T = 42$

hours. Although, similarly to Figure 5.5 (a), the bacterial load starts increasing exponentially at $T = 40$ hours. However, this time the bacterial load does not exceed $N_B = 2100$. Considering the fast replication rate of *E. Coli*, a four-fold increase during a 60 hours period is slow, which we attribute to the effects of Trimethoprim. A perfect example of the high replication rate *E. Coli* can be seen in Figure 5.5 (b), where the bacteria manage to achieve the activation threshold for bacterial shedding in well under $T = 12$ hours after being subdued by the immune system and treatment for the initial $T = 34$ hours.

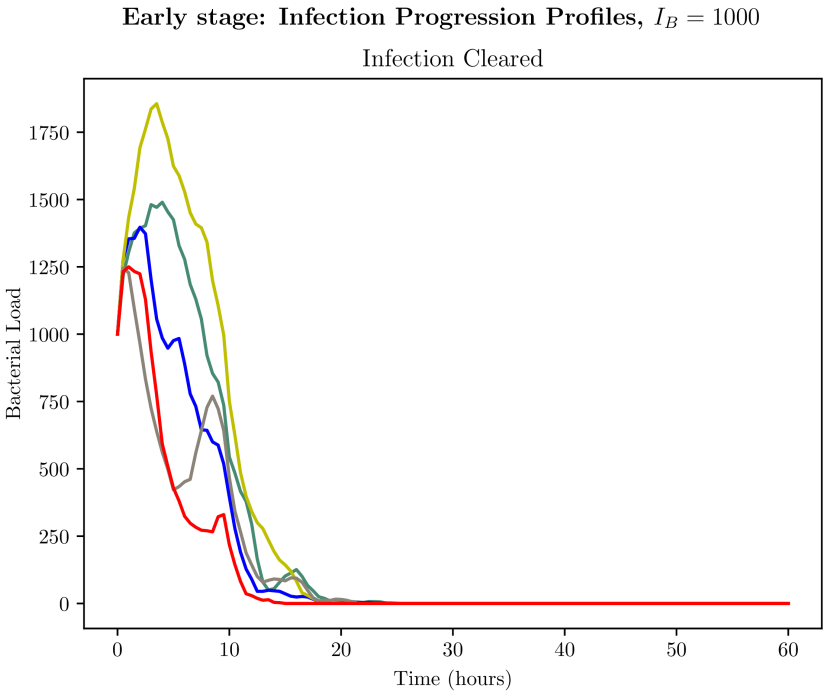

Figure 5.7: Bacterial growth profiles arising from 5 simulations where $I_B = 1000$ where the infections were cleared. Each colour refers to a different simulation, treatment is introduced to our environment at $T = 24$ hours.

5.3.1.4 Case where $I_B = 1000$

As expected, a higher initial bacterial load, in this case $I_B = 1000$, leads to profiles where bacterial shedding is almost always activated before $T = 60$ hours. As can be seen in Figure 5.8, profiles (a) and (c) present clear exponential growth before

shedding, while Figure 5.8 (b) and (d) show profiles where the effects of treatment can be clearly noted on the replication ability of bacteria. The profiles which conclude in clearance however, as can be shown in Figure 5.7, demonstrate quick bacterial clearance in a similar fashion to the profiles seen for lower initial bacterial loads. We believe this is due to the quick identification of the infection due to its larger initial size, this in turn promotes the initial rush of neutrophils and other immune cells.

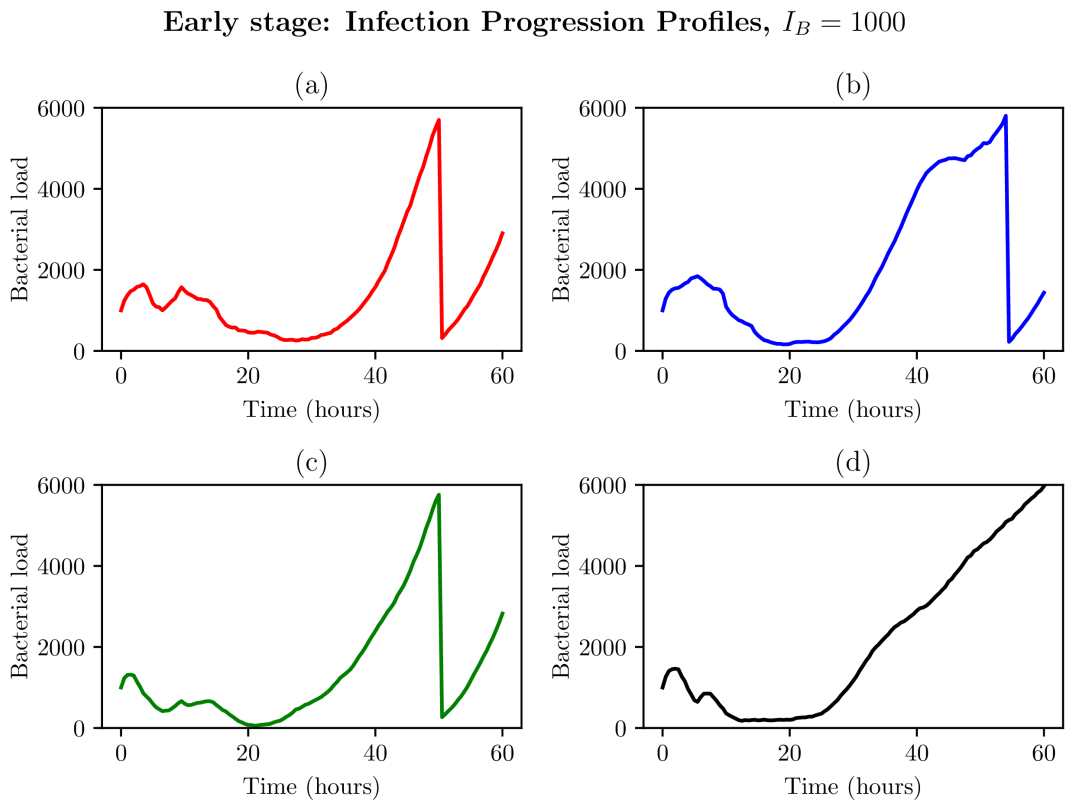

Figure 5.8: Simulations (a)-(d) represent the bacterial growth profiles arising from 4 representative example simulations for $I_B = 1000$ where the infection is not cleared in the early stages. Treatment is administered at $T = 24$ hours and bacterial shedding occurs if N_B exceeds 6000.

5.3.1.5 Aggregate results

To get a more general picture of our outcomes, we must also note the aggregate behaviour of all simulations when using our model to simulate a treatment protocol using a low dose of 20 mg to simulate a less intense course of treatment. As we've done in Chapter 3, we produce pie charts showing us the infection outcome states. As can be seen in Figure 5.9 the results are as expected, for low initial bacterial loads such as $I_B = 1, 100$, bacterial clearance is achieved in the majority of cases, for $I_B = 1$, clearance during the early stages is achieved in 60% of simulations. 20% of simulations indicated clearance during the middle stages while in 20% of simulations bacteria was able to evade clearance. In the case of $I_B = 100$, as we can see from Figure 5.10, bacterial clearance was not achieved in 35.8% of simulations, early clearance was the next most likely outcome, happening in 32.1% of simulations. 31.1% of simulations presented clearance during the middle stages of infection, while late clearance, took place in only 0.9% of cases.

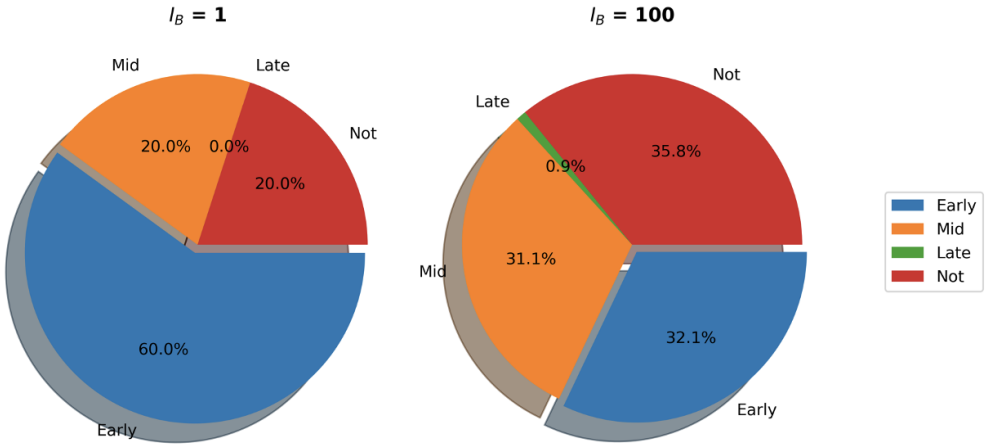

Figure 5.9: Aggregate analysis of $I_B = 1$ and $I_B = 100$, presenting UPEC clearance status and during which stages clearance occurs. These plots represent the result for simulations of treatment with a low initial antibiotic dose.

When looking at the outcomes from $I_B = 500$ presented in Figure 5.10, we see that

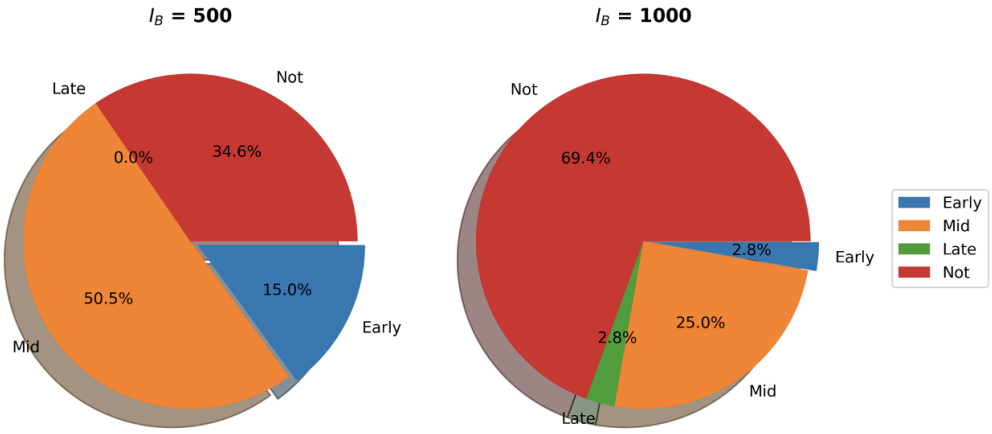

Figure 5.10: Aggregate analysis of $I_B = 500$ and $I_B = 1000$, presenting UPEC clearance status and during which stages clearance occurs.These plots represent the result for simulations of treatment with a low initial antibiotic dose.

bacteria was not cleared in 34.6%, a decrease from the value shown for $I_B = 100$. However, bacterial clearance during the middle stages was achieved in 50.5% of simulations. This is important to note as treatment is introduced to our model during the middle stage of the infection. With $I_B = 1000$ we can see that the majority of simulations do not present bacterial clearance. This is of course due to the high initial bacterial load. When clearance is achieved, it most likely will be during the middle stages which occurred in 25.0% of simulations, with late and early clearance both presenting in 2.8% of simulations.

5.3.2 High initial Trimethoprim dose

For the higher initial Trimethoprim dose (100 mg), we choose to set $I_B = 500, 1000$. We first begin by looking at the progression profiles for the infections as done in the previous section.

5.3.2.1 Case where I_B = 500

The profiles we can see in Figure 5.11 show the effects a high dose of treatment has on the bacterial growth within our model. As known, all infections are characterised by an initial rush to the infection site by the immune cells such as neutrophils and macrophages in which bacterial clearance is first attempted through such cells.

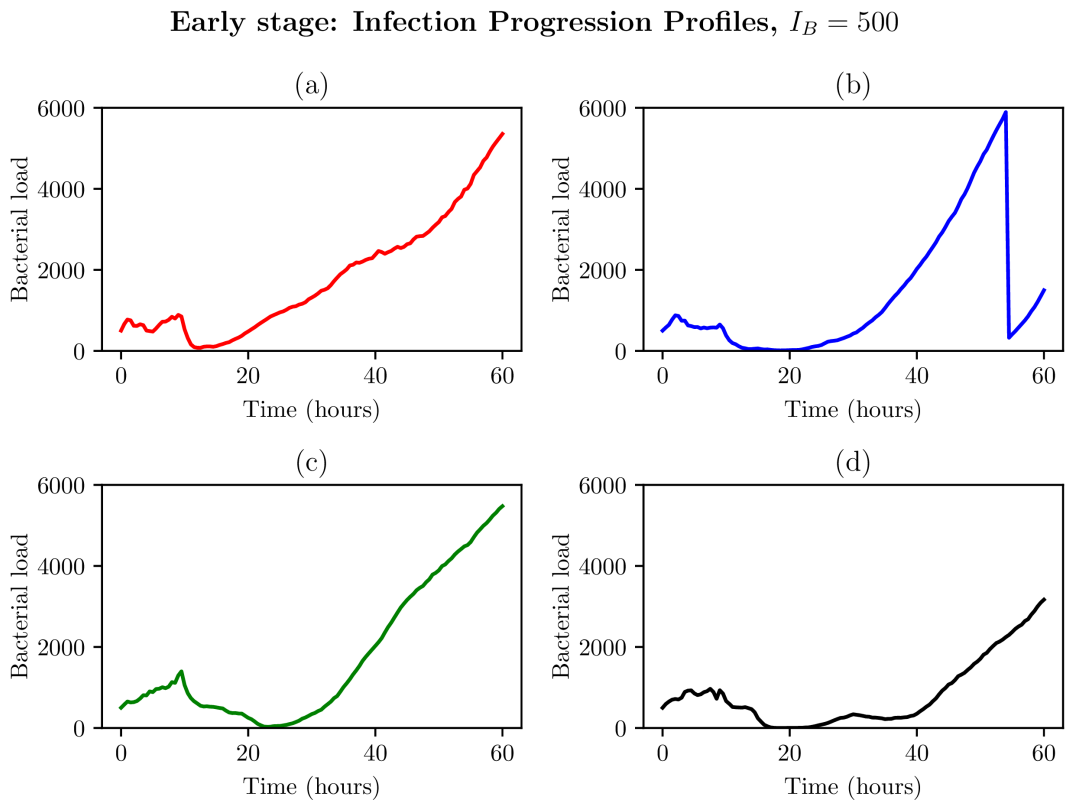

Figure 5.11: Simulations (a)-(d) represent the bacterial growth profiles arising from 4 representative example simulations for I_B = 500 where bacteria was not cleared during the early stage of the infection. Treatment is administered at T = 24 hours and bacterial shedding occurs if N_B exceeds 6000.

However, as we've seen in our previous simulations, due to the high replication rate of *E. Coli*, this initial rush of cells is often not enough to clear or stop the bacteria from replicating. However, as we can see in Figure 5.11 (a)-(c-d), with a high dose of Trimethoprim, bacterial replication during the early stages is hindered. This in turn results in fewer shedding episodes in our simulations, especially during the

early stages. This is important to note, as although bladder shedding is an important factor in bacterial clearance, overuse of this mechanism is known to have negative consequences such as the exposure of Bladder epithelium cells (BECs) to the toxic outer environment. Nevertheless, as can be seen in Figure 5.11 (c), even when simulating high treatment doses, *E. Coli* is able to replicate from very low numbers. In this simulation the bacterial load reaches $N_b = 40$ at $T = 23$ hours, a sharp decrease from the initial bacterial load. However, the bacteria is able to replicate and establish infection during the early stage, as can be seen in Figure 5.11.

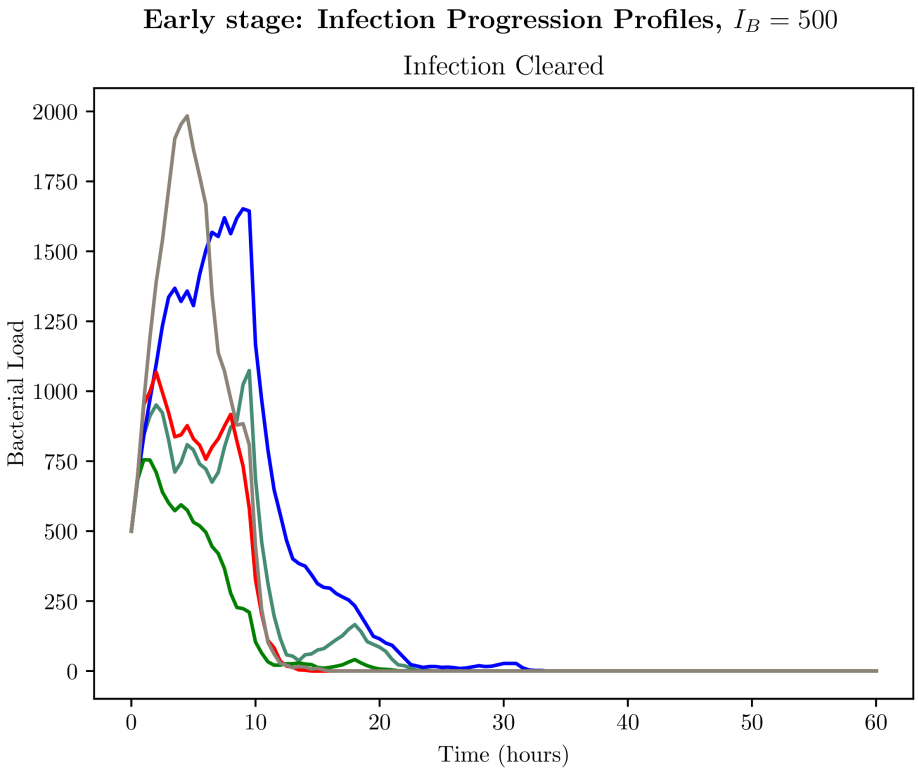

Figure 5.12: Bacterial growth profiles arising from 5 simulations where $I_B = 500$ where the infections were cleared during the early stages. Each colour represents a different simulations and treatment is administered at $T = 24$ hours.

5.3.2.2 Case where $I_B = 1000$

When simulating instances of high initial bacterial load and high dose of treatment, early progression profiles are split between exponential growth followed by shedding,

as can be seen in Figure 5.15 (c-d) or slow growth, Figure 5.15 (a-b). The profiles that initially present exponential growth will however not maintain such a rate for the entire simulation, as in contrast with the simulations in Section 5.3.1, continuous episodes of bacterial shedding are non existent in our high dose simulations. During the entire simulated time of 240 hours, the average number of bacterial sheddings until the clearance of infection is 3. This shows that treatment within our model lowers the need and therefore frequency of bacterial shedding episodes. This in turn, lowers the associated risks with over-regulation of the mechanism of bladder shedding. As can be seen from Figure 5.14, which shows us the bacterial load throughout the entire simulation for the infection profile (d) from Figure 5.15, even the simulations presenting with an early profile of exponential growth are usually subdued after the third episode of bacterial shedding.

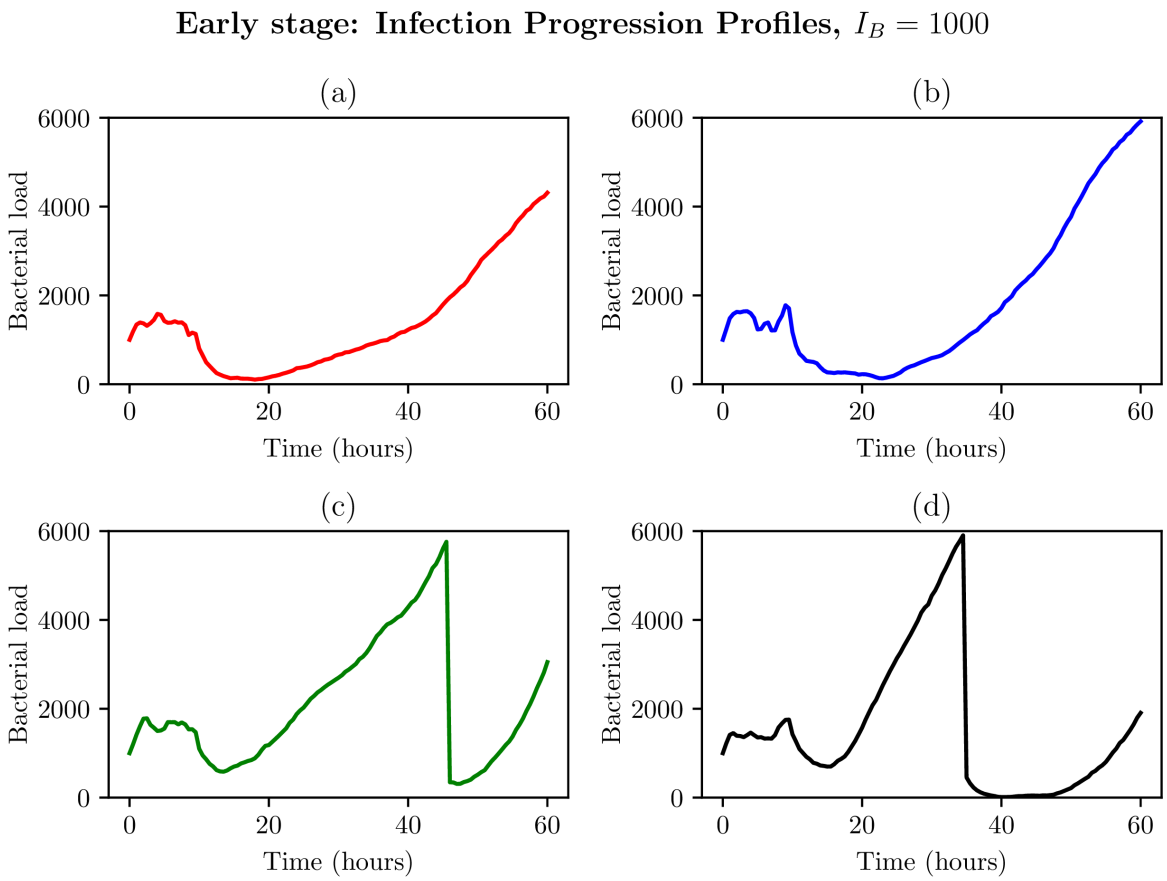

Figure 5.13: Simulations (a)-(d) represent the bacterial growth profiles arising from 4 simulations with I_B = 1000 where bacteria was not cleared during the early stage of the infection. Treatment is administered at T = 24 hours and each colour represents a different simulation. Bacterial shedding occurs when N_B = 6000

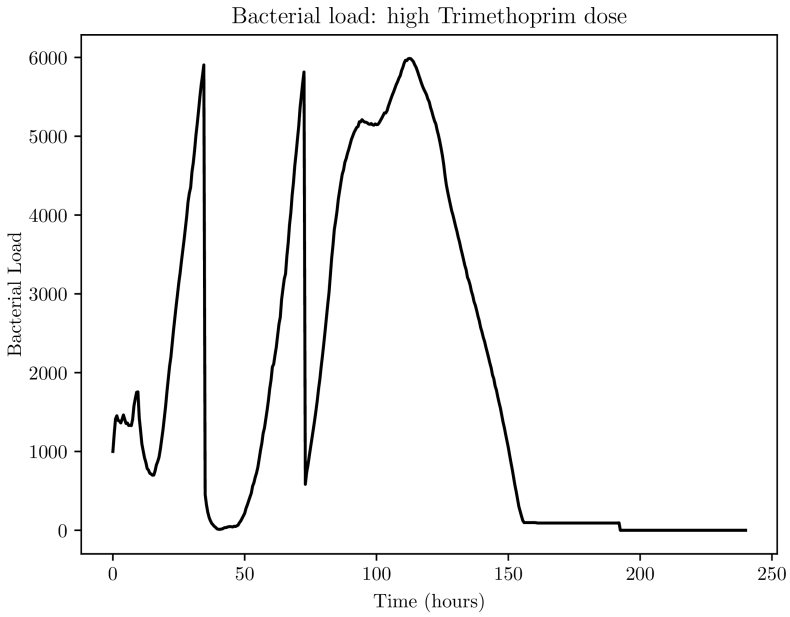

Figure 5.14: Bacterial load of simulation (d) in Fig 5.15.

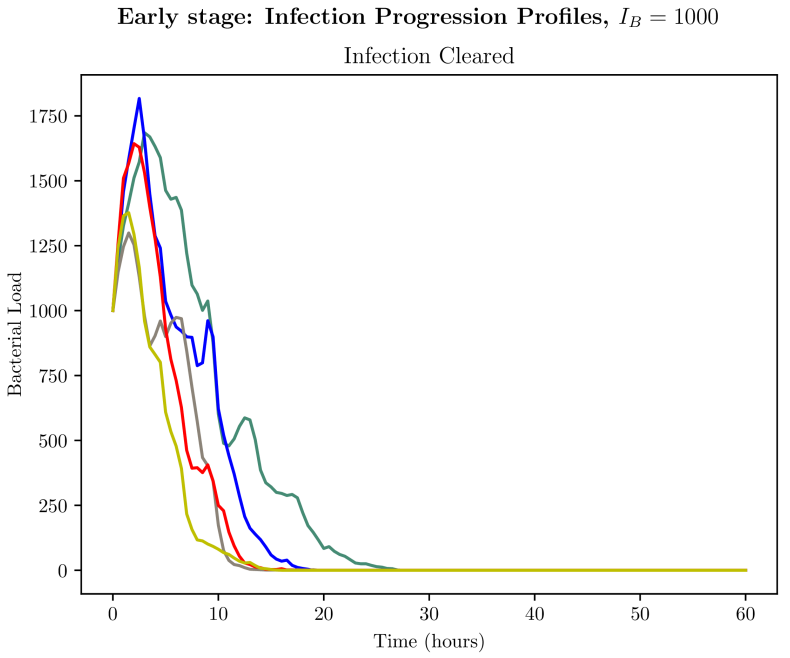

Figure 5.15: The bacterial growth profiles arising from 5 simulations with $I_B = 1000$ where the infections were cleared during the early stages. Treatment is administered at $T = 24$ hours and each colour represents a different simulation.

5.3.2.3 Analysis of aggregate results

We can also see the aggregate results for our model when used to simulate a treatment protocol with a high initial antibiotic load. This allows us to simulate a course of treatment using Trimethoprim for a patient who presents with an aggressive bladder infection. As discussed in Section 5.2, more aggressive infections are sometimes prescribed a higher dose of Trimethoprim. When using our model to simulate a treatment protocol using a dosing value of 100 mg, which is well above the MIC determined in our experiments in Chapter 4 and through the data collected (shown in Section 5.2), we get a new bacterial clearance profile. We find that when looking at simulations with an initial bacterial load of $I_B = 500$, 60.8% resulted in bacterial clearance when $200 \leq T < 240$ hours. We call this profile "Post" as can be seen in Figure 5.16. The simulations which did not result in bacterial clearance at the "Post" phase were also all cleared during the earlier phases of the simulations. 9.2% of simulations presented an early clearance profile while 27.7% of simulations resulted in clearance during the middle stage. Only 2.3% of simulations resulted in early bacterial clearance. Hence, when looking at the results of a higher initial load of $I_B = 1000$, we expect our bacteria to not be cleared during the early stages, thus, allowing for our treatment to show its effectiveness. As can be seen in Figure 5.16, simulations with an initial load of 1000 bacteria only present with two profiles. These simulations are either cleared during the middle stage, with 11.1% of our simulations doing so. However, the most expected outcome in bacterial clearance during the "Post" phase.

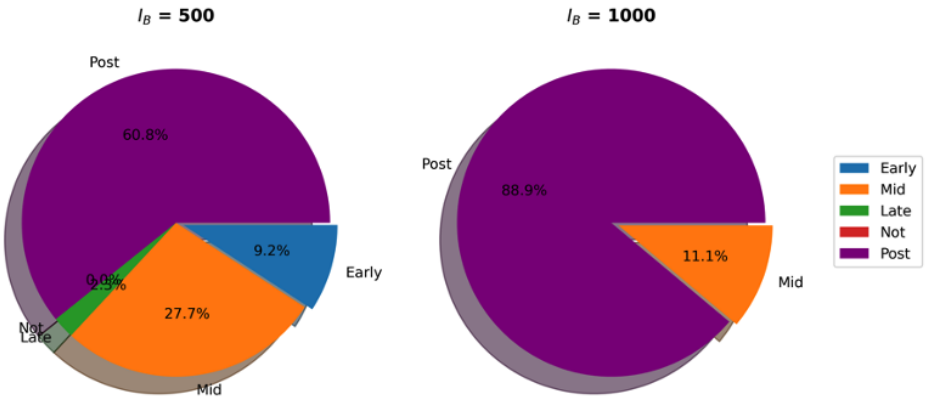

Figure 5.16: Aggregate analysis of $I_B = 500$ and $I_B = 1000$, presenting UPEC clearance status and during which stages clearance occurs. These plots represent the result for simulations of treatment with a high initial antibiotic dose

5.3.3 Summary of Trimethoprim effects

As can be seen from Figure 5.17, the simulations with a higher initial dose of antibiotic, present the expected profile of bacterial clearance. Around $T = 130$ hours (5 doses into the simulated treatment), Trimethoprim is able to halt the usual pattern of bacterial growth and shedding prevalent during the early stages of the infection. Following a short period of non replication, all *E. Coli* is cleared before the simulation is finished. This pattern of bacterial clearance is what we expect from simulations where the treatment concentration value is well above the MIC. On the other hand, when selecting lower doses of the drug, as can be seen from the yellow line in Figure 5.17, our model shows continued bacterial growth, opposed only by periodic episodes of bacterial shedding.

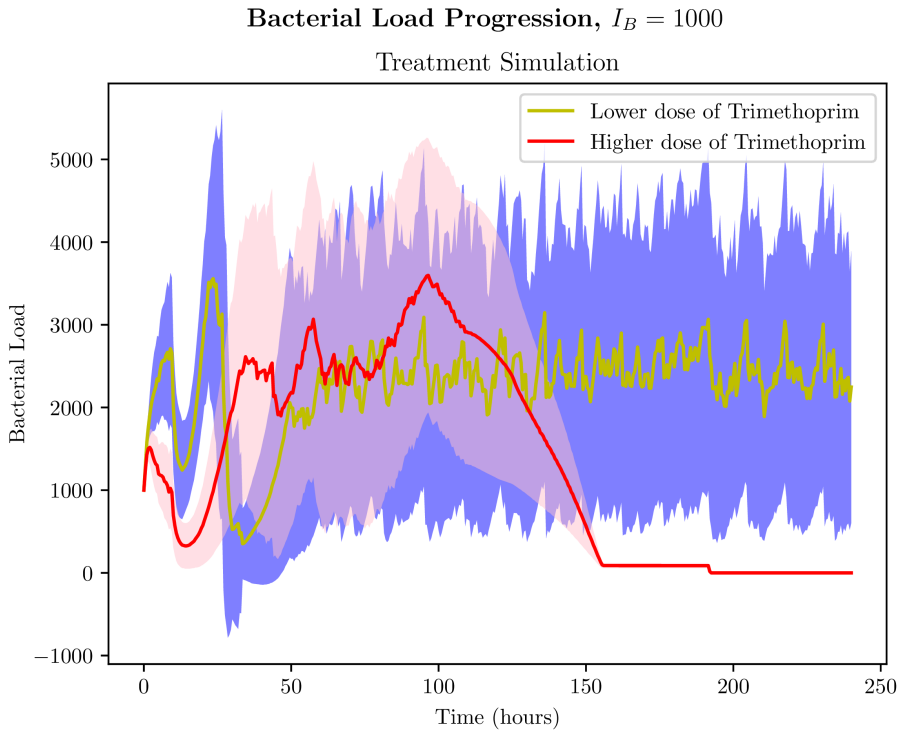

Figure 5.17: Average bacterial load over our simulations. In red, we have the simulations where the initial Trimethoprim dose is 100 mg. In yellow, we have the simulations where the initial dose of Trimethoprim is 20 mg. In both instances, the initial bacterial load is $I_B = 1000$. The shaded regions represent the 95% confidence intervals of our data.

5.4 Visualising *UTImodel* simulations

In this section we present visualisations of our model with different initial bacterial loads. This gives us a better insight into the effects of spatial location and allows us to track the bacterial growth through observation of clusters responsible for such growth. It is also important to determine the outcome of the early stage of such infections as it also shows us the effects Trimethoprim treatment has on the bacteria during the early stages. Current treatment as mentioned in Section 5.2 can range from 3 to 7 days. Thus, by investigating the effects of treatment (with an initial dose of 100 mg) on the early stages of infection progression we are able to see whether a shorter length of treatment is equally effective at clearing bacteria within our model depending on the initial bacterial load.

Looking at Figure 5.18, we can see an example of a simulation where $I_B = 1$ and the bacteria manages to establish infection during the early stages of the infection. We can note the effects of the chemokine diffusion and how this leads immune cells to the site of infection, which is due to the chemokine release by activated resident macrophages as explained in Section 2.2.4. At $T = 15$ hours we can see how the neutrophils are already at the site of infection carrying out bacterial clearance. At this time during our simulation we note 1 main bacterial cluster, and 2 other smaller clusters closer to the centre of our environment. At $T = 30$ hours the first dose of treatment is already introduced ($T = 24$ hours), the infection remains under control in addition to an increase in the load of neutrophils which allows the immune system to counteract bacterial growth in a more efficient way. Bacterial clusters remain with an increased size from those seen at $T = 15$ hours, however bacterial growth is clearly hindered as *E. Coli* replicates at a much higher rate under optimal conditions in the absence of the immune system and antibiotic treatment as is shown in Chapter 4. At $T = 45$ hours however, we can see the fast growth characteristic of *E. Coli*. Neutrophils are still present and fighting the infection however due to the exponential increase of bacteria, they are not able to counteract the infection. It's

worth noting that 3 hours (at T = 48 hours) later within the simulation the second dose of treatment will be administered which will further inhibit bacterial growth during the late stages of the infection. However, the profile shown in Figure 5.18 will lead to 2 episodes of shedding prior to the treatment and antibiotic being able to bring the infection under control.

Bacterial Replication: $I_B = 1$

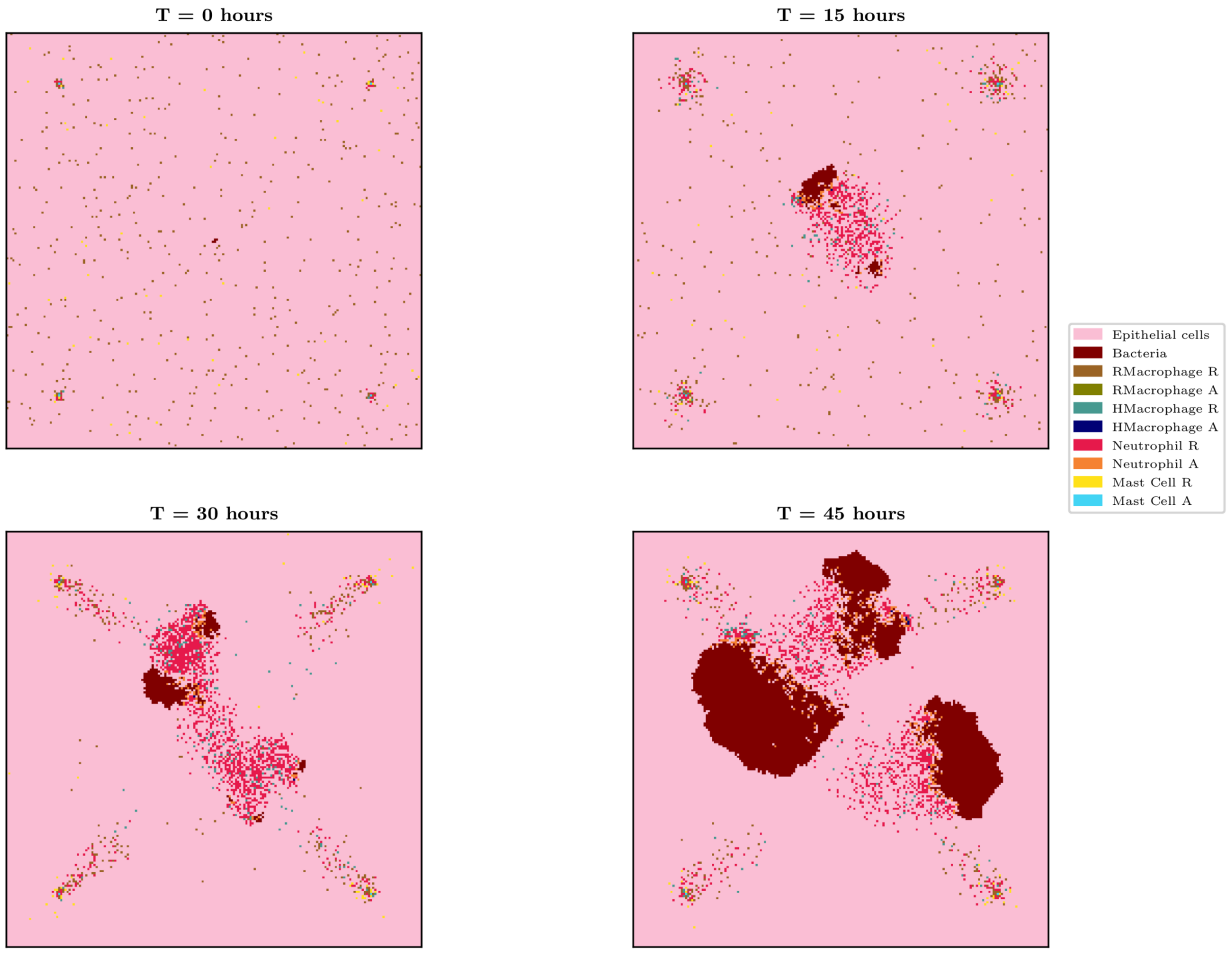

Figure 5.18: A model simulation arising from I_B = 1.

In the case of I_B = 100, as we can see from Figure 5.19 the infection is even more contained than the one previously seen in Figure 5.18. This may be due to the ability of the immune system to detect the bacteria early as it is a larger initial bacterial load. Nevertheless, bacterial growth is hindered completely during the early stages as can

be seen at T = 15 hours by the recruitment of neutrophils to the site of infection. We cannot see any large bacterial clusters at T = 15 hours and T = 30 hours, which is due to the actions of the immune system during the first 24 hours of the infection and the antibiotic treatment with the first dose administered at T = 24 hours. Hence at T = 15 hours we can only see two small clusters within the environment, one of which is cleared, as can be seen by T = 30 hours. The other remaining cluster however manages to establish a small infection which can be seen at T = 45 hours forming towards the upper side of our model domain.

Bacterial Replication: $I_B = 100$

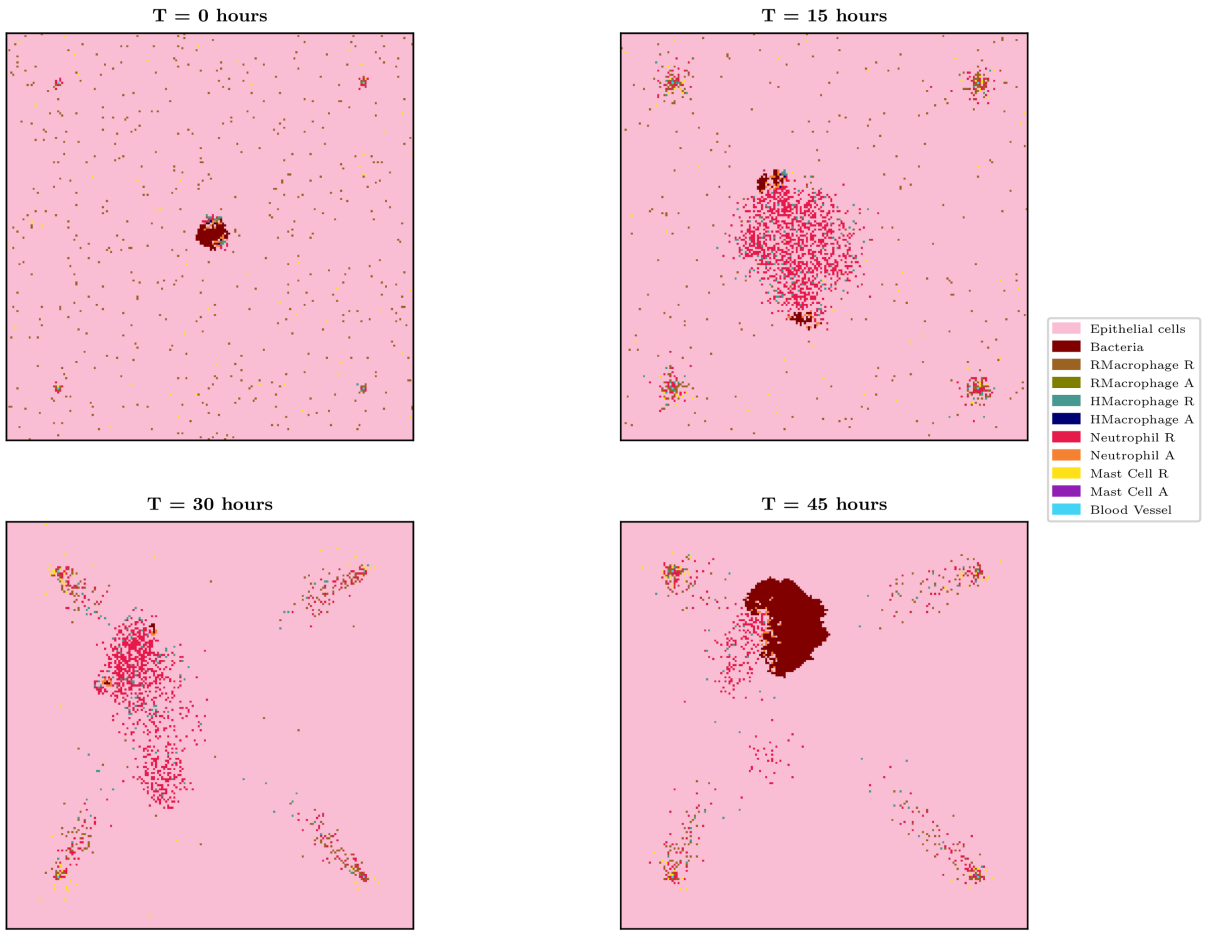

Figure 5.19: A model simulation arising from I_B = 100.

As opposed to Figure 5.18, the infection in Figure 5.19 does not present a high

growth profile towards the end of the early stages of the infection. This may be due to a range of factors, such as the timing for treatment. In Figure 5.18, at $T = 20$ hours, 4 hours before the first dose of treatment is administered the infection is not completely under controlled as two cluster can be seen clearly. However, at the same stage of infection, in Figure 5.19, the infection is completely under control with any remaining bacteria barely noticeable in our simulation.

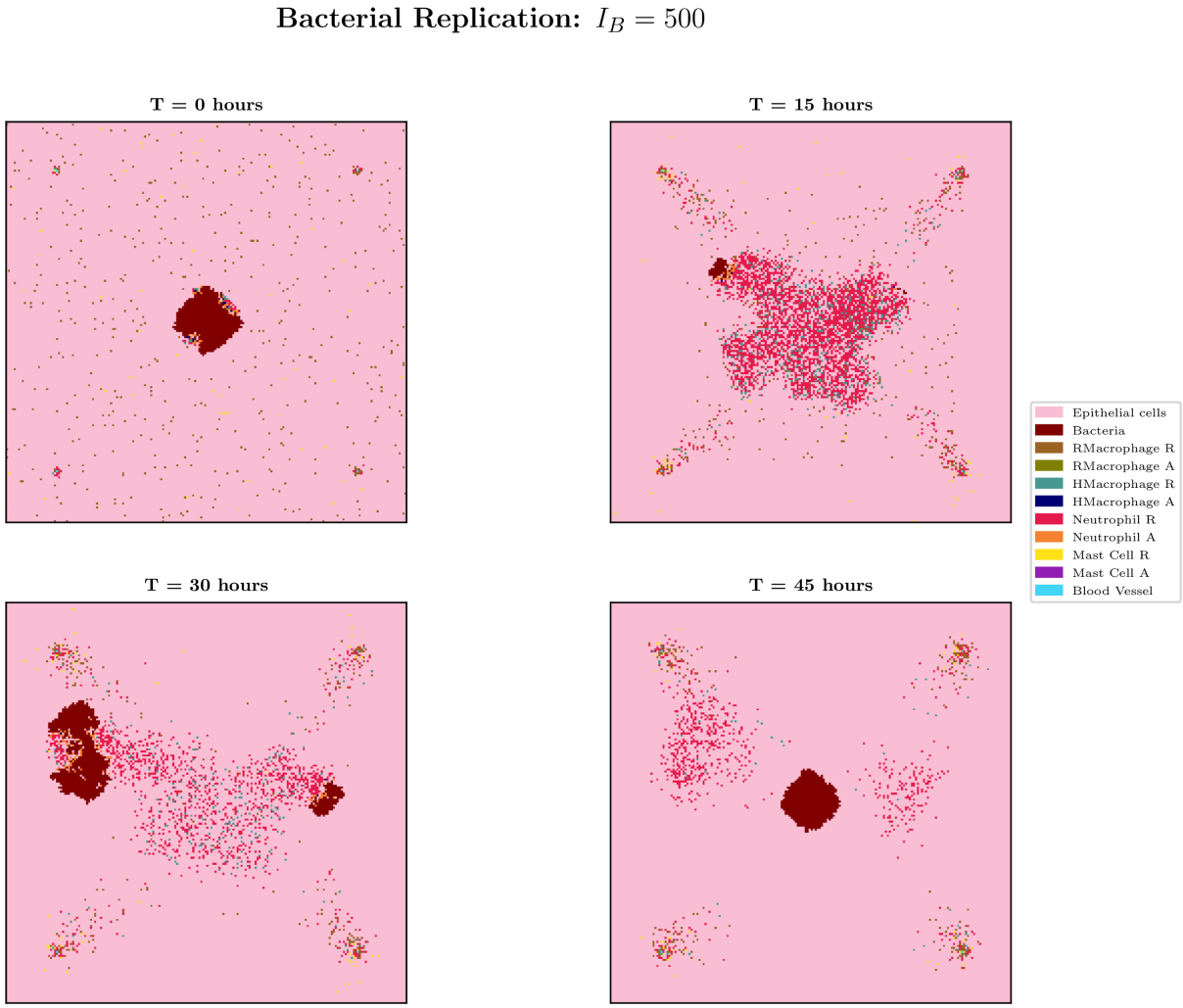

Figure 5.20: A model simulation arising from $I_B = 500$.

In addition to this, the number of bacterial clusters and location is more optimal in Figure 5.19 than that seen in Figure 5.18. The latter presents with more clusters positioned further away from the blood vessels which is the source of treatment

than the cluster seen at T = 45 hours in Figure 5.19, highlighting the importance of bacterial location in determining outcome.

In the case of I_B = 500, as can be seen in Figure 5.20, we can see the effects the increase in the initial bacterial load has on the outcome of the early stage of infection. What is also important to note is the neutrophil load which as can be seen in Figure 5.20 is much greater than that shown in Figure 5.18 and Figure 5.19.

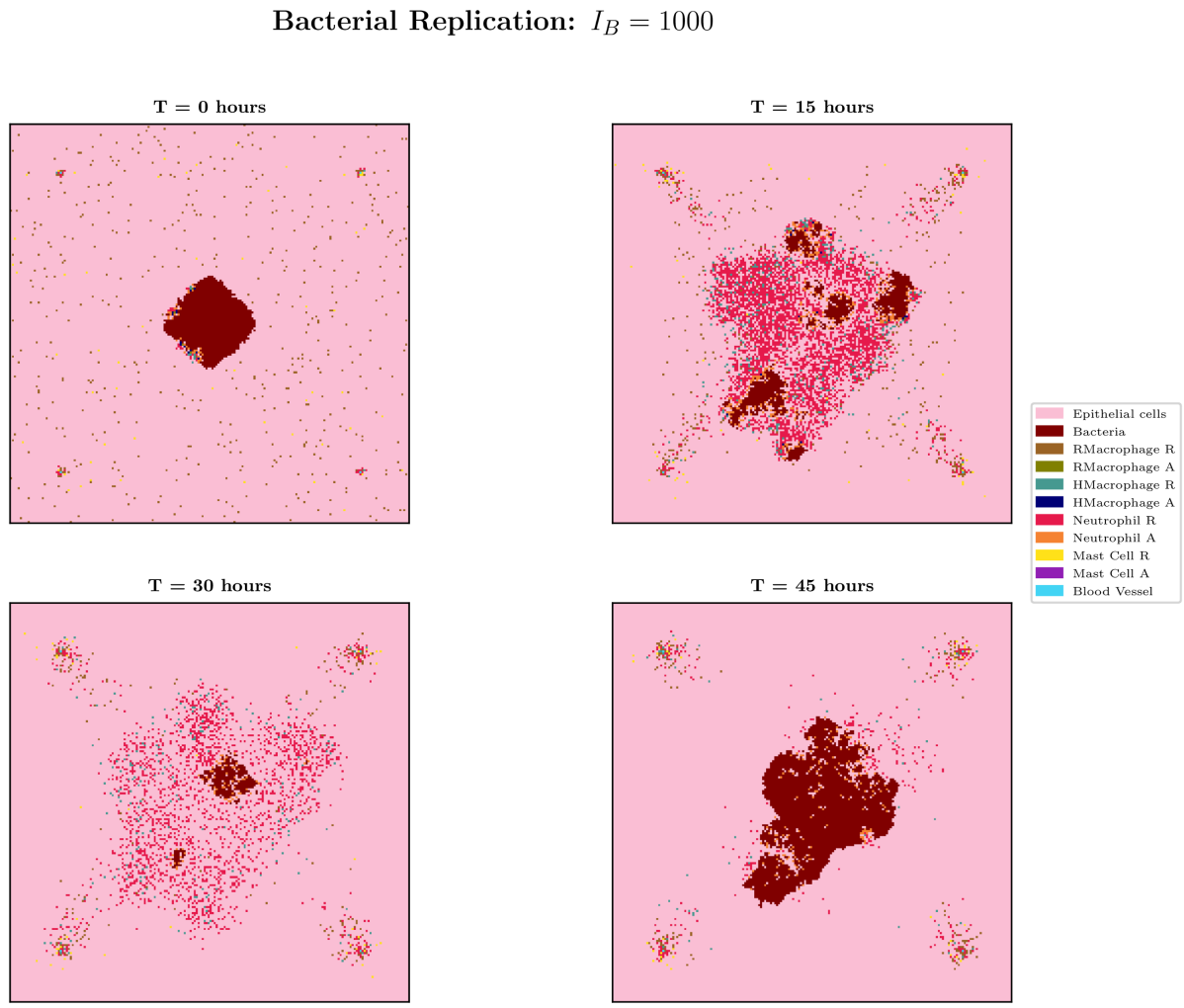

Figure 5.21: A model simulation arising from I_B = 1000.

Although at T = 15 hours no large clusters are present and the infection seems to be controlled, at T = 30 hours we can see 2 bacterial clusters in opposite sides of the environment. What happens next in this simulation is exponential bacterial growth

from $T = 30$ hours to $T = 44$ hours, leading to an episode of bacterial shedding triggered when N_B reaches 6000, after which that was able to evade killing and penetrate the superficial bladder wall is then reseeded into the environment, thus simulating deeper layers of the bladder. After the early episode of shedding. We can see neutrophils present however in lower numbers than those at $T = 15$ and $T = 30$ hours. As bacterial shedding happens just prior to the time of administration of the second dose of Trimethoprim within our model, the bacterial cluster will be located in the centre of the environment and hence be less affected by the treatment than the cluster seen in Figure 5.19, for example.

As expected, in the case of $I_B = 1000$, which represents a high initial bacterial load, the bacteria is able to establish a larger infection. The number of bacterial clusters seen in Figure 5.21 during the early stages especially at $T = 15$ hours and $T = 30$ hours is far greater than that seen in Figure 5.19 and Figure 5.20. The number of neutrophils during the initial stages of the infection is also, as expected, higher than that seen in lower initial bacterial loads. However due to the increased size of bacteria clusters and the dispersed nature of these clusters, the immune cells are not able to keep the infection under control during the early stages of infection. After the first dose of treatment ($T = 24$ hours), the number of clusters is reduced to 2 as can be seen in Figure 5.21 with only one sizeable cluster at the centre of our environment. Towards the end of the early infection stage however, we see how the infection is able to grow and how the immune system is not able to keep with the exponential replication rate presented by *E. Coli*. This exponential replication may lead to various shedding episodes until the treatment is able to clear the bacteria. In the case of $I_B = 1000$, the spatial location of the bacteria may have influenced on the outcome as the bacterial cluster which managed to establish infection is placed in the middle of the environment.

5.5 Conclusion

In this chapter, we incorporated the treatment framework into our *UTImodel* to examine the impact of treatment on infection outcome. We developed a framework that can simulate the treatment protocol for Trimethopriom, the preferred drug for bladder infections, and parameterized it with values from the literature (Section 5.2) and experiments conducted in Chapter 4. Typically, the treatment course for recurrent uncomplicated bladder infections using Trimethoprim lasts for 3-7 days, while patients with severe infections receive longer treatment. Consequently, we simulated our model for 240 hours to analyze the results while simulating a full course of treatment for a patient with a recurrent uncomplicated bladder infection.

Initially, we generated multiple simulations that examined the impact of low Trimethoprim doses (20 mg) on different initial bacterial loads ($I_B = 1, 100, 500, 1000$). The results showed that a low concentration of Trimethoprim does not make a significant difference to the infection outcome, especially in the early stages of infection, as demonstrated by the yellow line in Figure 5.17, which represents the average bacterial loads for our simulations with low Trimethoprim concentration (where $I_B = 1000$). In these simulations, the infection outcome is unfavorable, as bacteria continue to replicate and establish infection, interrupted only by periodic episodes of shedding.

Furthermore, we analyzed the effects of different initial bacterial loads, which yielded expected results, as seen in Chapter 3: higher initial bacterial loads lead to worse infection outcomes. Although more severe initial infections elicit a greater response from the immune system, immune cells are unable to counteract the exponential bacterial growth resulting from a severe infection. Consequently, the infection persists throughout the simulation without bacterial clearance post-treatment. We also noted for a second time what as confirmed in Chapter 3 that even one bacteria may result in the establishment of an infection when the treatment concentration

is lower than needed under the right conditions (see Figure 5.1) thus confirming experimental results.

However, when looking at cases where the initial Trimethoprim dose is high (100 mg), bacterial clearance was the only outcome, with clearance happening mostly between 160 hours and 190 hours as can be seen in Figure 5.17, a phase we refer to as post-treatment. These results coincide with what we have seen in Chapter 4 where we conducted *in vitro* experiments to determine both the replication rate of *E. Coli* and the effects of Trimethoprim on the growth rate of the bacteria.

Within the literature, the high MBC value for Trimethoprim makes it a predominantly bacteriostatic agent, which means it is able to halt the growth of bacteria at normal doses such the ones prescribed for treatment in Section 5.2 (100 mg, 200 mg), however, on its own Trimethoprim is not able to kill bacteria at such doses. Nonetheless, even at treatment doses, when combined with the action of the immune system, Trimethoprim is able to greatly affect the outcome of the infection. *E. Coli* is known for its low infectious doses meaning the replication rate of the bacteria is a great factor in the establishment of infection. With the combination of immune cells actions and Trimethoprim diffusion the effects on the infection outcome suggest that Trimethoprim is effective at current prescribed doses of treatment. In addition to this, Trimethoprim is also sometimes prescribed along with Sulfamethoxazole which is a bactericidal agent, allowing for more clearance during the treatment process. As we develop our model to include many lines of treatment we can explore more complex treatment strategies such as Trimethoprim-Sulfamethoxazole.

We also present simulations of our model in order to perform a visual analysis of the effects of spatial location and the presence of bacterial clusters on the infection outcome. Looking at Figure 5.18, Figure 5.19, Figure 5.20 and Figure 5.21 we can see how simulations presenting with bacterial clusters further away from the blood vessels are usually tougher to clear. This is expected as blood vessels are the source of Trimethoprim and recruited immune cells. In future work we also plan to

incorporate a Pharmacokinetic ODE model to more realistically mimic appropriate dosing of Trimethoprim.

Chapter 6

CONCLUSION

6.1 Summary

We have developed a spatio-temporal mathematical model to investigate the pathogen-host response in typical bladder infections and also inducing the effects of antibiotic treatment. In a 2-dimensional $16mm^2$ section of the bladder, we use our hybrid agent-based model to simulate Uropathogenic *E. Coli* as individual elements, as well as immune cells. In particular, we model resident and helper macrophages, neutrophils and mast cells the key immune cells acting during bladder infections. In addition to these discrete elements, we also model a generic chemokine in order to act as a chemoattractant. This molecule directs the immune cells to the site of infection, diffusing into the spatial domain via a PDE. Our model also captures bacterial shedding which is triggered once the bacterial load within the environment reaches $N_B = 6000$.

We conducted uncertainty and sensitivity analysis on our model, and in doing so, we determined the effects that our parameters (independent variables) have on the several outputs of our model such as bacterial load, number of bacteria killed by neutrophils, and others. We found that neutrophil associated parameters, such as movement rate and activation probability, were the most sensitive parameters, highlighting their importance in the model. In addition to this, the recruitment of macrophages during the early stages of infection also carried significance to the subsequent bacterial clearance or establishment of infection. This confirms the current available data regarding the importance of these immune cell types in bladder infections [51, 52]. Early recruitment of macrophages is crucial to the detection of the infection and subsequent attraction of other immune cells, such as neutrophils, which are in turn responsible for bacterial clearance. In addition to this, resident

macrophages will help guide other immune cells towards the site of infection through the secretion of a generic chemokine within the environment.

When investigating bladder infections, the bacterial load is known to be a determining factor towards the progression of the infection and hence clinicians usually take this as a factor when arranging a treatment protocol. By investigating the effects of the initial bacterial load on infection outcome we are able to determine the profiles resulting from host-pathogen interactions and use our model to confirm whether higher initial bacterial loads do in fact lead to a more severe infection. We also confirm that even though low initial bacterial loads usually lead to bacterial clearance during the early stages of infection, it is possible for bacterial replication to overtake the immune system and establishment of an infection to emanate from low initial bacterial loads.

We also were able to use our model to simulate other properties of an immunodeficient environment. We did so by modifying the initial number of resident macrophages, I_{rM} and mast cells, I_{MC}, as can be seen in Section 3.4. Our simulations resulting from this are in line with the literature, showing a greater chance of infection establishment and heavier bacterial loads throughout the infection.

In Chapter 5, we introduced a treatment framework to our model which we use to simulate treatment protocols for the antibiotic Trimethoprim, the most common treatment option for bladder infections, through experiments where we determine the bacterial growth profile of *E. Coli* and its susceptibility to Trimethoprim, as shown in Chapter 4. This, in combination with the results found in the literature in Section 5.2 helped us further parameterise our treatment framework. An analysis of this framework was conducted in Chapter 5, where we simulated treatment protocols for recurrent uncomplicated bladder infections with varying initial concentration of the antibiotic and initial bacterial load. This allowed us to investigate the effects of Trimethoprim on the infection progress and outcome. We also visualised simulations in order to capture the effects of spatial location on the infection progression.

This is an important subject as the blood vessels present within our environment are the source of Trimethoprim and recruited immune cells. Thus, the location of these vessels affects the infection progression as seen in Figure 5.18, Figure 5.19, Figure 5.20 and Figure 5.21.

With our novel hybrid agent-based model we are able to simulate the progression of *E. Coli* within the bladder over the full course of recommended Trimethoprim treatment for uncomplicated infections (see Section 5.2). This opens up a new simulation framework for UTIs and bladder infections, where we are able to use computational simulations parameterised by *in vitro* experiments we conducted, in addition to results from *in vivo* experiments available in the literature.

6.2 Practical impact of this work

Our approach to modelling bladder infections provides a simulation framework that is capable of providing researchers and clinicians a tool to explore different treatment strategies and their effects on the infection outcome. By modifying parameters such as initial bacterial load, drug concentration and treatment duration we are able to explore new strategies, identifying the individual profiles arising from such strategies and the aggregate outcome as was done in Chapter 3. This approach has the potential to inform clinical decision-making and improve patient outcomes by providing a more comprehensive understanding of the complex interactions between bacteria, immune cells, and drugs. Therefore, the practical use of an agent-based model studying bladder infections with treatment can provide valuable insights into the underlying mechanisms of infection and the potential effectiveness of different treatment strategies. In addition to studying the effects of new treatment strategies on the outcome of bladder infection, our model can also allow clinicians to devise individually tailored treatment strategies. This can be done through the introduction of parameters such as age and gender (the parameters will influence the other parameter values in the model by capturing what we know so far about the effects of the new parameters on the development of the infection) and modifying existing ones such as bacterial load and immune status to match the patient profile. This personalized approach has the potential to revolutionize clinical practice by allowing clinicians to tailor treatment strategies to individual patients based on their unique characteristics and disease history.

Studies have shown that recurrent UTIs are a common problem, with up to 25% of women experiencing a second infection within six months of their first UTI. The risk of recurrence is even higher for women who have had multiple UTIs in the past, with some studies reporting a recurrence rate of up to 80% [33]. While antibiotics have been a mainstay of UTI treatment for decades, the emergence of antibiotic-resistant strains of bacteria highlights the need for alternative approaches.

Traditional methods of studying UTIs, such as laboratory cultures and animal models, have provided valuable insights into the biology of these infections. However, these approaches have limitations when it comes to understanding the interactions between bacteria and the host immune system, as well as the effects of different treatment strategies. Agent-based models have the potential to address these limitations by allowing researchers to study the behavior of individual bacteria and immune cells in a simulated environment. In addition to this, we have have also constructed a UASA framework allowing us to study the effects of any newly introduced initial parameters to our model.

This has been done in the cancer field, agent-based models have been used to simulate these interactions and predict the effectiveness of different treatment strategies. For example, a study published in the journal Cancer Research used an agent-based model to simulate the effects of chemotherapy on tumor growth in patients with glioblastoma, a type of brain cancer. The model incorporated data on the growth rates of cancer cells, the activity of immune cells, and the pharmacokinetics of the chemotherapy drug. The results of the model showed that traditional chemotherapy regimens, which involved administering high doses of the drug over a short period of time, were less effective than alternative regimens that involved lower doses of the drug administered over a longer period of time. The model also predicted that combining chemotherapy with immunotherapy, which stimulates the immune system to attack cancer cells, could further improve treatment outcomes. Based on these findings, the researchers suggested that alternative chemotherapy regimens and combination therapies with immunotherapy may lead to better outcomes for patients with glioblastoma. This study highlights the potential of agent-based models to inform treatment decisions and improve patient outcomes in complex diseases.

6.3 Limitations and challenges

As with every other modelling techniques, there are certain limitations to consider utilising agent-based models in the study of complex biological phenomena. these limitations include:

- Over-simplification of the system to be investigated: It is very important to conduct an extensive review and analysis of the biological system to be modelled before building an agent-based model. This allows us to identify the key known mechanisms in the system and their respective roles. As we noted in Section 1.4.1, due to complex nature of the systems to be described, ABMs have to consider simplifications in order to satisfy computational constraints. However, when considering an over-simplified model, these simplifications may not capture the full complexity of the infection and may result in inaccurate or incomplete predictions. Hence, any earlier model simplifications should be examined, thus making sure this optimisation step is not at the cost of the model integrity.

- Parameter uncertainty: The accuracy of agent-based models is dependent on the quality and reliability of the input data used to parameterize the model. In many cases, data on key parameters such as bacterial growth rates, drug pharmacokinetics, and host immune responses may be limited or uncertain. In our research we conducted various experiments to validate important parameters within our model such as bacterial growth rate and the effects of treatment on infection outcome as can be seen in Chapter 4.

- Computational resources: Agent-based models can be computationally intensive, requiring significant computing power and time to run simulations. This may limit the ability to explore a large parameter space and can result in long simulation times. Our model run-time for a simulation of a complete course of treatment takes on average 17 minutes. When running multiple simulations

as done in Chapter 3 and Chapter 5 we also parallelise our model to run on all available machine cores. This allows us to further optimise against an increasing time complexity.

- Model validation: one of the most important things to note is that agent-based models require validation against experimental data to ensure that they accurately capture the behavior of the biological system being studied. This validation may often be challenging due to the complexity of the system and the difficulty in obtaining relevant experimental data.

All of these limitations have to be taken into consideration when implementing and parameterising our model. By first conducting UASA analysis on our model we are able to determine the sensitivity of certain parameters and in doing so explore the parameter uncertainty limitations. By conducting research and experiments to validate important parameters within our model, we were able to also overcome some of these limitations in our study. Despite these limitations, agent-based models remain a valuable tool for investigating and informing treatment strategies for complex infections such as bladder infections.

6.4 Future model developments

One area of future work is the integration of biofilms into the model. Biofilms are communities of microorganisms that adhere to surfaces and form a complex, three-dimensional structure embedded in a self-produced extracellular matrix. Biofilms are increasingly recognized as a key factor in the pathogenesis of chronic infections, including UTIs. In UTIs, bacteria can colonize the bladder and form biofilms on the surface of the bladder wall or on indwelling urinary catheters. Biofilm formation can increase the resistance of bacteria to antibiotics and host immune responses, and can also serve as a reservoir for recurrent infections.

In the context of bladder infections, biofilm formation has been shown to play a critical role in the development of recurrent infections. Studies have demonstrated that biofilm formation by UPEC was a key factor in the persistence of bladder infections. They found that UPEC was able to form biofilms on the surface of bladder epithelial cells and that these biofilms were able to resist host immune responses and antibiotic treatment. Similarly, another study has shown that biofilm formation by UPEC on catheter surfaces was a key factor in the development of catheter-associated UTIs. Integrating biofilm formation to our model will enable us to better understand the mechanisms by which biofilms contribute to recurrent infections and to develop new strategies to prevent or treat these infections. Future work in our agent-based model will focus on integrating biofilm formation and dynamics into our model, to enable us to simulate the effects of different interventions on biofilm formation and to explore new treatment strategies that target biofilms.

Another area of future work is the investigation of more complex treatment regimens. In this model, we have simulated a standard course of antibiotic treatment for bladder infections. However, there are many other potential treatment options that could be explored, such as combination therapy, alternative antibiotics, or even immunotherapy. By exploring these options, we can gain a better understanding of the most effective treatment strategies for different types of infections, and potentially

develop new treatment protocols.

As of now, we introduce Trimethoprim treatment through diffusion from the fixed vessels within our model, however it does not incorporate the full PK dynamics of Trimethoprim. This means we assume the drug immediately appears at the blood vessels in the bladder every 24 hours (thus not looking at the absorption profile from an oral dose). As a future development to our model, we intend to incorporate the full PK profile during treatment through an ODE system.

Furthermore, the current model focuses on acute bladder infections, which are typically resolved within a few days. However, chronic bladder infections are a significant problem, particularly in patients with indwelling catheters or other urinary tract abnormalities. By expanding the model to include chronic infections, we can investigate the factors that contribute to their persistence and potentially identify new treatment strategies.

As we further develop our existing model, we can also think of extending the simulated environment to capture other parts of the urinary tract such as the urethra. In addition to this we also plan to include the BECs as agents within the model in future iterations, as well as expand the model to three dimensions in order to more realistically simulate the environment. In doing so, we will be able to investigate UTIs through a wider lens.

BIBLIOGRAPHY

[1] SN Abraham and Y. Miao. “The nature of immune responses to urinary tract infections”. In: *Nat Rev Immunol.* 15.4 (2015), pp. 655–663. DOI: 10.1038/nri3887. URL: https://www.nature.com/articles/nri3887.

[2] Soman N. Abraham and Yuxuan Miao. “The nature of immune responses to urinary tract infections”. In: *Nature Reviews Immunology* 15.10 (2015), pp. 655–663. DOI: 10.1038/nri3887. URL: https://doi.org/10.1038/nri3887.

[3] G. An et al. “Optimization and Control of Agent-Based Models in Biology: A Perspective”. In: *Bulletin of Mathematical Biology* 79.1 (2017), pp. 63–87. DOI: 10.1007/s11538-016-0225-6. URL: https://doi.org/10.1007/s11538-016-0225-6.

[4] G. An et al. “Optimization and Control of Agent-Based Models in Biology: A Perspective”. In: *Bulletin of Mathematical Biology* 79 (2017), pp. 63–87. DOI: 10.1007/s11538-016-0225-6. URL: https://doi.org/10.1007/s11538-016-0225-6.

[5] Thomas E. Andersen et al. “Escherichia coli Uropathogenesis In Vitro: Invasion, Cellular Escape, and Secondary Infection Analyzed in a Human Bladder Cell Infection Model”. In: *Infection and Immunity* 80.5 (2012), pp. 1858–1867. DOI: 10.1128/IAI.06075-11. eprint: https://journals.asm.org/doi/pdf/10.1128/IAI.06075-11. URL: https://journals.asm.org/doi/abs/10.1128/IAI.06075-11.

[6] Hélène Arduin et al. “An agent-based model simulation of influenza interactions at the host level: insight into the influenza-related burden of pneumococcal infections”. In: *BMC Infectious Diseases* 17.1 (2017), p. 382. DOI:

10.1186/s12879-017-2464-z. URL: https://doi.org/10.1186/s12879-017-2464-z.

[7] Anna AU Zychlinsky Scharff, Matthew L. AU Albert, and Molly A. AU Ingersoll. "Urinary Tract Infection in a Small Animal Model: Transurethral Catheterization of Male and Female Mice". In: *JoVE* 130 (2017), e54432.

[8] Amelia E. Barber et al. "Strengths and Limitations of Model Systems for the Study of Urinary Tract Infections and Related Pathologies". In: *Microbiology and Molecular Biology Reviews* 80.2 (2016), pp. 351–367. DOI: 10.1128/MMBR.00067-15. eprint: https://journals.asm.org/doi/pdf/10.1128/MMBR.00067-15. URL: https://journals.asm.org/doi/abs/10.1128/MMBR.00067-15.

[9] Kate B Barnes, Gerda Szakonyi, and M D'enes Gyurk'o. "Trimethoprim: mechanism of action, resistance, and new developments". In: *Biomolecules* 9.11 (2019), p. 236. DOI: 10.3390/biom9110236.

[10] Francisco Barros-Becker et al. "Live imaging reveals distinct modes of neutrophil and macrophage migration within interstitial tissues". In: *Journal of Cell Science* 130.22 (Nov. 2017), pp. 3801–3808. ISSN: 0021-9533. DOI: 10.1242/jcs.206128. eprint: https://journals.biologists.com/jcs/article-pdf/130/22/3801/1948692/jcs206128.pdf. URL: https://doi.org/10.1242/jcs.206128.

[11] Francisco Barros-Becker et al. "Live imaging reveals distinct modes of neutrophil and macrophage migration within interstitial tissues". In: *Journal of Cell Science* 130.22 (Nov. 2017), pp. 3801–3808. ISSN: 0021-9533. DOI: 10.1242/jcs.206128. eprint: https://journals.biologists.com/jcs/article-pdf/130/22/3801/1948692/jcs206128.pdf. URL: https://doi.org/10.1242/jcs.206128.

[12] Erin N Bodine et al. “Agent-Based Modeling and Simulation in Mathematics and Biology Education.” In: *Bull Math Biol* 82 (2020). ISSN: 1522-9602 (Electronic); 0092-8240 (Print); 0092-8240 (Linking). DOI: 10.1007/s11538-020-00778-z.

[13] Şebnem Bora and Sevcan Emek. “Agent-Based Modeling and Simulation of Biological Systems”. In: *Modeling and Computer Simulation*. Ed. by Dragan Cvetković. Rijeka: IntechOpen, 2018. Chap. 3. DOI: 10.5772/intechopen.80070. URL: https://doi.org/10.5772/intechopen.80070.

[14] Ruth Bowness et al. “Modelling the effects of bacterial cell state and spatial location on tuberculosis treatment: Insights from a hybrid multiscale cellular automaton model”. In: *Journal of Theoretical Biology* 446 (2018), pp. 87–100. ISSN: 0022-5193. DOI: https://doi.org/10.1016/j.jtbi.2018.03.006. URL: https://www.sciencedirect.com/science/article/pii/S0022519318301206.

[15] Jolanda K. Brons et al. “Fast identification of Escherichia coli in urinary tract infections using a virulence gene based PCR approach in a novel thermal cycler”. In: *Journal of Microbiological Methods* 169 (2020), p. 105799.

[16] Cheryl Y. Chan, Ashley L. St. John, and Soman N. Abraham. “Mast Cell Interleukin-10 Drives Localized Tolerance in Chronic Bladder Infection”. In: *Immunity* 38.2 (2013), pp. 349–359. ISSN: 1074-7613. DOI: https://doi.org/10.1016/j.immuni.2012.10.019. URL: https://www.sciencedirect.com/science/article/pii/S1074761313000502.

[17] Cheryl Y Chan, Ashley L St John, and Soman N Abraham. “Mast cell interleukin-10 drives localized tolerance in chronic bladder infection.” In: 38.2 (2013), pp. 349–359. DOI: 10.1016/j.immuni.2012.10.019.

[18] Godefroid Charbon et al. “Counting Replication Origins to Measure Growth of Pathogens”. In: *Antibiotics* 9.5 (2020).

[19] Hong-Song Chen et al. “Computational fluid dynamics modeling approaches to assess lower urinary tract hydraulic dynamics in posterior urethral valve before and after endoscopic valve ablation: a pilot study”. In: *World Journal of Urology* 40.2 (2022), pp. 505–511.

[20] Alison Chisholm et al. “Diagnosis, management, and outcome of women with symptoms of urinary tract infection in primary care: prospective cohort study”. In: *BMJ* 341 (2010), p. c3565. DOI: 10.1136/bmj.c3565.

[21] Ashok Chockalingam et al. “Evaluation of Immunocompetent Urinary Tract Infected Balb/C Mouse Model For the Study of Antibiotic Resistance Development Using Escherichia Coli CFT073 Infection”. In: *Antibiotics* 8.4 (2019).

[22] Hae Woong Choi et al. “Loss of Bladder Epithelium Induced by Cytolytic Mast Cell Granules”. In: *Immunity* 45.6 (2016), pp. 1258–1269. ISSN: 1074-7613. DOI: https://doi.org/10.1016/j.immuni.2016.11.003. URL: https://www.sciencedirect.com/science/article/pii/S1074761316304757.

[23] Milan Chromek et al. “The antimicrobial peptide cathelicidin protects the urinary tract against invasive bacterial infection”. In: *Nature Medicine* 12.6 (2006), pp. 636–641. DOI: 10.1038/nm1407. URL: https://doi.org/10.1038/nm1407.

[24] Andrew J. Cohen et al. “Computational Fluid Dynamic Modeling of Urethral Strictures”. In: *Journal of Urology* 202.2 (2019), pp. 347–353.

[25] Richard Colgan and Mozella Williams. “Diagnosis and treatment of acute uncomplicated cystitis”. In: *American Family Physician (AFP)* 84.07 (2011), pp. 771–6. DOI: 22010614.

[26] N. A. Cornick and A. F. Helgerson. “Transmission and Infectious Dose of Escherichia coli O157:H7 in Swine”. In: *Applied and Environmental Microbiology* 70.9 (2004), pp. 5331–5335. DOI: 10.1128/AEM.70.9.5331-5335.2004. eprint: https://journals.asm.org/doi/pdf/10.1128/AEM.70.9.5331-5335.2004. URL: https://journals.asm.org/doi/abs/10.1128/AEM.70.9.5331-5335.2004.

[27] “Crosstalk between Sentinel and Helper Macrophages Permits Neutrophil Migration into Infected Uroepithelium”. In: *Cell* 156.3 (2014), pp. 456–468. ISSN: 0092-8674. DOI: https://doi.org/10.1016/j.cell.2014.01.006. URL: https://www.sciencedirect.com/science/article/pii/S0092867414000166.

[28] “Cyclic AMP–regulated exocytosis of Escherichia coli from infected bladder epithelial cells”. In: *Nature Medicine* 13.5 (2007), pp. 625–630. DOI: 10.1038/nm1572. URL: https://doi.org/10.1038/nm1572.

[29] PETER DE Man et al. “Bacterial adherence as a virulence factor in urinary tract infection”. In: *APMIS* 98.7-12 (1990), pp. 1053–1060. DOI: https://doi.org/10.1111/j.1699-0463.1990.tb05034.x. eprint: https://onlinelibrary.wiley.com/doi/pdf/10.1111/j.1699-0463.1990.tb05034.x. URL: https://onlinelibrary.wiley.com/doi/abs/10.1111/j.1699-0463.1990.tb05034.x.

[30] Nicole J. De Nisco et al. “Direct Detection of Tissue-Resident Bacteria and Chronic Inflammation in the Bladder Wall of Postmenopausal Women with Recurrent Urinary Tract Infection”. In: *Journal of Molecular Biology* 431.21 (2019). Mechanisms and Strategies of Host Response to Pathogens, pp. 4368–4379. ISSN: 0022-2836. DOI: https://doi.org/10.1016/j.jmb.2019.04.008. URL: https://www.sciencedirect.com/science/article/pii/S0022283619302025.

[31] Benjamin L. Duell et al. “Human Bladder Uroepithelial Cells Synergize with Monocytes to Promote IL-10 Synthesis and Other Cytokine Responses to Uropathogenic Escherichia coli”. In: *PLOS ONE* 8.10 (Oct. 2013), null. DOI: 10.1371/journal.pone.0078013. URL: https://doi.org/10.1371/journal.pone.0078013.

[32] T.S.J. Elliott et al. “Bacteriology and ultrastructure of the bladder in patients with urinary tract infections”. In: *Journal of Infection* 11.3 (1985), pp. 191–199. ISSN: 0163-4453. DOI: https://doi.org/10.1016/S0163-4453(85)92997-4. URL: https://www.sciencedirect.com/science/article/pii/S0163445385929974.

[33] Ana L Flores-Mireles et al. “Urinary Tract Infections: Epidemiology, Mechanisms of Infection and Treatment Options”. eng. In: *Nature reviews. Microbiology* 13.5 (2015), pp. 269–284. ISSN: 1740-1526.

[34] Valerie S. Forsyth et al. “Rapid Growth of Uropathogenic Escherichia coli during Human Urinary Tract Infection”. In: *mBio* 9.2 (2018), e00186–18. DOI: 10.1128/mBio.00186-18. eprint: https://journals.asm.org/doi/pdf/10.1128/mBio.00186-18. URL: https://journals.asm.org/doi/abs/10.1128/mBio.00186-18.

[35] Valerie S. Forsyth et al. “Rapid Growth of Uropathogenic Escherichia coli during Human Urinary Tract Infection”. In: *mBio* 9.2 (2018), e00186–18. DOI: 10.1128/mBio.00186-18. eprint: https://journals.asm.org/doi/pdf/10.1128/mBio.00186-18. URL: https://journals.asm.org/doi/abs/10.1128/mBio.00186-18.

[36] Betsy Foxman et al. “Urinary tract infection: self-reported incidence and associated costs”. In: *Annals of epidemiology* 10.2 (2000), pp. 509–515. DOI: 10.1016/s1047-2797(99)00072-7.

[37] Mar'ia Garc'ia-Castillo et al. "Pharmacodynamics of trimethoprim alone and in combination with sulfamethoxazole in a murine model of urinary tract infection caused by Escherichia coli". In: *Antimicrobial agents and chemotherapy* 64.10 (2020). DOI: 10.1128/AAC.01144-20.

[38] Pranav S. Garimella et al. "Urinary Uromodulin and Risk of Urinary Tract Infections: The Cardiovascular Health Study". In: *American Journal of Kidney Diseases* 69.6 (2017), pp. 744–751. ISSN: 0272-6386. DOI: https://doi.org/10.1053/j.ajkd.2016.08.022. URL: https://www.sciencedirect.com/science/article/pii/S0272638616304863.

[39] Janina K. Geißert et al. "A Computational Model of Bacterial Population Dynamics in Gastrointestinal Yersinia enterocolitica Infections in Mice". In: *Biology* 11.2 (2022).

[40] Michael Getz et al. "Iterative community-driven development of a SARS-CoV-2 tissue simulator". In: *bioRxiv* (2021). DOI: 10.1101/2020.04.02.019075. eprint: https://www.biorxiv.org/content/early/2021/11/10/2020.04.02.019075.full.pdf. URL: https://www.biorxiv.org/content/early/2021/11/10/2020.04.02.019075.

[41] Beth Gibson et al. "The distribution of bacterial doubling times in the wild". In: *Proceedings of the Royal Society B: Biological Sciences* 285.1880 (2018), p. 20180789.

[42] G Godaly et al. "Neutrophil recruitment, chemokine receptors, and resistance to mucosal infection." eng. In: *J Leukoc Biol* 69.6 (2001), pp. 899–906. ISSN: 0741-5400 (Print); 0741-5400 (Linking).

[43] Sherwood L Gorbach, John G Bartlett, and Neil R Blacklow. "Effect of trimethoprim-sulfamethoxazole on the intestinal flora of human volunteers and patients". In: *New England Journal of Medicine* 292.14 (1975), pp. 735–741. DOI: 10.1056/NEJM197504032921402.

[44] Larissa Grigoryan, Barbara W Trautner, and Kalpana Gupta. "Diagnosis and management of urinary tract infections in the outpatient setting: a review". In: *JAMA* 312.16 (2014), pp. 1677–1684. DOI: 10.1001/jama.2014.12842.

[45] West Essex Clinical Commissioning Group. *Antibiotic Prophylaxis Guidelines for Recurrent Urinary Tract Infections in Adults*. https://westessexccg.nhs.uk/your-health/medicines-optimisation-and-pharmacy/clinical-guidelines-and-prescribing-formularies/05-infections/2514-antibiotic-prophylaxis-guidelines-for-recurrent-urinary-tract-infections-in-adults/file. Accessed on May 7th, 2023.

[46] Kalpana Gupta et al. "International clinical practice guidelines for the treatment of acute uncomplicated cystitis and pyelonephritis in women: A 2010 update by the Infectious Diseases Society of America and the European Society for Microbiology and Infectious Diseases". In: *Clinical Infectious Diseases* 52.5 (2011), e103–e120.

[47] Robert J. H. Hammond et al. "A simple label-free method reveals bacterial growth dynamics and antibiotic action in real-time". English. In: *Scientific Reports* 12.1 (Nov. 2022). Funding Information: The authors gratefully acknowledge the financial support of Scottish Enterprise, NESTA Longitude Prize and the University of St Andrews. We thank Dr Samantha Pitt, Dr Ben Parcell and Dr Frank Kloprogge for their critical review of the manuscript. ISSN: 2045-2322. DOI: 10.1038/s41598-022-22671-6.

[48] Thomas J. Hannan and David A. Hunstad. "A Murine Model for Escherichia coli Urinary Tract Infection". In: *Bacterial Persistence: Methods and Protocols*. Ed. by Jan Michiels and Maarten Fauvart. New York, NY: Springer New York, 2016, pp. 159–175. ISBN: 978-1-4939-2854-5. DOI: 10.1007/978-

1-4939-2854-5_14. URL: https://doi.org/10.1007/978-1-4939-2854-5_14.

[49] Thomas J. Hannan et al. "Early Severe Inflammatory Responses to Uropathogenic E. coli Predispose to Chronic and Recurrent Urinary Tract Infection". In: *PLOS Pathogens* 6.8 (Aug. 2010), pp. 1–19. DOI: 10.1371/journal.ppat.1001042. URL: https://doi.org/10.1371/journal.ppat.1001042.

[50] Thomas J. Hannan et al. "Host–pathogen checkpoints and population bottlenecks in persistent and intracellular uropathogenic Escherichia coli bladder infection". In: *FEMS Microbiology Reviews* 36.3 (May 2012), pp. 616–648. ISSN: 0168-6445. DOI: 10.1111/j.1574-6976.2012.00339.x. eprint: https://academic.oup.com/femsre/article-pdf/36/3/616/18129212/36-3-616.pdf. URL: https://doi.org/10.1111/j.1574-6976.2012.00339.x.

[51] Masashi Haraoka et al. "Neutrophil Recruitment and Resistance to Urinary Tract Infection". In: *The Journal of Infectious Diseases* 180.4 (Oct. 1999), pp. 1220–1229.

[52] Byron W. Hayes and Soman N. Abraham. "Innate Immune Responses to Bladder Infection". In: *Microbiology Spectrum* 4.6 (2016), p. 4.6.45. DOI: 10.1128/microbiolspec.UTI-0024-2016. eprint: https://journals.asm.org/doi/pdf/10.1128/microbiolspec.UTI-0024-2016. URL: https://journals.asm.org/doi/abs/10.1128/microbiolspec.UTI-0024-2016.

[53] Byron W. Hayes et al. "Innate Immune Responses to Bladder Infection". In: *Microbiology Spectrum* 4.6 (2016), p. 4.6.45. DOI: 10.1128/microbiolspec.UTI-0024-2016. eprint: https://journals.asm.org/doi/pdf/10.

1128/microbiolspec.UTI-0024-2016. URL: https://journals.asm.org/doi/abs/10.1128/microbiolspec.UTI-0024-2016.

[54] J. C. Helton and F. J. Davis. "Illustration of Sampling-Based Methods for Uncertainty and Sensitivity Analysis". In: *Risk Analysis* 22.3 (2002), pp. 591–622.

[55] Andrés Hidalgo et al. "The Neutrophil Life Cycle". In: *Trends in Immunology* 40.7 (2019). Special Issue: New Advances in Neutrophil Immunity, pp. 584–597. ISSN: 1471-4906. DOI: https://doi.org/10.1016/j.it.2019.04.013. URL: https://www.sciencedirect.com/science/article/pii/S1471490619301024.

[56] Anh N. Hoang et al. "Measuring neutrophil speed and directionality during chemotaxis, directly from a droplet of whole blood". In: *TECHNOLOGY* 01.01 (2013), pp. 49–57. DOI: 10.1142/S2339547813500040. eprint: https://doi.org/10.1142/S2339547813500040. URL: https://doi.org/10.1142/S2339547813500040.

[57] TM Hooton et al. "Voided midstream urine culture and acute cystitis in premenopausal women". In: *New England Journal of Medicine* 329.15 (1993), pp. 977–981.

[58] Kim Young Hyo Jang Tae Young. "Interleukin-33 and Mast Cells Bridge Innate and Adaptive Immunity: From the Allergologist's Perspective". In: *Int Neurourol J* 19.3 (2015), pp. 142–150. DOI: 10.5213/inj.2015.19.3.142. eprint: http://www.einj.org/journal/view.php?number=535. URL: http://www.einj.org/journal/view.php?number=535.

[59] James R. Johnson. "Virulence factors in Escherichia coli urinary tract infection". English (US). In: *Clinical Microbiology Reviews* 4.1 (Jan. 1991), pp. 80–128. ISSN: 0893-8512. DOI: 10.1128/CMR.4.1.80.

[60] Carl-Fredrik Johnzon, Elin Rönnberg, and Gunnar Pejler. “The Role of Mast Cells in Bacterial Infection”. In: *The American Journal of Pathology* 186.1 (2016), pp. 4–14. ISSN: 0002-9440. DOI: https://doi.org/10.1016/j.ajpath.2015.06.024. URL: https://www.sciencedirect.com/science/article/pii/S0002944015005398.

[61] Gunnar Kahlmeter and Hanna Odén Poulsen. “Antimicrobial susceptibility of Escherichia coli from community-acquired urinary tract infections in Europe: the ECO·SENS study revisited”. In: *International Journal of Antimicrobial Agents* 39.1 (2012), pp. 45–51.

[62] Cheng-Yen Kao et al. “Characterization of host and escherichia coli strains causing recurrent urinary tract infections based on molecular typing”. In: *BMC Microbiology* 23.1 (2023), p. 90. DOI: 10.1186/s12866-023-02820-1. URL: https://doi.org/10.1186/s12866-023-02820-1.

[63] Ahmad Keshtkar, Asghar Keshtkar, and Pat Lawford. “Cellular morphological parameters of the human urinary bladder (malignant and normal)”. In: *International Journal of Experimental Pathology* 88.3 (2007), pp. 185–190. DOI: https://doi.org/10.1111/j.1365-2613.2006.00520.x. eprint: https://onlinelibrary.wiley.com/doi/pdf/10.1111/j.1365-2613.2006.00520.x. URL: https://onlinelibrary.wiley.com/doi/abs/10.1111/j.1365-2613.2006.00520.x.

[64] Hee Youn Kim et al. “Microbiological Characteristics of Unresolved Acute Uncomplicated Cystitis.” eng. In: *Microb Drug Resist* 22.5 (2016), pp. 387–391. ISSN: 1931-8448 (Electronic); 1076-6294 (Linking). DOI: 10.1089/mdr.2015.0241.

[65] Maria Kostakioti, Scott J. Hultgren, and Maria Hadjifrangiskou. “Molecular blueprint of uropathogenic Escherichia coli virulence provides clues toward the development of anti-virulence therapeutics”. In: *Virulence* 3.7

(2012). PMID: 23154288, pp. 592–593. DOI: 10.4161/viru.22364. eprint: https://doi.org/10.4161/viru.22364. URL: https://doi.org/10.4161/viru.22364.

[66] Maria Kostakioti, Scott J Hultgren, and Maria Hadjifrangiskou. "Molecular blueprint of uropathogenic Escherichia coli virulence provides clues toward the development of anti-virulence therapeutics." eng. In: *Virulence* 3.7 (2012), pp. 592–594. ISSN: 2150-5608 (Electronic); 2150-5594 (Print); 2150-5594 (Linking). DOI: 10.4161/viru.22364.

[67] Anas Lasri Doukkali et al. "A hybrid individual-based mathematical model to study bladder infections". In: *Frontiers in Applied Mathematics and Statistics* 9 (2023). ISSN: 2297-4687. DOI: 10.3389/fams.2023.1090334. URL: https://www.frontiersin.org/articles/10.3389/fams.2023.1090334.

[68] Fiona R. Macfarlane, Tommaso Lorenzi, and Mark A. J. Chaplain. "Modelling the Immune Response to Cancer: An Individual-Based Approach Accounting for the Difference in Movement Between Inactive and Activated T Cells". In: *Bulletin of Mathematical Biology* 80.6 (2018), pp. 1539–1562. DOI: 10.1007/s11538-018-0412-8. URL: https://doi.org/10.1007/s11538-018-0412-8.

[69] Livia Mariano and Molly Ingersoll. "The immune response to infection in the bladder". In: *Nature Reviews Urology* 17 (July 2020), pp. 1–20. DOI: 10.1038/s41585-020-0350-8.

[70] Simeone Marino et al. "A methodology for performing global uncertainty and sensitivity analysis in systems biology". In: *Journal of Theoretical Biology* 254.1 (2008), pp. 178–196. ISSN: 0022-5193. DOI: https://doi.org/10.1016/j.jtbi.2008.04.011. URL: https://www.sciencedirect.com/science/article/pii/S0022519308001896.

[71] Jenna M. McCracken and Lee-Ann H. Allen. “Regulation of Human Neutrophil Apoptosis and Lifespan in Health and Disease”. In: *Journal of Cell Death* 7 (2014). PMID: 25278783, JCD.S11038. DOI: 10.4137/JCD.S11038. eprint: https://doi.org/10.4137/JCD.S11038. URL: https://doi.org/10.4137/JCD.S11038.

[72] Subhashis Mitra and George John Alangaden. “Recurrent urinary tract infections in kidney transplant recipients”. In: *Current infectious disease reports* 13.6 (2011), pp. 579–587.

[73] Gabriela Mora-Bau et al. “Macrophages Subvert Adaptive Immunity to Urinary Tract Infection”. In: *PLOS Pathogens* 11.7 (July 2015), pp. 1–23. DOI: 10.1371/journal.ppat.1005044. URL: https://doi.org/10.1371/journal.ppat.1005044.

[74] Matthew A. Mulvey, Joel D. Schilling, and Scott J. Hultgren. “Establishment of a Persistent Escherichia coli Reservoir during the Acute Phase of a Bladder Infection”. In: *Infection and Immunity* 69.7 (2001), pp. 4572–4579. DOI: 10.1128/IAI.69.7.4572-4579.2001. eprint: https://journals.asm.org/doi/pdf/10.1128/IAI.69.7.4572-4579.2001. URL: https://journals.asm.org/doi/abs/10.1128/IAI.69.7.4572-4579.2001.

[75] Indira U. Mysorekar and Scott J. Hultgren. “Mechanisms of uropathogenic Escherichia coli persistence and eradication from the urinary tract”. In: *Proceedings of the National Academy of Sciences* 103.38 (2006), pp. 14170–14175. DOI: 10.1073/pnas.0602136103. eprint: https://www.pnas.org/doi/pdf/10.1073/pnas.0602136103. URL: https://www.pnas.org/doi/abs/10.1073/pnas.0602136103.

[76] Indira U. Mysorekar et al. “Bone Morphogenetic Protein 4 Signaling Regulates Epithelial Renewal in the Urinary Tract in Response to Uropathogenic

Infection". In: *Cell Host Microbe* 5.5 (2009), pp. 463–475. ISSN: 1931-3128. DOI: https://doi.org/10.1016/j.chom.2009.04.005. URL: https://www.sciencedirect.com/science/article/pii/S1931312809001061.

[77] Kurt G Naber. "Epidemiology of urinary tract infections: incidence, morbidity, and economic costs". In: *The American journal of medicine* 113.1 (2001), 5S–13S. DOI: 10.1016/s0002-9343(01)00949-0.

[78] National Institute for Health and Care Excellence. *Urinary tract infection (lower): antimicrobial prescribing*. https://www.nice.org.uk/guidance/ng109. 2018.

[79] Taiji NISHIMURA et al. "Macrophages in the Urine in Acute Bacterial Cystitis". In: *Journal of the Japanese Association for Infectious Diseases* 67.7 (1993), pp. 659–664. DOI: 10.11150/kansenshogakuzasshi1970.67.659.

[80] Amit A. Patel, Florent Ginhoux, and Simon Yona. "Monocytes, macrophages, dendritic cells and neutrophils: an update on lifespan kinetics in health and disease". In: *Immunology* 163.3 (2021), pp. 250–261. DOI: https://doi.org/10.1111/imm.13320. eprint: https://onlinelibrary.wiley.com/doi/pdf/10.1111/imm.13320. URL: https://onlinelibrary.wiley.com/doi/abs/10.1111/imm.13320.

[81] Alan S. Perelson and Ruy M. Ribeiro. "Introduction to modeling viral infections and immunity". In: *Immunological Reviews* 285.1 (2018), pp. 5–8. DOI: https://doi.org/10.1111/imr.12700. eprint: https://onlinelibrary.wiley.com/doi/pdf/10.1111/imr.12700. URL: https://onlinelibrary.wiley.com/doi/abs/10.1111/imr.12700.

[82] James Peterson et al. “Single-dose compared with 3-day norfloxacin for uncomplicated urinary tract infection in women: a double-blind, randomized trial”. In: *Annals of internal medicine* 148.6 (2008), pp. 409–417. DOI: 10.7326/0003-4819-148-6-200803180-00004.

[83] Gibin G. Powathil et al. “Modelling the effects of cell-cycle heterogeneity on the response of a solid tumour to chemotherapy: Biological insights from a hybrid multiscale cellular automaton model”. In: *Journal of Theoretical Biology* 308 (2012), pp. 1–19. ISSN: 0022-5193. DOI: https://doi.org/10.1016/j.jtbi.2012.05.015. URL: https://www.sciencedirect.com/science/article/pii/S0022519312002573.

[84] C’eline Pulcini et al. “New antibiotic development: barriers and opportunities in the antibiotic pipeline”. In: *Clinical microbiology and infection* 26.8 (2020), pp. 941–946. DOI: 10.1016/j.cmi.2020.03.014.

[85] Elias Rahal et al. “Escherichia coli O157:H7—Clinical aspects and novel treatment approaches”. In: *Frontiers in Cellular and Infection Microbiology* 2 (2012). ISSN: 2235-2988. DOI: 10.3389/fcimb.2012.00138. URL: https://www.frontiersin.org/article/10.3389/fcimb.2012.00138.

[86] Joan J. Ratner et al. “Bacteria-Specific Antibody in the Urine of Patients with Acute Pyelonephritis and Cystitis”. In: *The Journal of Infectious Diseases* 143.3 (Mar. 1981), pp. 404–412. ISSN: 0022-1899. DOI: 10.1093/infdis/143.3.404. eprint: https://academic.oup.com/jid/article-pdf/143/3/404/2565895/143-3-404.pdf. URL: https://doi.org/10.1093/infdis/143.3.404.

[87] Ploy Rattanaumpawan and Sudchai Boonsong. “Antibiotic use in uncomplicated urinary tract infection in adult women in primary care: a systematic

review". In: *Journal of the Medical Association of Thailand= Chotmaihet thangphaet* 100.1 (2017), pp. 87–93.

[88] Gregor Reid and Jack D. Sobel. "Bacterial Adherence in the Pathogenesis of Urinary Tract Infection: A Review". In: *Reviews of Infectious Diseases* 9.3 (1987), pp. 470–487. ISSN: 01620886. URL: http://www.jstor.org/stable/4454123 (visited on 05/10/2023).

[89] Sara Roccabianca and Tamara Bush. "Understanding the mechanics of the bladder through experiments and theoretical models: Where we started and where we are heading". In: *TECHNOLOGY* 04 (Mar. 2016), pp. 1–12. DOI: 10.1142/S2339547816400082.

[90] Aislinn D. Rowan-Nash et al. "Cross-Domain and Viral Interactions in the Microbiome". In: *Microbiology and Molecular Biology Reviews* 83.1 (2019), e00044–18.

[91] C. F. Rowlatt et al. "Modelling the within-host spread of SARS-CoV-2 infection, and the subsequent immune response, using a hybrid, multiscale, individual-based model. Part I: Macrophages". In: *bioRxiv* (2022). DOI: 10.1101/2022.05.06.490883. eprint: https://www.biorxiv.org/content/early/2022/05/06/2022.05.06.490883.full.pdf. URL: https://www.biorxiv.org/content/early/2022/05/06/2022.05.06.490883.

[92] H. S. Rugo et al. "Local cytokine production in a murine model of Escherichia coli pyelonephritis." In: *The Journal of clinical investigation* 89 3 (1992), pp. 1032–9.

[93] Seongmi K. Russell et al. "Uropathogenic Escherichia coli infection-induced epithelial trained immunity impacts urinary tract disease outcome". In: *Nature Microbiology* 8.5 (2023), pp. 875–888.

[94] Andrea Saltelli et al. “Why so Many Published Sensitivity Analyses Are False: A Systematic Review of Sensitivity Analysis Practices”. In: *Environ. Model. Softw.* 114.C (2019), 29–39. ISSN: 1364-8152. DOI: 10.1016/j.envsoft.2019.01.012. URL: https://doi.org/10.1016/j.envsoft.2019.01.012.

[95] Guido Schmiemann et al. “The diagnosis of urinary tract infection: a systematic review”. In: *Deutsches Arzteblatt International* 107.21 (2010), pp. 361–367. DOI: 10.3238/arztebl.2010.0361.

[96] National Health Service. *Trimethoprim*. https://www.nhs.uk/medicines/trimethoprim/. Accessed on May 7th, 2023.

[97] R D Shahin et al. “Neutrophil recruitment and bacterial clearance correlated with LPS responsiveness in local gram-negative infection.” In: *The Journal of Immunology* 138.10 (May 1987), pp. 3475–3480. ISSN: 0022-1767. DOI: 10.4049/jimmunol.138.10.3475. eprint: https://journals.aai.org/jimmunol/article-pdf/138/10/3475/1030633/3475.pdf. URL: https://doi.org/10.4049/jimmunol.138.10.3475.

[98] Kunal Sharma et al. “Dynamic persistence of UPEC intracellular bacterial communities in a human bladder-chip model of urinary tract infection”. In: *eLife* 10 (2021), e66481.

[99] Scott I. Simon and Min-Ho Kim. “A day (or 5) in a neutrophil’s life”. In: *Blood* 116.4 (July 2010), pp. 511–512. ISSN: 0006-4971. DOI: 10.1182/blood-2010-05-283184. eprint: https://ashpublications.org/blood/article-pdf/116/4/511/1332643/zh803010000511.pdf. URL: https://doi.org/10.1182/blood-2010-05-283184.

[100] Elliott Sober and David Sloan Wilson. *Unto Others: The Evolution and Psychology of Unselfish Behavior*. Harvard University Press, 1998.

[101] Jeongmin Song et al. “TLR4-mediated expulsion of bacteria from infected bladder epithelial cells”. In: *Proceedings of the National Academy of Sciences* 106.35 (2009), pp. 14966–14971. DOI: 10.1073/pnas.0900527106. eprint: https://www.pnas.org/doi/pdf/10.1073/pnas.0900527106. URL: https://www.pnas.org/doi/abs/10.1073/pnas.0900527106.

[102] Afsaneh Soruri et al. “-Defensins chemoattract macrophages and mast cells but not lymphocytes and dendritic cells: CCR6 is not involved”. In: *European Journal of Immunology* 37.9 (2007), pp. 2474–2486. DOI: https://doi.org/10.1002/eji.200737292. eprint: https://onlinelibrary.wiley.com/doi/pdf/10.1002/eji.200737292. URL: https://onlinelibrary.wiley.com/doi/abs/10.1002/eji.200737292.

[103] Kristian Stærk, Morten Østergaard Andersen, and Thomas Emil Andersen. “Uropathogenic Escherichia coli can cause cystitis at extremely low inocula in a pig model”. In: *Journal of Medical Microbiology* 71.4 (2022), p. 001537.

[104] Walter E Stamm, Thomas M Hooton, and James R Johnson. “Urinary tract infections: from pathogenesis to treatment”. In: *Journal of Infectious Diseases* 159.3 (1989), pp. 400–406.

[105] Walter E. Stamm and S. Ragnar Norrby. “Urinary Tract Infections: Disease Panorama and Challenges”. In: *The Journal of Infectious Diseases* 183.Supplement_1 (Mar. 2001), S1–S4. ISSN: 0022-1899. DOI: 10.1086/318850. eprint: https://academic.oup.com/jid/article-pdf/183/Supplement_1/S1/6463288/183-Supplement_1-S1.pdf. URL: https://doi.org/10.1086/318850.

[106] Sargurunathan Subashchandrabose et al. “Host-specific induction of Escherichia coli fitness genes during human urinary tract infection”. In: *Proceedings of the National Academy of Sciences* 111.51 (2014), pp. 18327–18332. DOI: 10.1073/pnas.1415959112. eprint: https://www.pnas.org/doi/

pdf/10.1073/pnas.1415959112. URL: https://www.pnas.org/doi/abs/10.1073/pnas.1415959112.

[107] Susanne Säve and Katarina Persson. "Extracellular ATP and P2Y Receptor Activation Induce a Proinflammatory Host Response in the Human Urinary Tract". In: *Infection and Immunity* 78.8 (2010), pp. 3609–3615. DOI: 10.1128/IAI.00074-10. eprint: https://journals.asm.org/doi/pdf/10.1128/IAI.00074-10. URL: https://journals.asm.org/doi/abs/10.1128/IAI.00074-10.

[108] Maria E. Terlizzi, Giorgio Gribaudo, and Massimo E. Maffei. "UroPathogenic Escherichia coli (UPEC) Infections: Virulence Factors, Bladder Responses, Antibiotic, and Non-antibiotic Antimicrobial Strategies". In: *Frontiers in Microbiology* 8 (). ISSN: 1664-302X. DOI: 10.3389/fmicb.2017.01566. URL: https://www.frontiersin.org/article/10.3389/fmicb.2017.01566.

[109] Jaime Simão Sichman, Rosaria Conte, and Nigel Gilbert, eds. *Agent-Based Modeling vs. Equation-Based Modeling: A Case Study and Users'Guide*. Berlin, Heidelberg: Springer Berlin Heidelberg, 1998, pp. 10–25. ISBN: 978-3-540-49246-7.

[110] Xu Wang et al. "Evidence for the Role of Mast Cells in Cystitis-Associated Lower Urinary Tract Dysfunction: A Multidisciplinary Approach to the Study of Chronic Pelvic Pain Research Network Animal Model Study". In: *PLOS ONE* 11.12 (Dec. 2016), pp. 1–12. DOI: 10.1371/journal.pone.0168772. URL: https://doi.org/10.1371/journal.pone.0168772.

[111] John W Warren et al. "Guidelines for antimicrobial treatment of uncomplicated acute bacterial cystitis and acute pyelonephritis in women. Infectious Diseases Society of America (IDSA)". In: *Clinical infectious diseases* 29.4 (1999), pp. 745–758. DOI: 10.1086/520427.

[112] Chuanqi Wei et al. “Evaluation of Trimethoprim/Sulfamethoxazole (SXT), Minocycline, Tigecycline, Moxifloxacin, and Ceftazidime Alone and in Combinations for SXT-Susceptible and SXT-Resistant Stenotrophomonas maltophilia by In Vitro Time-Kill Experiments”. In: *PLOS ONE* 11.3 (Mar. 2016), pp. 1–9.

[113] Uri Wilensky and William Rand. *An Introduction to Agent-Based Modeling: Modeling Natural, Social, and Engineered Complex Systems with NetLogo*. The MIT Press, 2015. ISBN: 9780262731898. URL: http://www.jstor.org/stable/j.ctt17kk851 (visited on 05/10/2023).

[114] Uri Wilensky and Kenneth Reisman. “Thinking Like a Wolf, a Sheep, or a Firefly: Learning Biology Through Constructing and Testing Computational Theories—An Embodied Modeling Approach”. In: *Cognition and Instruction* 24.2 (2006), pp. 171–209. DOI: 10.1207/s1532690xci2402_1.

[115] Jianxuan Wu, Yuxuan Miao, and Soman N. Abraham. “The multiple antibacterial activities of the bladder epithelium”. In: *Annals of Translational Medicine* 5.2 (2017). ISSN: 2305-5847. URL: https://atm.amegroups.com/article/view/13315.

[116] Vanaporn Wuthiekanun et al. “Trimethoprim/sulfamethoxazole resistance in clinical isolates of Burkholderia pseudomallei”. In: *Journal of Antimicrobial Chemotherapy* 55.6 (Apr. 2005), pp. 1029–1031. DOI: 10.1093/jac/dki151. eprint: https://academic.oup.com/jac/article-pdf/55/6/1029/2155878/dki151.pdf. URL: https://doi.org/10.1093/jac/dki151.

[117] George G Zhanel et al. “Antibiotic resistance in outpatient urinary isolates: final results from the North American Urinary Tract Infection Collaborative Alliance (NAUTICA)”. In: *International journal of antimicrobial agents* 26.3 (2005), pp. 380–388. DOI: 10.1016/j.ijantimicag.2005.06.005.